STUDIES OF EQUATORIAL AND POLAR LIGHT CHARGED PARTICLES EMITTED IN NUCLEAR FISSION AND DETERMINATION OF SCISSION CONFIGURATION

A Thesis Submitted
in Partial Fulfilment of the Requirements
for the Degree of

DOCTOR OF PHILOSOPHY

by

AJIT KUMAR SINHA

to the

DEPARTMENT OF PHYSICS

INDIAN INSTITUTE OF TECHNOLOGY KANPUR

DECEMBER, 1981

TO

MY PARENTS

CERTIFICATE

Certified that the work presented in this thesis entitled "Studies of Equatorial and Polar Light Charged Particles Emitted in Nuclear Fission and Determination of Scission Configuration" by Mr. Ajit Kumar Sinha, has been done under my supervision and that it has not been submitted elsewhere for a degree.

G. K. Mehta
Professor
Department of Physics
Indian Institute of Technology,
Kanpur.

December 1981.

ACKNOWLEDGEMENTS

With my apologies for those not acknowledged explicitly below, I begin with my attempt to acknowledge the enormous amount of help extended to me from various corners during my research carrier in I.I.T. Kanpur.

My most sincere thanks are due to Prof. G.K. Mehta for his invaluable and concrete guidance right from the search for the problem investigated to the completion of the project. His infinite patience in helping me (in his carefully planned way) to familiarize with various facets of the research methodology and elucidating various theoretical and experimental aspects of the fission physics has been of singular importance in carrying out the present work. His most decent treatment extended to me and technique* used in getting me to work have made an indelible impression on me and I thank him for the important lessons I have derived from his personality.

I wish to thank Dr. Sudhir Sen for his help in the initial stages of the project, Dr. H.S. Mani for useful discussions on trajectory calculations, Dr. R.K. Popli for his useful comments on detection efficiency calculations, Dr. B. Krishnarajulu for his help in trajectory calculations and Dr. S.C.L. Sharma for his help at various stages of work. Participation from Dr. D.M. Nadkarni, BARC, India in the experiment undertaken is deeply acknowledged. I express my gratitude for the help derived from discussions with Dr. S.S. Kapoor, Dr. V.S. Ramamurthy, Dr. R.K. Choudhury, Dr. C.V.K. Baba from BARC, Bombay.

I thank Mr. D.S. Mishra, Mr. Muddu Krishna and Mr. N.V. Nair for their patient and cooperative attitude during the lab-work. I express my sincere thanks for the help

---

*The technique simply consisted of a practical demonstration of hard work extending beyond 10 hrs. per day.

from Dr. H.C. Verma, Mrs. Veena Joshi, Mr. A.K. Singh, Dr. K.M. Varier, Dr. A.K. Nayak and Dr. C.V. Srinivas Rao.

Mr. M.M. Sharma is thanked specially for his active cooperation during the experimental work and data analysis and for his helpful attitude. I have immense pleasure in acknowledging the continual technical help extended to me from Mr. K. Masood, Mr. V.K. Sharma, Mr. M.M. Gupta and Mr. V.K. Jain. I wish to acknowledge the most helpful attitude of Mr. K.M.L. Jha and express my gratitude for excellent maintenance of the Van de Graaff laboratory by his technical team of Mr. M.M. Gupta, Mr. K. Masood and Mr. V.K. Sharma. Help provided by Mr. K. Masood, Mr. S.P. Tripathi and Mr. C.B. Srivastava for 'round the clock' operation of the machine during the experimental runs is most sincerely acknowledged. I acknowledge the help derived from the good maintenance of various electronic equipments by Mr. A.R. Korde, Mr. Kamal Kumar, Mr. Vishal Saxena and Mrs. Fatima Naqvi.

I have derived an unique help through my friend D.S. Mishra by his inspiring company which has surpassed the level of 10 hrs. per day during last two years of my stay in I.I.T. Kanpur. I must express my deepest gratitude for various helps of crucial nature provided by him as well as by Mr. M. Rafat, Dr. H.C. Verma, Mr. N.V. Nair, Mr. Shailendra Agnihotri, Dr. P.N. Dixit and Dr. Ashok Kumar. During my stay in I.I.T. Kanpur, I have been guided by some of my friends into work related to the social service, which helped me in getting the much needed peace of mind. In this regard, I must thank the guidance of respectable Dr. Y.R. Waghmare and cooperation from friends Mr. G.D. Bagaria, Mr. S. Major, Mr. V.S.P. Srivastava, Mr. S.K. Nigam, Mr. Amarendra, Mr. M. Rafat, Mr. N.V. Nair, Mr. D.S. Mishra and Ms. R.M. Roy.

I thank Sri N. Abraham, Principal, Ch. Ch. College, Mr. A.N. Dixit, Head, Physics Dept., Ch.Ch. College and my colleagues in the Physics Dept., Ch. Ch. College for the

cooperative attitude and substantial help throughout my part-time research in I.I.T. Kanpur.

The financial help from DAE, India and Physics Dept., I.I.T. Kanpur is acknowledged.

I thank Mr. B.K. Jain for his excellent drawing, Mr. L.S. Bajpai for his excellent typing and Mr. H.K. Panda and Mr. L.S. Rathore for neat cyclostyling. Last, but not least, I take this opportunity to thank Mr. Ram Nath and Mr. Shiva Prakash for their caring attitude and generous help throughout my stay in I.I.T. Kanpur.

Ajit Kumar Sinha

CONTENTS

Page

Page

LIST OF TABLES

LIST OF FIGURES

SYNOPSIS

STUDIES OF EQUATORIAL AND POLAR LIGHT CHARGED PARTICLES EMITTED IN NUCLEAR FISSION AND DETERMINATION OF SCISSION CONFIGURATION

AJIT KUMAR SINHA
Ph.D.
Department of Physics
Indian Institute of Technology, Kanpur
September 1981

Nuclear fission is one of the important manifestations of large scale collective motion of nucleons involving a complicated interplay between the single particle and collective degrees of freedom. Inspite of nearly four decades of extensive investigations, an unified description of this process has not as yet emerged which is able to command general acceptance.

The observed distributions in mass, charge, spin, kinetic energy and excitation energy etc. of the fission fragments depend sensitively upon the motion of the fissioning nucleus from the saddle point to the scission point. The initial conditions of such a motion are believed to be set at the saddle point. Various fission theories follow this motion under different assumptions regarding the coupling strengths among the particle and collective degrees of freedom.

Studies in the light charged particle (LCP) accompanied fission (LCPF) bear a strong potential of probing the scission point configuration. In addition, it is believed that some characteristics of the LCPs such as the dependence of their yield on the excitation energy of the compound nucleus may

reflect the saddle point effects.

The LCPs observed in LCPF have been categorized as the equatorial LCPs and the polar LCPs. The former are emitted preferentially at right angles to the fission axis while the latter are emitted preferentially along the fission axis. Equatorial LCPs are believed to be emitted from the neck region at the scission point while situation in the case of the polar LCPs is ambiguous. Due to extremely low probability of polar emission, the experimental study of this mode of fission is quite difficult. More experimental information comparing the characteristics of the equatorial and the polar LCPs will be helpful for a clearer understanding of the mechanism of the polar emission.

The first part of the present thesis aims at studying some of the characteristics of the equatorial and polar LCPs in the neutron induced fission of ^{235}U upon a change in the excitation energy of the compound nucleus. The experiment was done for thermal and 600 keV neutron energies. Such a range of neutron energy was chosen in view of the earlier observation of the variation in the LCP yield with neutron energy in the keV neutron induced fission of ^{235}U. The experiment was done by using a novel geometry providing a simultaneous detection of the polar and equatorial LCPs and permitting use of large area fission source without sacrificing the angular resolution. Such a simultaneous measurement of the equatorial and polar emissions provides a mutual comparison of the two

processes and it is expected to provide a clue to the mechanism of the polar emission. To the best of our knowledge, such a study for the polar LCPs has been done for the first time.

The second part of the thesis concerns with the determination of the scission point configuration by using the method of trajectory calculations. The calculations have been performed under point charge approximation utilizing some recently studied correlations in the alpha-particle accompanied fission. Improvements have been made in the method by incorporating the nuclear forces and fragment deformations and effect of such improvements in the determination of scission point configuration has been investigated. Attempt has been made to see if we can explain the polar emission by incorporation of the nuclear interaction.

First chapter gives a short introduction to some important experimental and theoretical aspects of the fission process. Importance of an accurate knowledge of the scission point configuration has been brought out.

Chapter II summarizes the work done on the equatorial and the polar light charged particles (LCP) emitted in nuclear fission, with emphasis on the polar LCPs. Various models proposed for the polar and the equatorial LCPs are described. Need of further experiments is pointed out and motivation of the present experiment is presented.

The chapter III presents the details of the geometry used for the measurements of the polar and equatorial LCP

yields, the associated electronics and data recording arrangement, the data analysis, results and discussion. Monte Carlo method, used for calculating the detection efficiencies of the polar and equatorial LCPs and their possible intermixing in the process of identification has been described. The results show a variation in the yields of the polar and equatorial LCPs when the neutron energy changes from the thermal value to the 600 keV. These results have been discussed in the perspective of emission mechanism of polar LCPs.

Chapter IV introduces the method of trajectory calculations. The problems associated with the reconstructing of the scission point configuration by trajectory calculations are discussed and a survey of the earlier works has been presented.

Chapter V starts with the trajectory calculations performed by using the point charge model. The method used in this work allows a free variation of all the scission point parameters except for some restrictions on the interfragment distance. The calculations were done for different ranges of values of the interfragment distance attempting to test the validity of different models regarding the saddle to scission point motion. The results of such calculations are presented and it has been shown that by a proper choice of the range of interfragment distance one can explain nearly all the experimental correlations in alpha-particle accompanied fission including some recent results on the angular distribution of the alpha-particle as a function of the total

fragment kinetic energy. A relatively compact scission point configuration is favoured by these calculations.

Incorporation of the nuclear interaction among the alpha-particle and fragments and an approximate inclusion of the deformation of the fragments have been done in the trajectory calculations to see the effects of the approximations made in the point charge model calculations, especially in view of the compact scission point configuration predicted by this model. All the initial parameters describing the scission point configuration are permitted a free variation and selection of the initial phase space is done by using the experimentally studied correlations in the asymptotic values of the dynamical variables. Attempt is made to provide a proper time scale in the calculations so that the origin coincides with the actual scission point. The results obtained are presented and they indicate significant changes in the scission point configuration. Due to the presence of nuclear interaction, some of the alpha-particle trajectories are bent into the polar region. The results obtained for the polar alpha-particles are encouraging and show reasonable agreement with the experimental results in view of the sensitive dependence of the calculated characteristics of the polar alpha-particles to the parameters of the nuclear potential etc. The need for further improvements in the trajectory calculations, e.g. more realistic fragment deformations, their time dependence, the frictional forces in the nuclear interaction etc. are discussed.

Lastly, the chapter VI contains a brief summary of the results of the experimental work and their interpretation and the results of the trajectory calculations.

CHAPTER I

NUCLEAR FISSION

1.1 Experimental Aspects

The nuclear fission is a type of nuclear reaction that results in the splitting of a nucleus into atleast two comparable parts. It was first identified by Hahn and Strassman[1] after a series of radiochemical studies of neutron induced reaction in uranium. Nuclear fission is a very complex nuclear reaction. Inspite of very extensive theoretical and experimental investigations, an unified picture of the fission process has not emerged.

An isolated nucleus with a given excitation energy may decay via various channels like γ-emission, nucleon or nucleon cluster emission, β-emission or fission. The fission mode of decay assume significant probability relative to the other modes for heavy nuclei or for highly excited nuclei. Light nuclei, viz. gold, bismuth etc., are observed to decay significantly by the fission mode at high excitation energy while fission even with zero excitation energy (termed as spontaneous fission) occurs for heavy nuclei ($A > 230$). Spontaneous fission enjoys an unique position towards understanding the fission phenomenon as in this, the initial state of the fissioning nucleus is a pure quantum state and known accurately. A fissioning excited nucleus can be produced by several

methods, such as, by absorption of nucleons(p or n)[2-3], nuclei (^{2}H, ^{4}He etc.)[4], photons[5], by partial absorption like in a direct reaction (d,pf)[6] or by inelastic collision ($\alpha,\alpha'f$)[7]. Excitation may also be imparted by a fast changing electromagnetic field (Coulomb excitation) like in electron induced fission[8] or muon induced fission[9]. These different modes of formation of the excited nucleus essentially produce their characteristic population densities of different excited states in the nucleus.

1.1A Different Modes of Fission

A nucleus, undergoing fission, most predominantly divides into two nuclei of comparable masses. This mode of fission of a nucleus is called the binary fission. Possibility of a division into three (or even more) comparable parts exists. Such a mode of fission is very rare and has not been studied extensively[10] and we shall not be discussing it any further. Another interesting mode of fission has been studied in which a light charged particle (like ^{1}H, ^{2}H, ^{3}H, ^{4}He, ^{6}He etc.) is produced in addition to the two heavier nuclei. In the following we shall discuss some of the experimental characteristics of the binary fission and the light charged particle accompanied fission.

(i) Binary Fission

A fissioning nucleus undergoes large deformations

before reaching the scission point, a stage in the fission process when division of the nucleus is complete with negligible nuclear interaction remaining between the resulting parts. The nuclei formed at the scission point accelerate due to the mutual Coulomb repulsion and are called the primary fragments. The primary fragments are highly excited and neutron rich (Excitation Energy $\approx$ 30 MeV) and within a short time (10^{-19} sec), some neutrons are evaporated from them, which are known as prompt neutrons[11]. Some of the characteristics of the prompt neutrons[12] (e.g., the angular distribution with respect to the fragment direction) indicate that a part of them might have originated from the fissioning nucleus itself while it was on its way towards the split.

The nuclei formed after the emission of prompt neutrons are called fission fragments. These are unstable towards β^- emission and from stable isotopes, known as fission products, after a series of β^- transformations accompanied by the emission of the so called delayed γ-rays and the delayed neutrons. De-excitation of the primary fragments is also possible by prompt γ-emission, however, it becomes competitive with prompt neutron emission only when the excitation energy approaches a value near the neutron binding energy. On an average about 9 MeV of the excitation energy is disposed of by gamma ray emission. In addition, γ-rays take away a large part of the fragment angular momentum as indicated by the large anisotropies in the gamma ray angular distribution

with respect to the fragments[13].

Sharing of the nucleons among the fission fragments is a topic of immense theoretical interest and has been studied rather extensively. Nucleon distributions (viz., proton distribution, neutron distribution or their combined distribution) in nuclear fission has been studied by several methods like radiochemical analysis[15], simultaneous velocity or energy measurements of the two fragments[16-18], study of the X-rays and the γ-rays from the fragments[18], mass spectroscopy of the fragments[19], the ΔE-E method using gas filled ionization chamber[20] etc. At low energies, the most probable mode of division for nuclei with $A > 229$ is the asymmetric mode in which the fragments possess unequal numbers of nucleons. Consequently the mass distribution shows two humps corresponding to the light and the heavy groups of the fragments. For lighter nuclei (with $Z < 83$), mass distribution is single peaked indicating a dominant symmetric mode. For intermediate nuclei (like Ra, Ac) mass distribution is triple humped. A similar behaviour with increasing preference for symmetric division is indicated in the mass distribution of very heavy nuclei like francium[21]. However, as the excitation energy is increased, the symmetric mode becomes relatively more and more prominent in all studied cases. The yield distributions of the isobars and the isotones produced in the fission process have been studied by several workers[19]. Isobars with even atomic number are found to be relatively more abundant as

compared to those with odd atomic numbers. Distribution of mass has been studied more extensively as compared to the distribution of protons (charge distribution) and the distribution of neutrons. Attempts have been made to study the proton and neutron distributions and look for systematic trends which might be reflected more clearly in their separate distributions rather than in their combined distribution, viz., the mass distribution.

Kinetic energy[22] of the fission fragments has been of great interest for understanding the fission process. The observed kinetic energy is contributed mainly by the potential energy of Coulomb interaction between the fragments just after the scission, except for a small contribution due to their initial kinetic energy at the scission point. Knowledge of the latter contribution plays an important role in the understanding of the fission phenomenon.

A lot of work is devoted in studying the correlations among the various characteristics of the fission fragments (mass and energy), the prompt neutrons and the prompt γ-rays produced in the binary fission.

In addition, angular distribution[23] of the fragments relative to the direction of the particle inducing the fission has been studied for many nuclei. Such a study essentially provides experimental informations regarding the population of the excited levels in the fissioning nucleus and dynamical aspects of the fission process.

(ii) Light Charged Particle Accompanied Fission (LCPF)

In LCPF[27], the nucleus splits into two nuclei of comparable masses and an additional light charged particle (LCP), e.g. p, d, ^{3}H, ^{4}He, ^{6}He etc., ^{4}He being the most frequently emitted LCP.

No drastic difference has been noted in the mass and the kinetic energy distributions of the fragments in the LCPF and binary fission. The observed difference is accountable by considerations of the mass and the kinetic energy taken away by the LCP. This result points to the essential similarity of the two processes.

Angular distributions of the LCP's with respect to the fragments, which is found to be sharply peaked nearly at right angles to the fission axis, quite definitively indicate that they are produced in the neck region nearly contemporaneous to the scission moment. Energy distribution of the LCP together with its intercorrelations with the angular distribution and the fragment mass and energy have been exploited by the method of trajectory calculations for finding out the scission point configuration in LCPF, which as indicated earlier, should closely resemble the scission configuration in binary fission.

Studies of the prompt neutrons from the fragments in LCPF have indicated that the fragment excitation energy is less as compared to that in binary fission. In addition, the shift in mass distribution in LCPF from that in binary

fission corresponds to the light fragment side in near symmetric region and heavy fragment side in the asymmetric region. The primary fragments corresponding to these mass regions are highly deformed at the scission point as indicated by the average number of prompt neutrons emitted from them. This point may be taken to relate the origin of LCP-emission with the fragment of larger deformation.

The LCP's discussed so far are the ones emitted preferentially along a direction nearly at right angles to the fission axis and are called the equatorial LCP's. While studying the angular distribution of the LCP's, Piasecki et al.[24] discovered that the yield of the LCP per unit solid angle shows a rising tendency in the fragment direction contrary to a monotonous decrease as anticipated from the angular distribution of the equatorial LCP's. These LCP's, which show a preference towards emission along the fission axis, are called the polar LCPs. The emission probability of the polar LCPs is found to be more towards the light fragments than the heavy fragments. The fragment mass and kinetic energy distributions in the polar LCP accompanied fission exhibit[25] characteristics similar to that in the binary fission or equatorial LCPF. Experimental characteristics of the polar LCPs, unlike the case of the equatorial LCPs, do not provide any unambiguous picture of the origin of the polar LCPs.

1.2 Theories of Nuclear Fission

Promptly after the discovery of nuclear fission, Meitner and Frisch[26] suggested that the liquid drop model (LDM) of the nucleus provides a natural explanation for it. Shortly afterward Bohr and Wheeler[27] provided a more quantitative description of the fission process using the liquid drop model. According to this model, the fissility parameter $x = (Z^2/A)$ decides the stability of the nucleus towards shape vibrations. It was found that for values of x less than a critical value, there exists a potential energy barrier towards fission, which is higher for lower values of x. Calculations of the potential energy of deformation based on LDM indicated a value larger than that obtained from the experimental data for the barrier height. In addition, the model favours symmetric mode of fission in contradiction to the experimental results on the fission of the actinides. The incorporation of the shell effects in the simple liquid drop model was recognised as a possible remedy. Several experimental findings (i.e., no shift in the position of the heavy fragment peak in the mass distributions for different actinide nuclei etc.) indicated the presence of shell effects.

Strutinsky[28] provided a framework for incorporation of the shell effects in the calculation of the potential energy of deformation. His method consists of adding to the liquid drop energy a deformation dependent shell

correction. Nilsson model[29] was used to calculate the single particle energy levels in the deformed nucleus. A smeared level density was obtained by averaging the calculated single particle level densities over a large energy interval ($\sim$ 8 MeV) so as to wash out the shell effects. The difference of the total energy of the nucleus obtained by the use of single particle level density from that calculated by using the smeared level density was used for the correction to the LDM potential energy.

A typical potential energy curve as a function of the deformation for an actinide nuclei is shown in Fig. 1.1. Shell corrected potential energy curve shows a double humped structure to be contrasted from the curve based upon the LDM also shown in the figure. Such a curve is obtained from a map of the potential energy of deformation calculated for a set of deformation parameters. The curve shown in the Fig. 1.1 reflects the variation in the potential energy along a contour in the multidimensional space of the deformation parameters, chosen in such a way that for all points on the contour there is a minima in the potential energy along the directions at right angle to the contour. A maxima thus obtained by climbing a hill along a trenched path, is called a saddle point and as suggested by A. Bohr[31] in his channel theory of fission plays a very significant role in the fission process. Angular distribution of the fission fragments in particle induced fission and the existence of sharp fission

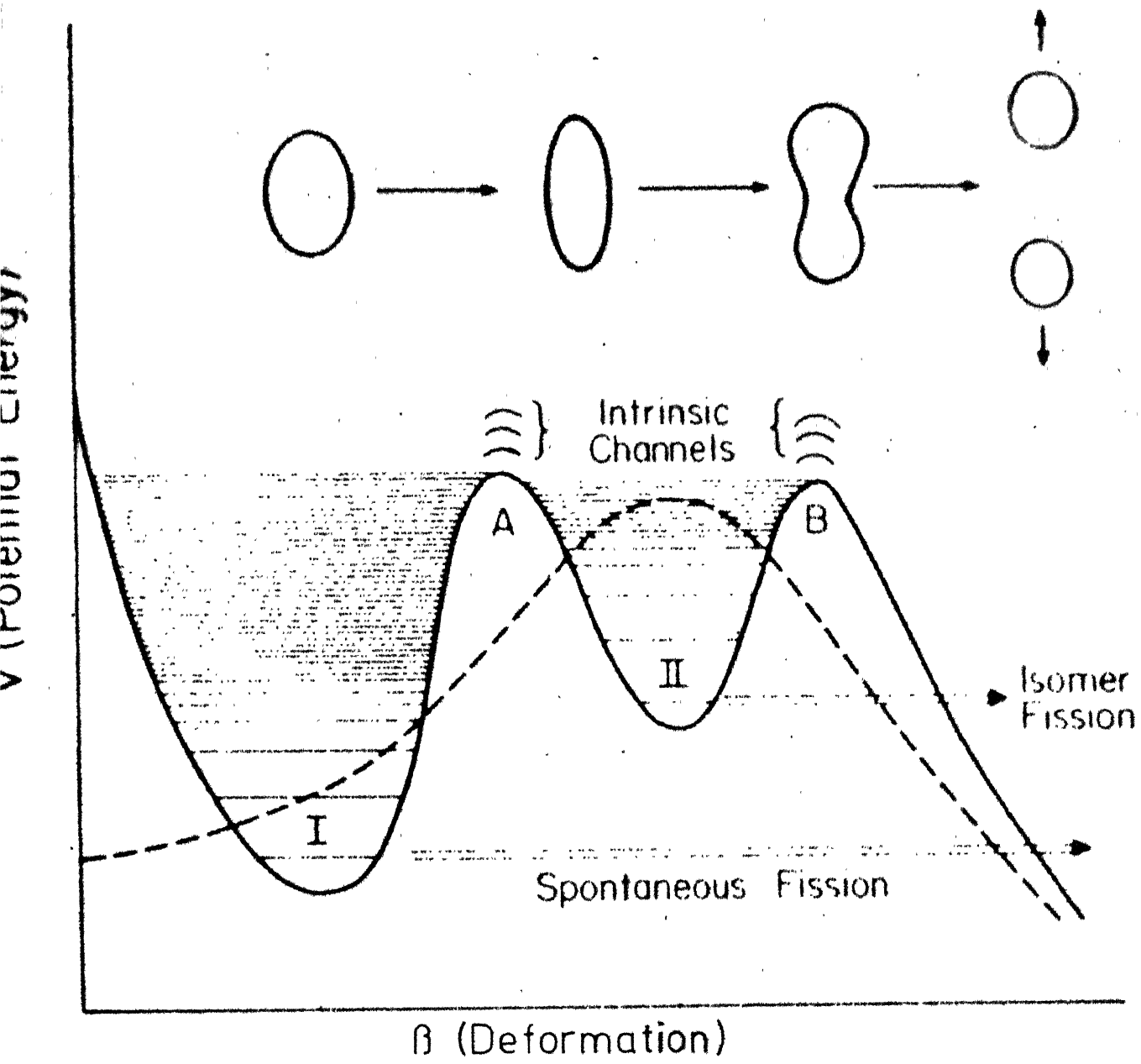

Fig. 1.1. Schematic illustrations of single-humped (---) and double-humped (——) fission barriers. Intrinsic excitations in the first and second wells are designated class I and class II states, respectively. Intrinsic channels at the two barriers are also illustrated. The transition in the shape of the nucleus as a function of deformation is schematically represented in the upper part of the figure. After Vandenbosch and Huizenga, [30]

resonances in slow neutron induced fission of odd-N nuclei have been successfully explained by the consideration of the saddle point quantum states. In such fission reactions, a large fraction of the excitation energy of the nucleus goes into the deformation energy at the saddle, leaving the nucleus cold. The level structure at the saddle point should resemble that of heavy nuclei with ground state deformation and thus are widely spaced at low excitation. This accounts for the observed sharp fission resonances. Angular distribution data are explained by considering the saddle wavefunction and assuming the conservation of the angular momentum about the nuclear symmetry axis during the motion from the saddle point to the scission point. Correlation of the odd parity states at saddle point with the observed mass asymmetry has also been suggested based on certain observations regarding the peak to valley ratio of the mass distribution in the keV-neutron induced fission of ^{235}U, ^{239}Pu etc.[32]. Evidence of the saddle point effects on the light charged particle characteristics in LCPF induced by the keV-neutrons has also been suggested[33].

Motion of the nucleus from the saddle point configuration to the scission stage is considered to play a crucial role in deciding various characteristics of the fission. As the nucleus proceeds saddle point onwards, the energy latent in the deformation becomes available to the other degrees of freedom corresponding to the collective motion and the particle motion. The coupling of the fission degree of freedom (which

corresponds to a collective motion in which the imminent fragments move apart) to the other collective and particle degrees of freedom is a point of debate among the various fission models. The adiabatic model assumes this coupling to be very weak and accordingly the released deformation energy should appear solely as the kinetic energy of the translation of the imminent fragments. On the other hand, the statistical model takes a strong coupling among all the degrees of freedom and assumes that the nucleus remains in a state of quasi-equilibrium throughout its descent till the scission point. Thus the fragments are supposed to possess comparatively small kinetic energies at the scission point. Some fission models (like Norenberg's[34]) take an intermediate stand and assume the coupling to be strong enough to have statistical equilibrium among the various collective degrees of freedom only. Norenberg further assumes that coupling between the collective and the particle degrees of motion becomes strong the moment the energy of the collective motion exceeds the energy needed for breaking a nucleon-pair. This model has met several successes and is being explored further.

Predictions regarding the various characteristics, such as the mass and the kinetic energy distributions of the fragments are made by either following the motion of the nucleus from the saddle to the scission point by solving the relevant equations of motion (the dynamical treatment[35]) or under the statistical model assumption by concentrating upon the scission point configuration (the statistical treatment[36]).

1.2A The Dynamical Treatment

In the dynamical treatment one considers the motion of the nucleus from the saddle point to the scission point by a suitable parameterisation of the shape of the nucleus and solves the relevant equations of motion to predict the shape of the nucleus at the scission point. The dynamical model assumes a complete statistical equilibrium in the distorting nucleus till the saddle point as this stage in the fission process is supposed to be veryslow ($\approx 10^{-15}$ Sec.) in comparison to the characteristic nuclear time ($\approx 10^{-21}$ Sec.). At saddle point, the energy is distributed among the various dynamical variables as given by the laws of statistical mechanics. A Monte Carlo technique is used to calculate the distributions in the values of the dynamical variables at the scission point by solving the equations of motions starting from the distributions at the saddle point. From these distributions, the mass, kinetic energy, excitation energy distributions can be calculated.

A knowledge of the various inertial parameters and nuclear viscosities for different collective degrees of motion (which determine the coupling between the collective and the particle degrees of freedom) and their dependence upon the nuclear deformation and temperature as well as an accurate potential energy map over the deformation space is essential for a successful dynamical calculation. A lot of present research[37] is devoted to achieve this information.

In addition, a versatile shape parameterisation is also required[38].

Initial dynamical calculations[35] with some simplying assumptions have not met much success and thus highlighted the need of more accurate knowledge of the various quantities used in the calculations.

Recent calculations[37] of the deformation energy curve for some actinide nuclei indicate that near the deformation corresponding to the second saddle, the nucleus becomes unstable towards mass asymmetric deformations. Thus a possibility of two nearly parallel barriers beyond the second saddle point has been suggested one leading to a preferential symmetric mass division while the other leading to a preferential asymmetric mass division. This concept of two modes of the fission decay has received considerable attention lately and some experimental evidence in its support has been suggested[27].

1.2B The Statistical Treatment

Under the perview of the statistical model, Fong[36] has developed an approach for predicting various fission characteristics. At any instant, during the descent of the nucleus from the saddle to the scission point, the assumption of the statistical equilibrium permits a determination of the configuration of the nucleus at that instant. Thus the scission

point configuration is determined by statistical methods without necessitating the solution of the equations of motion. For such a calculation, an accurate information of various nuclear properties like the energy level densities at various excitation energies and deformations for relevant nuclides, the ground state masses etc. is needed.

Due to comparative simplification arising due to the assumption of complete statistical equilibrium, the statistical approach provides a possibility of predicting a large number of fission characteristics, such as, the asymmetry in mass distribution for actinide fission, dependence of the total fragment kinetic energy and the prompt neutron yields from the fragments upon their masses, spins of the fragments, characteristics of the LCPF etc. Predictions thus made are in fair agreement with the experimental results and the remaining disagreements are, according to Fong, possibly due to inaccuracies in various nuclear data used in the calculations. However, inspite of a number of predictions of various fission characteristics in near agreement with experimental results (which provide an empirical support to the statistical approach), a conclusive fundamental justification for the statistical assumption is still awaited.

As indicated earlier, the motion from the saddle to the scission point may not be entirely adiabatic or entirely non-adiabatic. In fact, an entirely adiabatic motion will

tend to cause a fast tearing of the nucleus, resulting in a rapidly changing nuclear potential which may bring out particle excitations. This will imply a coupling with the particle degrees of freedom and thus invalidate a pure adiabatic model. Similarly, the strong coupling assumption of the statistical model will permit a slow saddle to scission point motion. But in such a slow motion, nucleons get enough time to rearrange to the lowest energy states which leads to a lowered value for inertial parameters. This may cause an acceleration in the descent of the nucleus making the statistical model assumption less valid. Thus motion from saddle to scission point may seem to alternate between slow and fast stages and exact picture is not clear.

An accurate information on the geometric and the dynamic configuration of the scission point seems crucial in ascertaining the validity of assumptions underlying different fission theories.

The phenomenon of light charged particle emission has been identified as an unique tool for determining scission configuration. Their characteristics are also expected to depend upon the saddle point configuration. A theoretical and experimental analysis of various characteristics of the LCPs bears a strong potential for testing various fission theories.

Among the LCPs, two different catagories namely equatorial and polar LCPs have been found, characterised by

their angles of emission relative to the fragment direction. Motivation of our work was to study the dependence of some characteristics of the two types of LCPs on the saddle point configuration and to look for a clue so as to understand the mechanism of the polar LCP emission.

In addition, attempt has been made to reconstruct the scission point configuration by the method of the trajectory calculations. Possibility of explaining the polar emission by trajectory calculation is also explored.

REFERENCES

1. O. Hahn and F. Strassman, Naturwissenschaften 26 (1938) 755
2. G.L. Bate and J.R. Huizenga, Phys. Rev. 133, B (1964) 1333
3. J.E. Simmons and R.L. Henkel, Phys. Rev. 120 (1960) 198
4. J.R. Huizenga, In 'Nuclear Structure and Electromagnetic Interactions' (N. MacDonald, ed.), Oliver and Boyd, Edinburgh, p. 319
5. A.P. Baerg, R.M. Bartholomew, F. Brown, L. Katz and S.B. Kowalski, Canadian J. of Phys. 37 (1959) 1418
6. H.C. Britt, W.R. Gribbs, J.J. Griffin, R.H. Stokes, Phys. Rev. 139, B (1965) 354
7. B.D. Wilkins, J.P. Unik and J.R. Huizenga, Phys. Lett. 12 (1964) 243
8. J.D.T. Arruda Neto, S.B. Herdade and I.C. Nascimento, Nucl. Phys. A334 (1980) 297
9. J.A. Maruhn, V.E. Oberacker, V. Maruhn - Rezwani, Phys. Rev. Lett. 44 (1980) 1576
10. R. Vandenbosch, J.R. Huizenga,"Nuclear Fission",, Academic Press, New York and London (1973) p. 400
11. H.R. Bowman, S.G. Thompson, J.C.D. Milton, W.J. Swiatecki, Phys. Rev. 126 (1962) 2120
12. R. Govil and R.K. Choudhury, J. Phys. G : Nucl. Phys. 7 (1981) 59

13. V.S. Ramamurthy, R.K. Choudhury and J.C. Mohana Krishna, Pramana 9 (1977) 623

14. A.C. Wahl, A.E. Norris, Proc. of Symp. on Physics and Chemistry of Fission (Vienna, 1969) IAEA, Vienna (1969) p. 51

15. J.C.D. Milton and J.S. Fraser, Can. J. Phys. 40 (1962) 1626

16. S.L. Whetstone, Jr., Phys. Rev. 131 (1963) 1232

17. H. Bowman and S.G. Thompson, Proc. of the Second United Nations Conference on the Peaceful Uses of Atomic Energy, Geneva (1958) p. 652

18. W. Reisdrof, J.P. Unik, H.C. Griffin and L.E. Glendenin, Nucl. Phys. A177(1971) 337

19. W. Lang, H.-G. Clerc, H.Wohlfarth, H. Schrader and K.-H. Schmidt, Nucl. Phys. A345 (1980) 34

20. G. Mariolopoulos, J.P. Bocquet, R. Brissot, H. Nifenecker, Ch. Ristori, A. Pequet, J. Girard, Nucl. Instr. and Meth. 180 (1981) 141

21. J.P. Balagna, G.P. Ford, D.C. Hoffman and J.D. Knight, Phys. Rev. Lett. 26 (1971) 145

22 J.P. Unik, J.E. Gindler, L.E. Glendenin, K.F. Flynn, A. Gorski, R.K. Sjoblom, Proc. of Symp. on Physics and Chemistry of Fission (Rochester, 1973), IAEA, Vienna,(1974) Vol. II, p. 19

23. R. Vandenbosch and J.R. Huizenga,"Nuclear Fission", Academic Press, New York and London (1973) p. 109

24. E. Piasecki, M. Dakowski, T. Krogulski, J. Tys, J. Chwaszczewska, Phys. Lett. 33B (1970) 568

25. E. Piasecki and L. Nowicki, Proc. of Sym. of Physics and Chemistry of Fission (Jülich, 1979), IAEA, Vienna (1979) p. 193

26. L. Meitner and O.R. Frisch, Nature (London) 143 (1939) 239

27. N. Bohr and J.A. Wheeler, Phys. Rev. 56 (1939) 426

28. V.M. Strutinsky, Nucl. Phys. A95 (1967) 420

29. S.G. Nilsson, Kgl. Dan. Vidensk. Selsk. Mat. Fys. Medd. 29, No. 16 (1955)

30. R. Vandenbosch and J.R. Huizenga,"Nuclear Fission", Academic Press, New York and London (1973) p. 97

31. A. Bohr, Proc. Int. Conf. on Peaceful Uses of Atomic Energy, (Geneva, 1956), United Nations, New York, 2, p. 151

32. L. Wilets and D.M. Chase, Phys. Rev. 103 (1956) 1296

33. B. krishnarajulu, S. Sen and G.K. Mehta, J. Phys. G : Nucl. Phys. 5 (1979) 319

34. W. Nörenberg, Proc. of Sym. on Physics and Chemistry of Fission (Vienna, 1969), IAEA, Vienna (1969) p. 51

35. J.R. Nix, Nucl. Phys. A130 (1969) 241; R.W. Hasse, Nucl. Phys. A128(1969) 609

36. P. Fong, Statistical Theory of Nuclear Fission, Gordon and Breach, New York (1969)

37. H.C. Britt, Proc. of Symp. on Physics and Chemistry of Fission (Jülich, 1979), IAEA, Vienna (1980) p. 3;
S. Bjørnholm and J.E. Lynn, Review of Modern Physics, 52 (1980) No. 4

38. S. Trentalange, S.E. Koonin, A.J. Sierk, Phys. Rev. C22 (1980) 1159

CHAPTER II

LIGHT CHARGED PARTICLE ACCOMPANIED FISSION

2.1 Equatorial Light Charged Particle Accompanied Fission

The phenomenon of emission of light charged particle (specifically, α-particle) in nuclear fission was first observed by Alvarez in 1943 (quoted from Farwell et al.[1]). However, published account of this phenomenon was given by Tsien[2]. Light charged particle accompanied fission (conventionally called as ternary fission) occurs once in about 300-500 normal fission events. The direction of emission of the particle was found to be preferentially at right angles to the direction of motion of the fission fragments (the adjective 'equatorial' is added to differentiate from comparatively small but significant number of 'polar' light charged particles which are found to be emitted preferentially along the fragment direction). This fact led to the belief that these particles are emitted close to the scission point in between the two fragments. Thus, this particular mode of fission was recognised as a potential probe for investigating the scission point configuration.

Besides the α-particles, which are most dominantly emitted, emission of other light charged particles (LCP) in fission such as the isotopes of hydrogen, other isotopes of

helium and some heavier isotopes (viz., those of lithium, berrylium, boron, carbon, nitrogen etc.) have been reported. As the α-particles form nearly 90 %. of all the LCPs, α-particle accompanied fission has been studied more extensively compared to the fission with the emission of other LCPs.

Relative probabilities of emissions of some of these particles in the spontaneous fission of ^{252}Cf and thermal neutron induced fission of ^{235}U along with the values of mean and full width at half maximum of their energy and angular distributions are presented in Table 2.1. The angle of emission of LCP is found to depend upon its energy and the mass ratio and kinetic energy of the fragments. Various investigations with multiparameter data acquisition systems have been carried out to study the energy - angle correlations in ternary fission. The average kinetic energy of the α-particles as a function of its angle of emission displays a minimum around the most probable angle[4]. The angular distribution of the α-particle becomes wider, with mild variations in the most probable angle of emission, as the kinetic energy of the α-particles increases[5]. The angular distribution of the α-particles is also seen to depend upon the fragment kinetic energy, being broader for lower values of the kinetic energy[4]. Mean angle of emission of α-particles with respect to the light fragment is found to decrease with the fragment mass ratio[4]. Average kinetic energy of the fragments decreases as a function of the

Table 2.1

Relative probabilities of emission and values of mean and full width at half maximum (FWHM) of the energy and angular distributions of equatorial light charged particles emitted in nuclear fission.

Light Charged Particle	Fissioning Nucleus	Yield (extrapolated per 100 α-particles	Energy Distribution		Angular Distribution with respect to light fragment	
			Mean (MeV)	FWHM (MeV)	Mean (in deg.)	FWHM (in deg.)
Proton	$^{236}U^{*}$	1.02 ± 0.01 [a]	8.9 ± 0.2 [a]	5.9 ± 0.4 [a]	-	-
	^{252}Cf	1.6 ± 0.2 [c]	9 ± 2 [c]	6 ± 2 [c]	91 [e]	90 [e]
Deutron	$^{236}U^{*}$	0.6 ± 0.02 [a]	7.5 ± 0.3 [a]	6.6 ± 0.6 [a]	-	-
	^{252}Cf	0.63 ± 0.03 [c]	7 ± 2 [c]	7 ± 1 [c]	91 [e]	66 [e]
Triton	$^{236}U^{*}$	6.67 ± 0.04 [a]	8.4 ± 0.1 [a]	6.7 ± 0.2 [a]	-	-
	^{252}Cf	5.9 ± 0.2 [c]	8.3 ± 0.5 [d]	7.0 ± 1.2 [d]	86.5 [d]	17 ± 1 [d]
^{4}He	$^{236}U^{*}$	100	16.0 ± 0.1 [a]	9.6 ± 0.2 [a]	81.5 ± 0.4 [b]	18.5 ± 0.8 [b]
	^{252}Cf	100	15.6 ± 0.5 [d]	11.2 ± 1.4 [d]	84.5 ± 0.5 [d]	17 ± 1 [d]
^{6}He	$^{236}U^{*}$	1.81 ± 0.02 [a]	12.2 ± 0.3 [a]	9.2 ± 0.6 [a]	-	-
	^{252}Cf	2.4 ± 0.5 [c]	12.5 ± 0.7 [d]	9.0 ± 1.0 [d]	86.0 ± 1 [d]	13 ± 3 [d]

i) Alpha-particle yield is taken as 100
ii) $^{236}U^{*}$ is formed by thermal neutron capture by ^{235}U
iii) Angular distribution data for proton and deuteron are obtained without distinguishing between light and heavy fragments
iv) a - [3]; b - [4]; c - [5] ; d - [6]; e - [7].

α-particle energy almost linearly[8]. In addition, several other correlations among energy-angle observables have been studied in the α-particle accompanied fission. Studies for other LCPs also indicate similar behaviour[6]. These data provide important input to the method of trajectory calculations employed for obtaining the configuration of the fissioning nucleus at the instant of LCP emission. A comparison of the characteristics of the alpha-particle accompanied fission and binary fission indicates that the scission configurations of the nucleus corresponding to these two modes of fission resemble each other closely. Thus the trajectory calculations provide informations relevant to the study of binary fission.

Kinetic energy and mass distributions of the fragments in the ternary fission with LCPs; protons, tritons and α-particles, have been measured[8-10]. The distributions in the kinetic energy of the fragments in the α-particle accompanied fission and binary fission are found to be nearly identical if an account is taken of the kinetic energy taken away by the α-particle. The observed fragment mass distribution in α-particle accompanied fission shows features very similar to those observed in the binary fission. When normalised to the same height, the lighter sides of both light and heavy peaks nearly overlap while their heavier sides are displaced relative to each other by ≈ 4 mass units. A similar trend is seen for the triton accompanied fission.

However, no unique information is derivable from these mass distributions as regards the dependence of the emission probability of LCP upon the fragment mass due to absence of any information of the relative nucleon contributions from the two fragments to the LCP. This point, as discussed by Halpern[11], prohibits an assessment of the one step or the two nature of the LCP accompanied fission on the basis of the fragment mass distributions. The mass distribution in the proton accompanied fission shows some distinctive feature as compared to the α-particle accompanied fission. The observed distribution shows a relative preference for the symmetric division and both the light and heavy peaks are shifted towards the symmetric valley. Another distinctive feature for the proton accompanied fission concerns with the comparatively very broad angular distribution of protons which is interpreted to imply a surface emission mechanism for these particles[12]. If we assume that the surface emission is realistic, the observed preference for the symmetric division appears qualitatively in the right direction as the symmetric division corresponds to comparatively more stretched scission configurationswith more surface area for emission(as indicated by a dip in the total kinetic energy in symmetric fragmentation).

The net energy release in the form of internal excitation and kinetic energy of the particles is about 2.5 MeV less in α-particle accompanied fission as compared to that in the binary fission. The internal excitation energy

is obtained from the average energy and number of prompt neutrons and γ-photons emitted from the fissioning nucleus and is a measure of the total 'deformation - excitation'' energy of the fragments at the scission point. A comparison of the internal excitation energy as a function of mass of fission fragments in the α-particle accompanied fission and binary fission indicates that the emission of α-particle occurs at the expense of energy of the fragments with high deformation - excitation energy.

The fall of ≈2.5 MeV in the total energy release in the α-particle accompanied fission in comparison to binary fission is less than that expected on the basis of the average separation energy of the α-particle of ≈ 5 MeV. This point has been suggested to indicate a preponderance of fragments with even number of protons or neutrons in α-particle accompanied fission which results in the release of additional energy in the form of the pairing energy. The observation that the energy for the α-particle emission dominantly comes from the fragment which has higher deformation - excitation energy forms the basis for the belief that the required energy for the emission of α-particle is imparted to it at the expense of the deformation energy of the fragments. Halpern[11] has suggested that this transfer of energy could occur due to a fast changing potential that will be seen by the α-particle due to a rapid snap and contraction of the protuberances of the nascent fragments. Rough calculations based on this sudden snap model of

Halpern have met partial success in explaining the relative yields of various light charged particles. However, no quantitative calculation on these lines exist. The pre-scission evaporation model proposed by Ramanna et al.[14] predict satisfactorily some characteristics of the light charged particles. However, a consideration of the energetics and the observed rather mild dependence of the light charged particle yield upon the excitation energy of the compound nucleus makes the evaporation mechanism as untenable for explaining the light charged particle accompanied fission. An earlier suggestion of alpha-emission from the heavy fragment shortly after scission by Feather[15] has been discarded on the basis of the prompt neutron yield data of Nardi et al.[16], as discussed in the review article by Feather[17]. Carjan[18] has advanced some arguments of qualitative nature in support of pre-scission emission of the α-particle based upon rather elaborate calculations performed for the α-particle cluster-formation probability over the surface of the nucleus near the scission stage[19]. However, further calculations providing a quantitative support to the theory have not been done.

Fong[20] has applied statistical theory for calculating the probability of α-particle emission. He arrives at a value for emission probability of α-particle in thermal neutron induced fission of ^{235}U in agreement with the experimental value. The calculated probability for the emission

depends sensitively upon the fragment excitation energy at the scission point. The observed decrease in the yield of prompt neutrons in α-particle accompanied fission as compared to binary fission is assumed to be entirely due to a loss in the excitation energy of the fragments at scission, the deformation energy being assumed to be nearly same in the α-particle accompanied fission and binary fission. Apart from this assumption, the calculation suffers from the uncertainties associated with various parameters it requires for evaluating the emission probability. In addition, calculations have not been done in the case of other light charged particle accompanied fission. Such calculations may provide a better test for the statistical model.

Efforts have been made to study the dependence of the characteristics of the light charged particle accompanied fission upon the excitation energy of the fissioning nucleus. In the range of excitation energy upto ≈ 20 MeV, a mild decrease in the yield of alpha-particle is observed while for still higher energy, the yield shows an increasing trend[21-24]. The results of such experiments are difficult to interpret as there is an admixture of the emissions from several nuclei at different excitation energies due to the occurence of second and higher chance fissions. Several workers have performed experiments with excitation energy below the threshold of the second chance fission for a clearer picture of the excitation energy dependence of the ternary fission probability. Results of Nadkarni et al.[25]

for the neutron induced fission of ^{235}U with neutron energy varied from 1 MeV to 4 MeV in steps of 1 MeV showed that the α-particle yield in ternary fission is nearly constant. In a subsequent work, Nadkarni et al.[26] found that the yield of LCPs with kinetic energy above 12 MeV remains constant while the yield of LCPs with energy below 12 MeV varied significantly for the neutron energy region of 0.75 MeV to 1.75 MeV. Fluss et al.[27] studied the yields of α-particle and tritium from neutron induced ternary fission of ^{235}U with neutron energy from thermal to 700 KeV. The alpha-particle yield was found to remain constant in contrast to a strong variation for the yield of tritons. Krishnarajulu et al.[28] studied the energy distribution and yield of the LCP at several neutron energies in the range from thermal to 1 MeV for the neutron induced ternary fission of ^{235}U and ^{239}Pu. The alpha-particle yield showed a mild structure in the neutron energy region around 200 KeV. They suggested that an explanation for the observed structure be sought in terms of properties (e.g., parity) of saddle point states of the fissioning nucleus. They also presented results for the tritium yield but the errors were large due to the difficulty in proper identification in the absence of the ΔE-E particle telescope. Sharma et al.[29] carried out extensive study of the yield of the protons, tritons and α-particles in the KeV neutron induced ternary fission of ^{235}U by employing a ΔE-E semiconductor telescope for particle identification. Their results confirm the findings

of Krishnarajulu et al.[28]. In addition, they found large increase in the yields of tritons and protons with neutron energy.

2.2 Polar Light Charged Particle Accompanied Fission

One of the most important characteristic of the equatorial light charged particles (LCP) in ternary fission concerns with their sharply peaked angular distribution with respect to the fission axis. This observation provides a crucial argument for assuming that the LCP-emission occurs from the neck region nearly contemporaneously with the scission point of the fissioning nucleus. The Coulomb repulsion due to the fragments is expected to prohibit the LCP to emerge in directions close to the fragment direction. However, several experiments[30-32] indicated that there may be some LCPs produced in fission which are emitted in directions very close to the fragment direction. Piasecki et al.[33] carried out systematic investigation in the thermal neutron induced fission of ^{235}U for these close angle emissions. Their experiment established the existence of the so called polar LCPs emitted close to the fragment direction. The result indicated even a possible increase in the α-particle intensity (yield per unit solid angle) for directions in close vicinity of the fission axis. The mechanism of emission of the polar LCPs appeared as yet another problem before a fission physicist. As compared to the case of equatorial LCPs, the experimental study of the polar LCPs

is quite difficult due to the lower probability of their emission (e.g., polar α-particle yield is about 1 % of yield of the equatorial α-particles). The uncertainties associated with the measurements on the polar LCPs as well as availability of only limited data on them make it difficult to assess the validity of various hypotheses advanced to interpret the polar LCP emission in fission.

2.2A Experimental Studies in Polar Emission

Observation of protons, tritons and α-particles in the polar direction has been reported[33-39] for thermal neutron induced fission of ^{233}U and ^{235}U, spontaneous fission of ^{252}Cf and in the fission of ^{238}U by 42 MeV protons. However, no definite statement can be made regarding the dependence of characteristics of the polar LCPs upon the fissioning nuclei. In addition, no experimental information† exists so far on the dependence of the characteristics of the polar LCPs upon the excitation energy of the fissioning nucleus. Such data concerning the characteristics of polar emission on parameters of fissioning nucleus could be very useful in understanding the mechanism of polar emission.

---

†Andreev et al.[36] studied the yield dependence of polar α-particles for the thermal neutron induced fission of ^{233}U and ^{235}U. They report that ratio of probability of normal ternary fission and polar LCP accompanied fission are nearly same for the two cases, while the absolute ternary fission probabilities are quite different.

(i) Angular Distribution, Intensity and Energy Distribution of Polar LCPs

Several workers have attempted to obtain information regarding the angular distribution of different polar LCPs. Due to the rarity of emission of polar LCPs, precise shape of their angular distribution is so far, not known.

Piasecki et al.[33] carried out a study of the angular distribution of α-particles over the entire range in the thermal neutron induced fission of ^{235}U. In the measurements for angles close to the fission axis, the angle between lines joining the centre of the fissile source to the centres of α-particle and fission detectors was 0°, however, a significant probability existed for the detection of α-particles emitted within $\pm 20^{\circ}$ from the fragment direction due to finite sizes of the detectors and the source. Angular detection efficiency curve was found to be peaked at about 12° with FWHM $\pm 16^{\circ}$. The angular distribution was reconstructed from the experimental yields at different angles by least squares method employing Monte Carlo technique. The reconstructed angular distribution (yield per unit solid angle) indicated a rise for directions in close vicinity (about 20°) of the fission axis. Adamov et al.[38] investigated the angular distribution of the polar LCPs using a semiconductor telescope for particle identification. Observed angular distribution showed a rise for extreme angles which was found to be larger for protons as compared

to that for α-particles.

Recently Caitucoli et al.[40] studied angular distribution of the α-particles in directions close to the fission axis. Their result indicates a mild increase in the yield for directions along the fission axis.

A determination of the intensity of polar LCPs calls for an appropriate definition of the polar LCPs. Piasecki et al.[41] suggested a border-line of $\approx 25^{\circ}$ for the angle of emission from fission axis for defining the polar LCPs based upon the shape of the observed angular distribution. In addition, derivation of intensity of polar LCPs from the experimental data demands a knowledge of their angular distributions due to finite experimental angular resolution. Using the angular distribution data obtained in Ref. 33, Piasecki et al.[41] estimated polar α-particle intensity as 5×10^{-3} of the equatorial α-particle in ^{235}U (n_{th},f). Relative intensities of the different polar LCPs also need be corrected for the effects due to differences in their angular distributions. It is found that the intensity of polar LCPs emitted towards the light fragment direction is different from intensity towards the heavy fragment direction, being lesser by a factor of 3-4 for the latter case. These data, though yet to be precisely known, provide useful informations for understanding the nature of polar emission. The available data on the intensity of various polar LCPs is summarised in Table 2.2.

Table 2.2

Experimental intensity ratios for polar light charged particles.

Particle	^{236}U polar emission Piasecki et al. [42]			P/E ratio*	^{252}Cf polar emission Nowicki et al. [43]		
	L-emission	H-emission	L/H ratio		L-emission	H-emission	L/H ratio
p	30.5±2(±0.6)	44.5±4(±1)	2.0±0.2	0.17±0.03	35±2(±1)	33±3(±1)	3.9±0.3
d	2.8±0.5(±0.6)	3.4±0.9(±0.7)	2.4±0.9	0.03±0.01	7.2±0.6(±1.5)	5.7±1.1(±1.2)	4.8±1
t	9.2±1.2(±0.9)	8.0±1.5(±0.8)	3.3±0.6	$(7.2\pm1.3)\times10^{-3}$	13±1(±2)	18±2(±3)	2.7±0.3
^4He	100	100	2.9±0.2	5×10^{-3}	100	100	3.8±0.2
^6He	0.06	0.2	-		0.05	0.2	-

L and H relate to emission along the light and heavy fragment trajectory respectively.
The errors given in the table are statistical ones and the estimated maximum systematic errors involved in particle identification are given in parentheses.

The α-particle intensity is assumed as 100.

*The P/E values were obtained basing on a 5×10^{-3} value for alphas.

After Piasecki et al. [41].

Energy distributions of the polar LCPs have been determined by various workers[33-41]. The mean energies of the polar LCPs are found to be higher as compared to the corresponding equatorial LCPs while their dispersions seem to be comparatively smaller. In addition, the mean energies seem to be nearly independent of the fragment mass. Table 2.3 lists the first two moments of their energy distributions. A knowledge of the dependence of the polar LCP kinetic energy on its angle of emission could be useful for testing hypotheses regarding polar emission, but such data are not available.

The kinetic energy of the fragments in polar LCP accompanied fission has been measured[36,42]. Average kinetic energy of fragments moving in the direction of polar α-particle is found to be less by about 15 MeV as compared to the corresponding value for the binary fission, while the decrease in the kinetic energy of the fragments moving opposite to polar LCPs is found to be much less ($\sim$ 2 MeV). Part of the decrease in kinetic energy of fragments in the direction of polar LCPs is due to the recoil effect, while the change in kinetic energy of the oppositely moving fragments is expected to be comparatively uneffected by such recoil effects and should provide a good probe for the scission configuration in the polar LCP accompanied fission.

Of interest is nearly linear fall in the kinetic energies of the polarly emitting fragments (that is, the

Table 2.3

Values of mean and standard deviation (in MeV) of the energy distributions of polar light charged particles.

Particle	Fissioning nucleus	Mean value		Dispersion		Reference
		L-emission	H-emission	L-emission	H-emission	
α	^{234}U	22.8±0.1	22.2±0.3	3.0±0.2	2.8±0.4	Andreev et al. [36]
	^{236}U	22.8±0.2	22.5±0.4	3.0±0.2	2.8±0.5	Andreev et al. [36]
	^{236}U	24.5±0.1	23.5±0.1	2.9±0.1	2.5±0.1	Piasecki et al. [42]
	^{252}Cf	25.5±0.1	24.8±0.1	3.4±0.1	2.7±0.1	Nowicki et al. [43]
t	^{236}U	15.3±0.2	13.6±0.3	2.7±0.2	2.0±0.2	Piasecki et al. [42]
	^{252}Cf	15.3±0.2	14.0±0.3	2.6±0.2	2.6±0.3	Nowicki et al. [43]
d	^{236}U	13.1±0.3	11.6±0.3			Piasecki et al. [42]
	^{252}Cf	13.6±0.2	12.8±0.5			Nowicki et al. [43]
p	^{236}U	11.2±0.1	11.2±0.2	2.5±0.2	2.8±0.3	Piasecki et al. [42]
	^{252}Cf	11.4±0.2	11.3±0.1	2.2±0.1	2.0±0.1	Nowicki et al. [43]

fragments moving in the direction of the polar LCP) with increasing mass of the polar LCP (Fig. 2.1). This observation seems to be related to a linear increase in the recoil with the mass of the polar LCP, which is expected on kinematic considerations. However, it is important to note that the effect of change of charge from ^{3}H to ^{4}He on fragment recoil is somehow getting annuled as there is not significant departure from the linear behaviour for this region.

Correlations between the kinetic energies of the polar LCPs and the fragments are not yet precisely determined. However, average LCP energy is found to be nearly independent of the total fragment kinetic energy. Average fragment energy as a function of the LCP-energy is not reported so far. Such an information will be interesting in view of the observed anticorrelation in the equatorial LCP accompanied fission which plays an important role in ascertaining the scission configuration.

Total kinetic energy released in polar LCP accompanied fission (sum of the kinetic energies of the LCP and fragments) is not much different from the kinetic energy released in binary fission. In the case of polar α-particle accompanied fission of ^{235}U by thermal neutrons, the net kinetic energy released exceeds the corresponding value for binary fission by about 3 MeV† while in the case of polar proton and triton

---

†Obtained from Ref. 42 after averaging for polar emissions along light and heavy fragments.

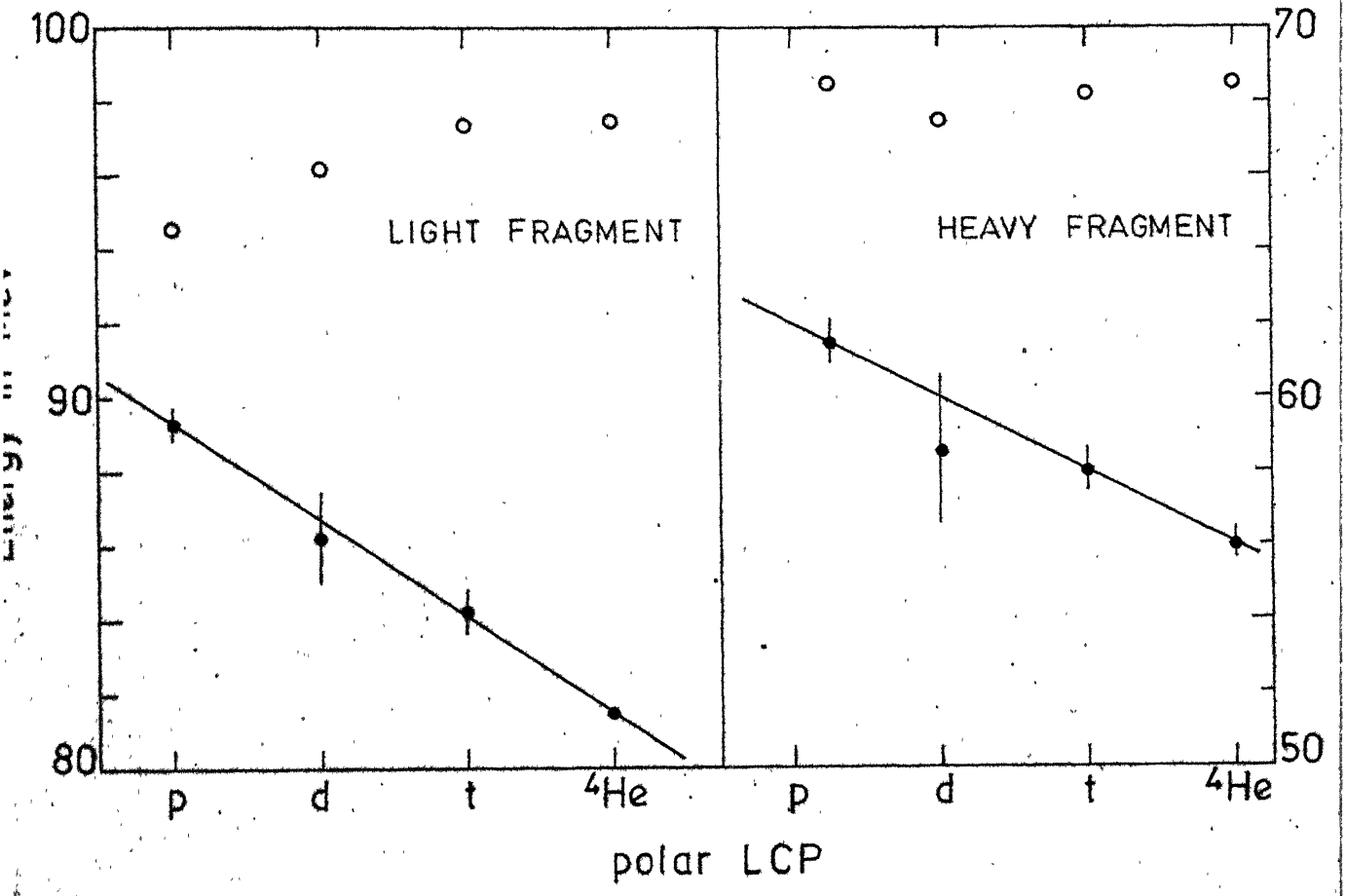

Fig. 2.1. Measured mean energies of light and heavy fragments moving along and opposite to the polar light charged particle (LCP) emitted in thermal neutron induced fission of ^{235}U. '●'- Corresponds to the fragments along the polar LCP while 'o'-corresponds to those moving in opposite direction. Lines are only visual fits. (Data taken from Piasecki et al.[42])

accompanied fission, it is lesser by about 2 MeV. These results are similar to those obtained for the equatorial LCP accompanied fission.

(ii) Fragment Mass Distribution in the Polar LCP Accompanied Fission

Fragment mass distribution in polar LCP accompanied fission has been determined for the thermal neutron induced fission of ^{233}U and ^{235}U and spontaneous fission of ^{252}Cf. Results on the thermal neutron induced fission of ^{235}U by Piasecki et al.[42] (and later confirmed by the work of Andreev et al.[36]) indicated a similarity in the mass distributions in the polar and equatorial LCP accompanied fission. Average masses of the light fragments moving along and opposite to the direction of polar α-particles is found to be lowered by about 2.5 amu and 0.7 amu respectively as compared to the corresponding value in binary fission. The corresponding shift in the light fragment mass is about 2 amu for the equatorial α-particle accompanied fission. However, if we consider all the fission events for which the α-particle is emitted along the fission axis within the polar cone, the average shift comes out to be 2.1 amu (obtained by a weighted average for the emissions along light and heavy fragments). This number is in good agreement with the shift observed for equatorial emission. For the proton accompanied fission of ^{235}U by thermal neutrons, a preference for the symmetric fission is revealed in both the polar emission

as well as in the equatorial emission.

Results of Nowicki et al.[43] for the polar α-particle accompanied spontaneous fission of ^{252}Cf indicate a very small decrease in the mean mass of light fragments as compared to the corresponding value for the binary fission. This result is in disagreement with the corresponding result for the equatorial α-particle accompanied fission of ^{252}Cf. However, their result for the polar proton accompanied spontaneous fission of ^{252}Cf indicates an increase of about 3.1 amu for the mean mass of light fragments (averaged for proton emission along and opposite to the fragment direction) in the polar emission which may be compared with value of about 3.2 amu obtained for equatorial proton accompanied spontaneous fission of ^{252}Cf.

2.2B Hypotheses on the Nature of Polar Emission

Unlike the case of equatorial LCPs, the characteristics of polar LCPs do not provide a clear indication of their origin and several models to explain their emission have been suggested. Several alternate assumptions can be made as to the place and time of their origin in the fission process. For example, these LCPs might have been produced in the neck region at about the scission moment and later due to appropriate turning provided by the nuclear attraction of the fragments, they may emerge in the polar direction. Or, they might by diffracted into the polar region, as the quantum mechanical effects may play a significant role

considering the de Broglie wavelength of the α-particle at the scission moment. Another possibility is that these LCPs are emitted from the poles of the fragments (ends of the imminent fragments away from the neck) at time close to the scission, the emission being made possible due to sudden retraction of the nuclear matter at the poles. Yet another mechanism for the emission of polar LCPs may be due to evaporation of the LCPs from the fragments. The evaporation of LCPs might be significant if the fragment excitation energy is large, as for lower excitation energies neutron evaporation will overshadow the LCP emission due to the absence of a Coulomb barrier for neutrons. The evaporation being a comparatively slower process will occur from fully accelerated fragments.

A large number of hypotheses thus seem possible which can qualitatively explain the emergence of LCPs in the polar direction and have been discussed in fair detail by Piasecki et al.[41].

One important question that seems relevant is whether the polar LCP accompanied fission is a three particle breakup process or a two step process with LCP emission occuring from one of the fragments after the binary division. In the later type of mechanism, contribution of nucleons for the LCP would be from the fragments moving along the direction of polar LCP (the possibility that polar LCP is emitted from the oppositely moving fragment is rejected as this would necessitate a very large kinetic energy of LCP at the

instant of emission). On the other hand, for the first type of mechanism, the nucleon contributions from the fragments to the LCP can not be precisely ascertained if the LCP is emitted from the neck region.

The only hypothesis which has been worked out in detail is the evaporation hypothesis[43,44] of the polar emission. This theory has met partial success in explaining some of the characteristics of polar LCPs, such as the relative intensities of different polar LCPs and energy spectra of some of the LCPs (it fails in case of the energy spectra of tritons as well as of polar α-particles emitted along the light fragments). The evaporation model permits a rather unambiguous prediction of the fragment mass distribution due to the assumed sequential nature of polar emission. Thus important test for the validity of evaporation hypothesis lies in the comparison of the predicted and experimental mass distributions for the polar LCP accompanied fission. Fig. 2.2 gives the required comparison. The observed disagreement seems difficult to be explained by the uncertainties associated with the evaporation calculations.

Apart from evaporation hypothesis, some calculations have been reported to test the validity of the hypotheses of nuclear orbitting of the LCPs in polar direction and quantum mechanical diffraction of LCP-wavepackets by the fragments. Calculations by Dakowski et al.[45] confirm that bending of the LCPs starting from the neck region due to nuclear attraction is possible with realistic values for

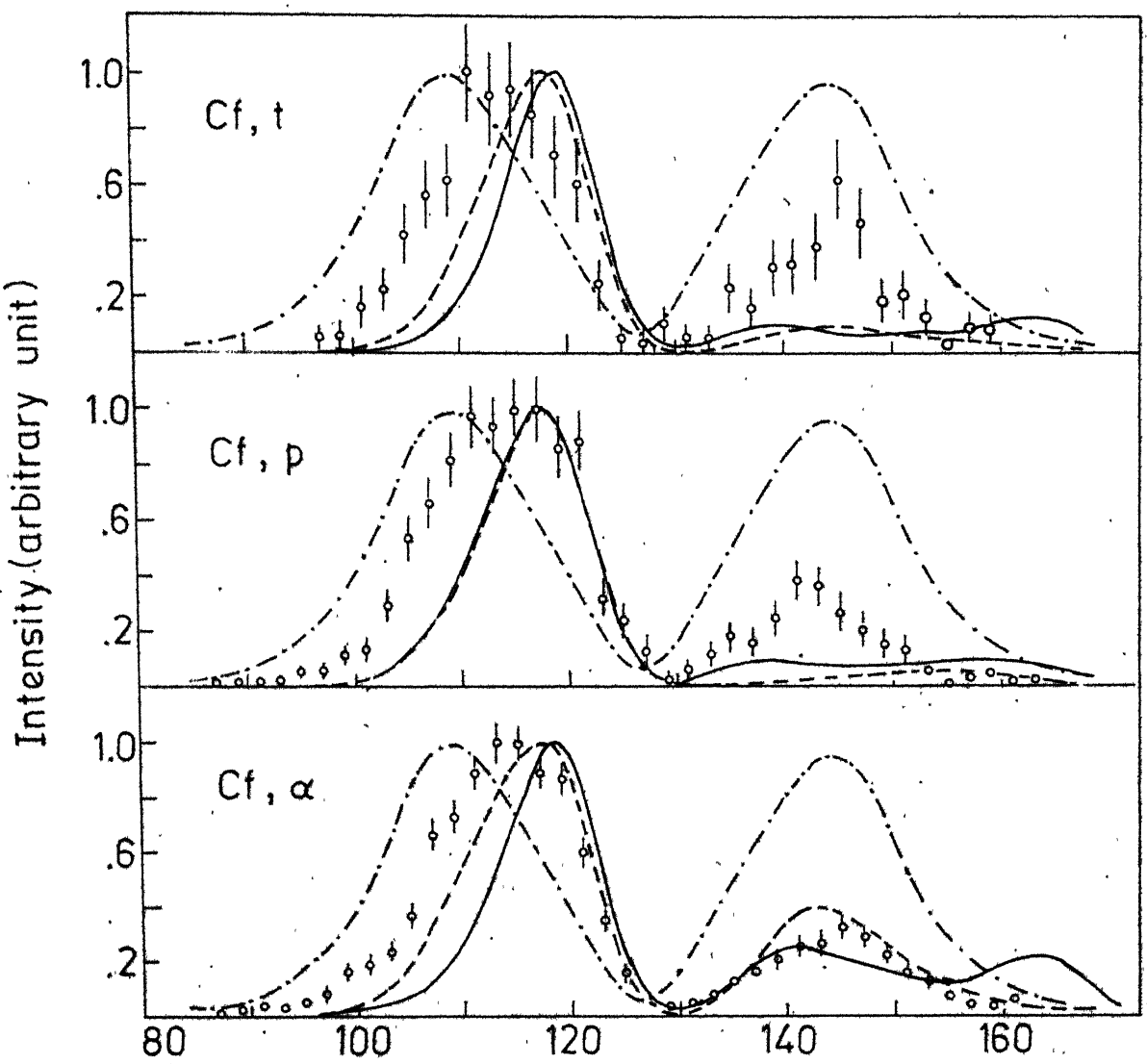

ig. 2.2. Comparison of the measured (shown by open circle) and calculated (pre-emission) mass distributions of the fragments moving along the polar LCP. The bipartition data are represented by dot-dashed line. The calculated curves are obtained by using various level density formulae employed in evaporation model calculations: Truran et al [47] (solid line) and Ignatyuk [48] (dashed line). After Piasecki et al [41].

the dynamical coordinates of the fragments and the LCP. They calculated the nuclear force between the α-particle and fragments by using the α-nucleus optical potential (real part) and considered the effect of inclusion of phenomenological friction term in calculating nuclear force. Fragment deformations at the scission point were considered. However, they conclude that a simultaneous reproduction of both the intensity and energy of the polar LCPs seems possible only if some dubious assumptions are made regarding the nuclear potential etc. Calculations on the quantum mechanical diffraction of LCPs are reported by Andreev et al.[36] and Kordyasz et al.[46]. Kordyasz has done calculations by assuming the fragments as stationary and of equal mass. Calculations indicate that the observed intensity ratio of the polar and the equatorial LCPs can be reproduced by such calculations. The calculated ratio of the polar and the equatorial intensities is found to be strongly dependent upon the scission point configuration. As such these calculations appear quite promising, however, detailed calculations with estimations of the effects due to various approximations made in solving the Schrödinger equation are not done.

Lastly, we shall mention yet another model for the polar emission which assumes a delayed emission of the LCP (the delayed tripartion model described in the review paper of Piasecki et al.[41]). Calculations have been performed to test this hypothesis[47]. These calculations with pure Coulomb force taken among the particles after LCP-emission

have, however, failed to explain the polar emission.

Thus we see that the present understanding of the phenomenon of polar emission is rather vague with a number of possible mechanisms prevailing. Experimental data on polar emission are limited. There is a need for more experimental data on the comparison of the characteristics of polar LCPs with those of comparatively well studied equatorial LCPs and on their dependence on the parameters of the fissioning nucleus. In the present work, we have attempted to study the dependence of the yields of polar LCPs emitted in the neutron induced fission on the neutron energy. Experiment has been done for the thermal and 0.6 MeV neutron energies. The experiment is devised to provide a simultaneous measurement on the equatorial LCP yields. The possible comparison between the changes in the yields of equatorial and polar LCP with neutron energy assumes significance as the experiments on equatorial LCPs have indicated significant variations in their yields in this neutron energy region.

13. I. Halpern, Proc. of Symp. on Physics and Chemistry of Fission, (Salzburg, 1965), IAEA, Vienna 2 (1965) p. 369

14. R. Ramanna, K.G. Nair and S.S. Kapoor, Phys. Rev. 129 (1963) 1350

15. N. Feather, Proc. of Royal Soc. of Edinburgh 66A (1964) 192

16. E. Nardi and Z. Fraenkel, Phys. Rev. Lett. 20 (1968) 1248

17. N. Feather, Proc. of Symp. on Physics and Chemistry of Fission, (Vienna, 1969), IAEA, Vienna (1969) p. 91

18. N. Carjan, Journ, de Phys. 37 (1976) 1279

19. N. Carjan, A. Sandulescu, V.V. Pashkevich, Phys. Rev. C11 (1975) 782

20. P. Fong, Phys. Rev. 102 (1956) 434

21. J.L. Coleman et al., Phys. Rev. 133 (1964) B 724

22. L.V. Draphinski, S.S. Kovalenkov, K.A. Petrzhak and I.I. Tyntyugin, Sov. J. At. Energy 16 (1964) 164

23. T.D. Thomas and S.L. Whetstone, Phys. Rev. 144 (1966) 1060

24. W.D. Loveland, A.W. Fairhall and I. Halpern, Phys. Rev. 163 (1967) 1315

25. D.M. Nadkarni and S.S. Kapoor, Proc. of Nucl. Phys. and Solid State Phys. Symp. (India) 13B

26. D.M. Nadkarni, R.K. Choudhury, P.N. Rama Rao and S.S. Kapoor, Proc. of Nucl. Phys. and Solid State Phys. Symp. (India) 18B (1975) 131

27. M.J. Fluss, N.D. Dudey and R.L. Malewicki, Phys. Rev. C6 (1972) 2252

28. B. Krishnarajulu, S. Sen and G.K. Mehta, J. Phys. G : Nucl. Phys. 5 (1979) 319

29. S.C.L. Sharma, G.K. Mehta, R.K. Choudhury, D.M. Nadkarni and S.S. Kapoor, Nucl. Phys. A355 (1981) 13

30. R.A. Atneosen and T.D. Thomas, Phys. Rev. 139 (1965) B 307

31. D.M. Narkarni, Report BARC-362 (1968), India

32. M. Scheeberger, Thesis, Vienna, 1969

33. E. Piasecki, M. Dakowski, T. Krogulski, J. Tys and J. Chwaszczewska, Phys. Lett. 33B (1970) 568

34. I.G. Schröder, Bull. Am. Phys. Soc. II 17 (1972) 441

35. D.M. Nadkarni, S.K. Kataria, S.S. Kapoor and P.N. Rama Rao, Nucl. Phys. A196 (1972) 209

36. V.N. Andreev, V.G. Nedopekin and V.I. Rogov, Sov. J. of Nucl. Phys. 18 (1974) 503 and 25 (1977) 732

37. J.A. Adams and R.R. Roy, Nucl. Sci. Eng. 63 (1977) 41

38. V.M. Adamov, L.V. Drapchinsky, S.S. Kovalenko, K.A. Petrzhak, L.A. Pleskacheosky, I.I. Tyutyugin, Phys. Lett. 48B (1973) 311

39. M. Rajagopalan and T.D. Thomas, Phys. Rev. C5 (1972) 1402

40. F. Caitucoli, B. Leroux, P. Perrin, G. Barreau, M. Asghar and N. Carjan, Proc. of Symp. on Physics and Chemistry of Fission, (Jülich, 1979), IAEA, Vienna (1980)

41. E. Piasecki and L. Nowicki, Proc. of Symp. on Physics and Chemistry of Fission, (Jülich, 1979), IAEA, Vienna (1980) p. 193

42. E. Piasecki, M. Sowinski, L. Nowicki, A. Kordyasz, E. Cieslak, and W. Czarnacki, Nucl. Phys. A255 (1975) 387

43. L. Nowicki, E. Piasecki, A. Kordyasz, M. Kisielinski, J. Sobolewski, W. Czarnacki, H. Karwowski, P. Koczon and C. Signarbieux, to be published (as reported in Ref. 41)

44. E. Piasecki and J. Blocki, Nucl. Phys. A208 (1973) 381; E. Piasecki and J. Blocki, Nucl. Phys. A212 (1973) 628

45. M. Dakowski, E. Piasecki and L. Nowicki, Acta Phys. Pol. B9 (1978) 933

46. A.J. Kordyasz, J. Phys. G : Nucl. Phys. 6 (1980) L-123

47. J.W. Truran, A.G.W. Cameron and E. Hiff, Proc. of Int. Conf. on the Properties of Nuclear Far from the Region of β-stability (Leysm, 1970) 2, CERN, Geneva (1970) p. 275

48. A.V. Ignatyuk, Proc. of the Summer School, Alushta (1978) 505.

CHAPTER III

POLAR AND EQUATORIAL EMISSION OF LIGHT CHARGED PARTICLES IN keV NEUTRON INDUCED FISSION

3.1 The Geometry

The geometry used in the experiment is shown in Fig. 3.1. The fission fragments were detected by a combination of two ionization chambers formed by division of a single ionization chamber into two parts by a multihole collimator. Such a geometry with two ionization chambers provides informations regarding the direction of emission of the particles, which is necessary for a proper identification of the equatorial or the polar nature of the detected LCP. The holes in the collimator form a hexagonal close packing structure and it is kept as close to the fission source as possible so as to minimise the uneffective area of the fission source. The separation of the nearest holes is chosen to ensure that the particles originating from a particular source area may pass through only one particular hole of the collimator. In addition, the collimator serves as a common electrode for the upper and the lower ionization chambers. The backing of the ^{235}U source forms the collector electrode for the lower ionization chamber (LIC) while an aluminium foil serves this purpose for the upper ionization chamber (UIC). A ΔE-E semiconductor telescope for the detection of the light charged particles (LCP) is placed above the aluminium

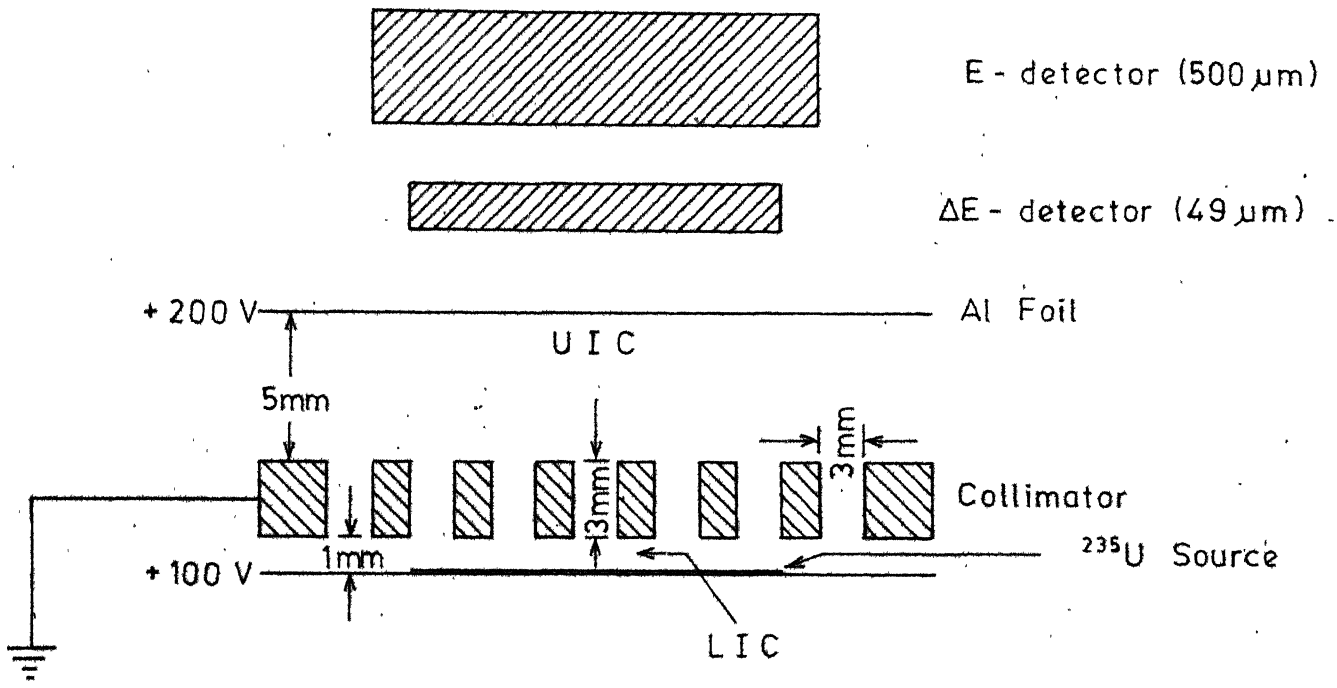

Fig. 3.1. Schematic diagram of the detection system.

foil. The aluminium foil is thick enough (≈ 4 mg/cm^2) to stop the fission fragments and the natural alpha-particles from the fission source. The chamber was filled with pure argon gas at a pressure of slightly more than the atmospheric pressure.

Depending upon the point of origin and the direction of emission, a fission fragment trajectory may fall into one of the three general types indicated in Fig. 3.2. For clarity, only one collimator hole is displayed in the figure. For a trajectory of type (a) or (b), a pulse is obtained from the LIC while for (c) type trajectory pulses are obtained from both LIC as well as UIC. Possibility of a small charge collection by UIC for some trajectories of type (b) exists. The amount of this possible charge collection is minimised by increasing the distance of the aluminium foil from the collimator and applying a lower electric field gradient in the UIC as compared to that in the LIC. Most of the charge produced inside the collimator hole due to trajectories of the type (b) either recombines due to very small electric field present or gets collected by the LIC. A consideration of the dimensions of the chamber implies a difference of atleast a factor of ≈ 5 between the UIC pulses originating due to the trajectories of type (c) and those due to the trajectories of type (b). In the experiment, the UIC pulses were found to be pretty large apart from very small pulses due to above mentioned cause and the natural alpha-particles. These small pulses were cutoff by the electronic circuit used in the experiment.

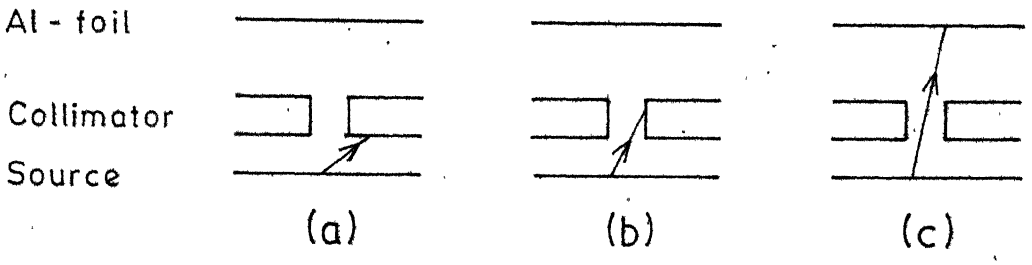

Fig. 3.2. Schematic illustration of typical fragment trajectories in the ionization chamber.

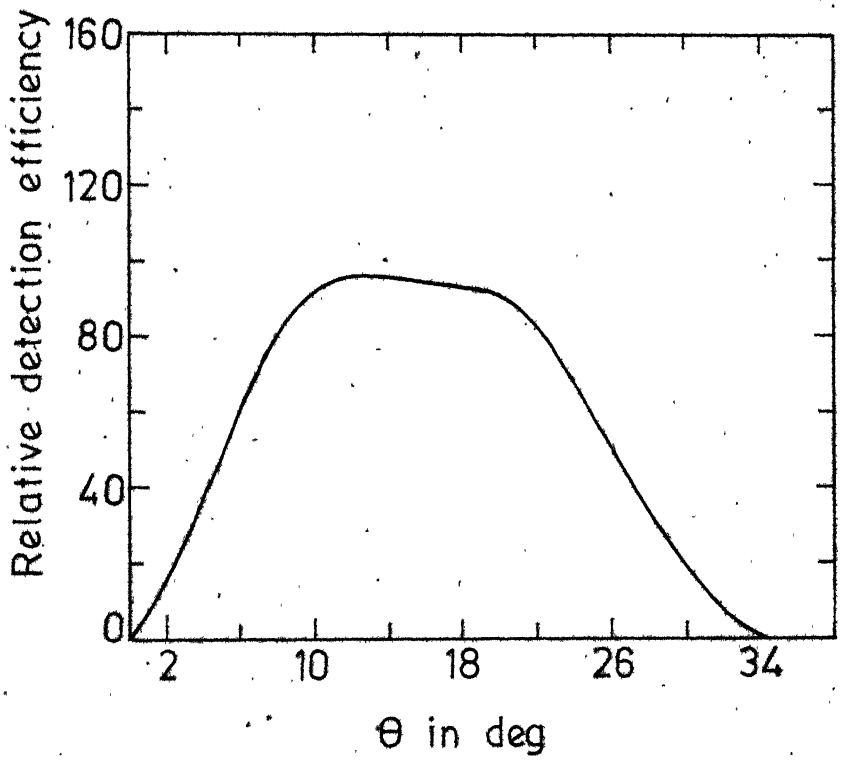

Fig. 3.3. Angular efficiency for the polar LCP detection.

The pulses derived from the LIC, the UIC, the ΔE-E detector and the E-detector were looked for the coincidences by the electronic circuit described later. A three-fold coincidence between the ΔE-detector pulse, the E-detector pulse and the LIC pulse indicates that the fragment trajectory is of the type (a) or (b) and the LCP has passed through the collimator hole so as to be detected by the ΔE-E detector telescope. Such a three-fold coincidence is taken to correspond to the detection of an equatorial LCP accompanied fission event. On the other hand a four-fold coincidence between the UIC pulse and the aforementioned three pulses indicates that both the LCP and the fragment have passed through the collimator hole. Thus such a four-fold coincidence is taken to correspond to the detection of a polar LCP accompanied fission event.

3.1A Choice of the Collimator Size

In deciding upon the size of a collimator-hole it is necessary to minimise possible contaminations to what we have designated as the equatorial events (identified by the three-fold coincidence requirement) from the LCPs which are actually emitted in the polar direction. Similarly contribution to the LCPs which have been claimed by us to be due to polar emission (identified by the four-fold coincidence requirement) from the LCPs that are actually emitted in the equatorial directions. Such contributions may be made arbitrarily small

by chosing finer collimators. However, employing a very fine collimator means a reduction in the count rate resulting in near impossibility of doing such an experiment with the available neutron flux due to extremely rare emission of the polar LCPs. The dimensions of the collimator holes (Fig. 3.1) have been chosen, in the present experiment, to provide a reasonably low 'polar-equatorial' mixing keeping in view the need of maximising the value of the detection efficiency for the LCPs. A Monte Carlo calculation (described later) has been done to estimate the possible polar contamination of the equatorial events and vice versa. It is estimated that nearly 7 %. of the detected equatorial alpha-particles might be actually produced in the polar emissions. Corresponding number for the contamination of the equatorial protons by the polar protons comes out to be nearly 14 %.. These numbers are the upper limit of the possible contaminations and have been calculated by using the equatorial and the polar data as given in the review paper by Piasecki et al.[1]. Similar calculations estimating the contaminations of the detected polar LCPs by the equatorial LCPs in our geometry indicate negligible contamination for the polar alpha-particles while the contamination of the polar protons by the equatorial protons comes out to be approximately 0.6 % . Thus we see that with the present choice of the collimator size, the contaminations due to 'equatorial-polar mixing' in our experiment is not significant (possible contamination due to scattering is estimated to be insignificant).

Figure 3.3 gives the relative detection efficiency for the LCP detected in coincidence with the UIC and the LIC pulses as a function of the angle between the LCP and the fragment. The efficiency is maximum around 14^{o} and falls to negligible value after 34^{o}. Thus the polar LCPs detected in the present experiment are emitted within a narrow cone around the fission axis.

The present geometry avoids the use of semiconductor fission detectors and permits the use of a broad fission source without sacrifying the angular resolution. Thus it is quite useful for studying the rare phenomenon of the polar emission in nuclear fission. In addition, a simultaneous study of the equatorial LCPs is also possible which provides a direct comparison of the characteristics of the polar and the equatorial LCPs. A possibility of studying the angular distributions of the various LCPs exists by using collimators of different hole-sizes. Work on this line is in progress[2].

3.2 Experimental Details

3.2A Details of the Double Ionization Chamber

Voltage applied in the UIC and the LIC were adjusted along with the time constants and the gains in the linear amplifiers to obtain nicely shaped pulses without reaching the saturation level of the amplifiers. The LIC pulses were found to be varying continuously from very low values to a

certain maximum value. The low height pulses from the LIC contain contributions from the natural alpha-particles and the fragments emitted at small angles to the source and were not detected by adjusting the lower cutoff in the Timing-Single-Channel Analyzer (ORTEC - 420). The UIC pulses were mostly large pulses apart from those due to the natural alpha-particles. In addition, the small pulses may also be, in part, due to the reason discussed in section 3.1. These pulses were discarded by suitably adjusting the lower cutoff value in the TSCA. The TSCAs were operated in the bipolar mode to obtain accurate timing signals from the LIC and the UIC pulses. With a known delay introduced in the UIC pulses, the fast negative timing signals from the two TSCAs were fed to the start and the stop inputs of a time to pulse height converter (TPHC, ORTEC-405) for studying the time relationship between the LIC and the UIC pulses. It was found that the two pulses (obtained when a fragment passes through the collimator hole) are coincident within 20 nS. The full width at one tenth of maximum of the peak in the spectrum of the TPHC output is nearly 80 nS.

3.2B Details of the LCP Detector

A ΔE-E semiconductor telescope supplied by the ORTEC, Inc., USA, was used for the detection and identification of the LCPs. The ΔE-detector was a transmission mounted 49 μm thick silicon detector with an active area of

300 mm^2 while the E-detector was 500 μm thick with an active area of 450 mm^2. The detector telescope was not kept very close to the collector foil of the UIC in view of the possibility of sparking due to the voltage applied to the collector.

3.2C Electronic Setup

The electronic setup used for the signal processing and the data acquisition in the experiment is shown schematically in Fig. 3.4. The circuit was planned to store informations on the values of the ΔE and E once a LCP is detected coincident with a fission fragments. In addition, arrangement was made to provide information whether the detected fragment pulse came from the LIC alone or from both LIC and UIC. Pulses from the UIC, ΔE-detector and E-detector were fed into the respective low noise preamplifiers (ORTEC 142A), which were kept close to the detection chamber. The preamplifier output pulses were transmitted to the linear amplifiers placed in the data acquisition room by shielded transmission cables of proper characteristic impedances to avoid reflection and distortion of the signals. The gains and the time constants of the linear amplifiers (ORTEC Models providing unipolar as well as bipolar outputs) were adjusted so as to provide nicely shaped pulses with their magnitudes within the working range (0 V - 10 V) of the linear amplifiers.

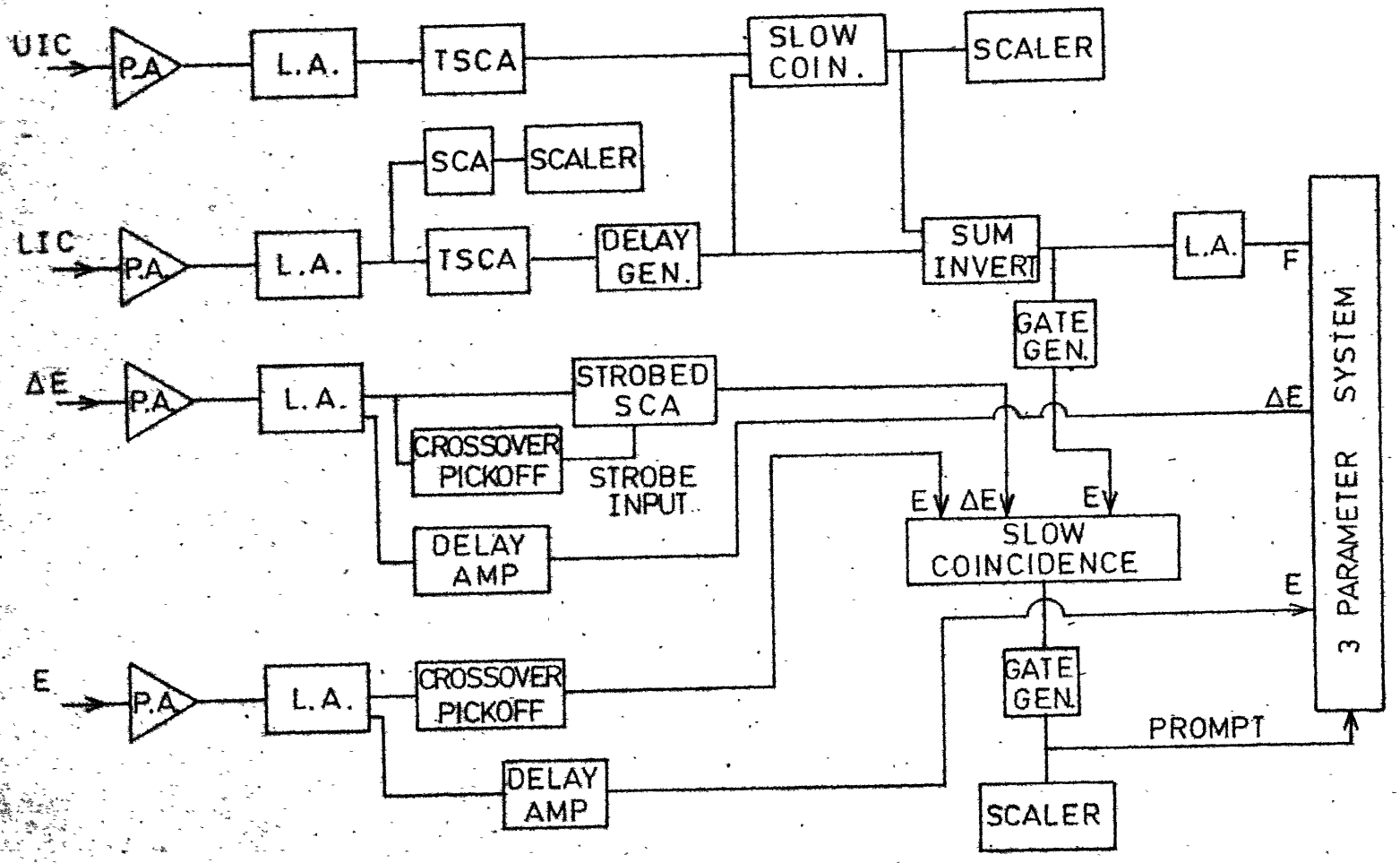

Fig. 3.4. Schematic diagram of the electronic circuit and data recording system.

The bipolar pulses of the linear amplifiers corresponding to the UIC and the LIC were fed to the timing single channel analyzers (ORTEC - 420) operated in the bipolar mode to achieve accurate timing signals. After a suitable delay in the LIC timing pulse to annul the time-mismatch arising due to a slight difference in the width of the LIC and the UIC pulses, the two timing signals (standard logic pulses of ≈ 0.5 μS width) are looked for coincidence by a slow coincidence unit (ORTEC - 409). The output of the coincidence unit was algebraically added to the LIC timing signal by the ORTEC 'SUM and INVERT' unit (Model - 433A). The pulse so obtained will have a higher amplitude in case of a coincidence between the LIC and the UIC pulses and a lower amplitude otherwise. This two level logic pulse provided information whether the fragment passed through a collimator hole or not and was recorded after inversion and proper shaping for each LCP-detection event. The ΔE-timing signal was derived from the corresponding bipolar pulse by using the CROSSOVER PICKOFF UNIT (ORTEC - 407) which provides a fast-rising pulse at the instant of the zero crossing of the bipolar pulse. This timing signal provided the strobe input to the STROBED SINGLE CHANNEL ANALYSER (ORTEC - 413). This arrangement provides accurate timing signal with adjustable lower cutoff value for the input pulses. The E-timing signal was obtained by using the CROSSOVER PICKOFF UNIT which itself provided the necessary lower cut off value (240 mV)

for the input pulses. The pulse widths of the E and ΔE pulses were chosen such that the timing pulses derived from them were coincident with each other as well as with the logic pulse derived from the output of the 'SUM and INVERT' unit described above. These three pulses were looked for the coincidence by a slow coincidence unit (ECIL - Model LG666). The output of this coincidence unit generated the gate pulse to activate the data recording unit. The unipolar pulses from the linear amplifiers corresponding to the ΔE and E detectors were brought in coincidence with this gate pulse by introducing the necessary time-delays with the help of the DELAY AMPLIFIER UNITS (ORTEC - 427; ECIL - DA671).

The data were recorded event by event on a magnetic tape with a three parameter data acquisition system which also provided a display of the 'channel numbers' of the three parameters. The three parameters were the ΔE-pulse, E-pulse and the two level logic pulse indicating the polar or the equatorial character of the detected LCP.

3.2D The Neutron Production

Neutrons were produced using the proton beam from the Van de Graaff accelerator at Indian Institute of Technology, Kanpur. The accelerator is capable of providing a total of 100 μA current of protons with their energy adjustable over a continuous range extending upto a maximum of 2 MeV. The intrinsic energy stability of the machine was

within ± 5 keV and it could be improved further upto ± 1 keV by using the slit stabilization system fabricated in the accelerator lab. The machine was calibrated for the proton energy by using the sharp thresholds in the (p,n) nuclear reactions with the ^{7}Li and the tritium targets.

The $^{7}Li(p,n)^{7}Be$ reaction was used for generating thermal neutrons. The thermalisation was achieved by using a 2'' thick paraffin block. Thick lithium targets were made by vacuum deposition of the lithium metal over copper backings. After the evaporation, dry nitrogen gas was filled in the evaporation chamber so as to provide a protective lithium nitride layer on the lithium target.

The $^{3}H(p,n)^{3}He$ reaction was used for generating 600 keV neutrons. The tritium target (obtained from the Isotope Division, BARC, Bombay) consisted of adsorbed tritium gas in the titanium layer deposited on copper discs, the ratio of the titanium atoms to the tritium atoms being 1:1. A 8 curie tritium target was used which caused a spread of nearly ± 160 keV in the energy of the neutrons.

Neutron target holder and the associated beam transport system are shown in Figs. 3.5 and 3.6. Chilled water was circulated in the copper tubes covering the neutron target holder to avoid deterioration of the target due to heating by the proton beam. The aluminium grill arrangement (Fig. 3.6) at the exposure site reduced the possible contamination to the direct neutrons at the fission source from

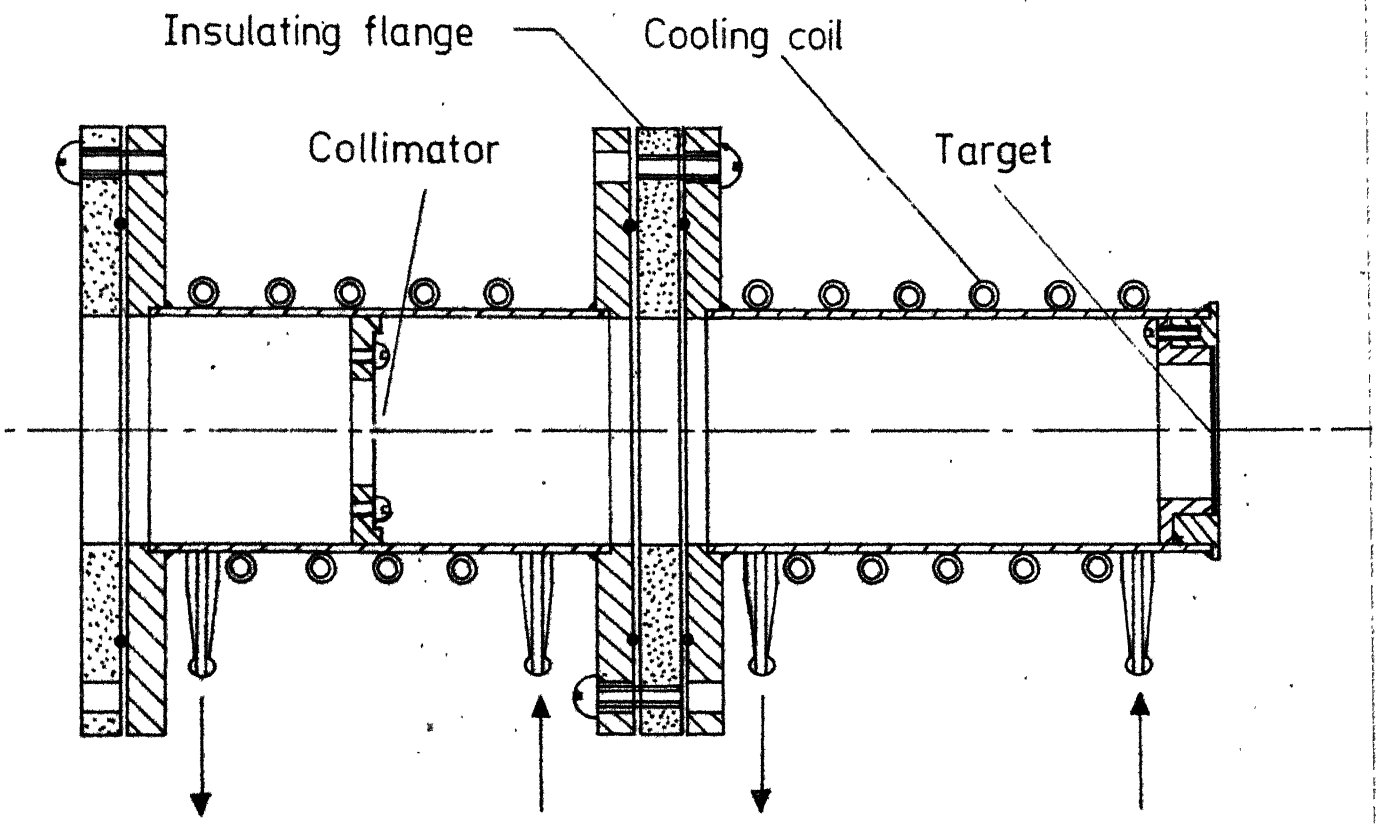

Fig. 3.5. The neutron target holder and collimator.

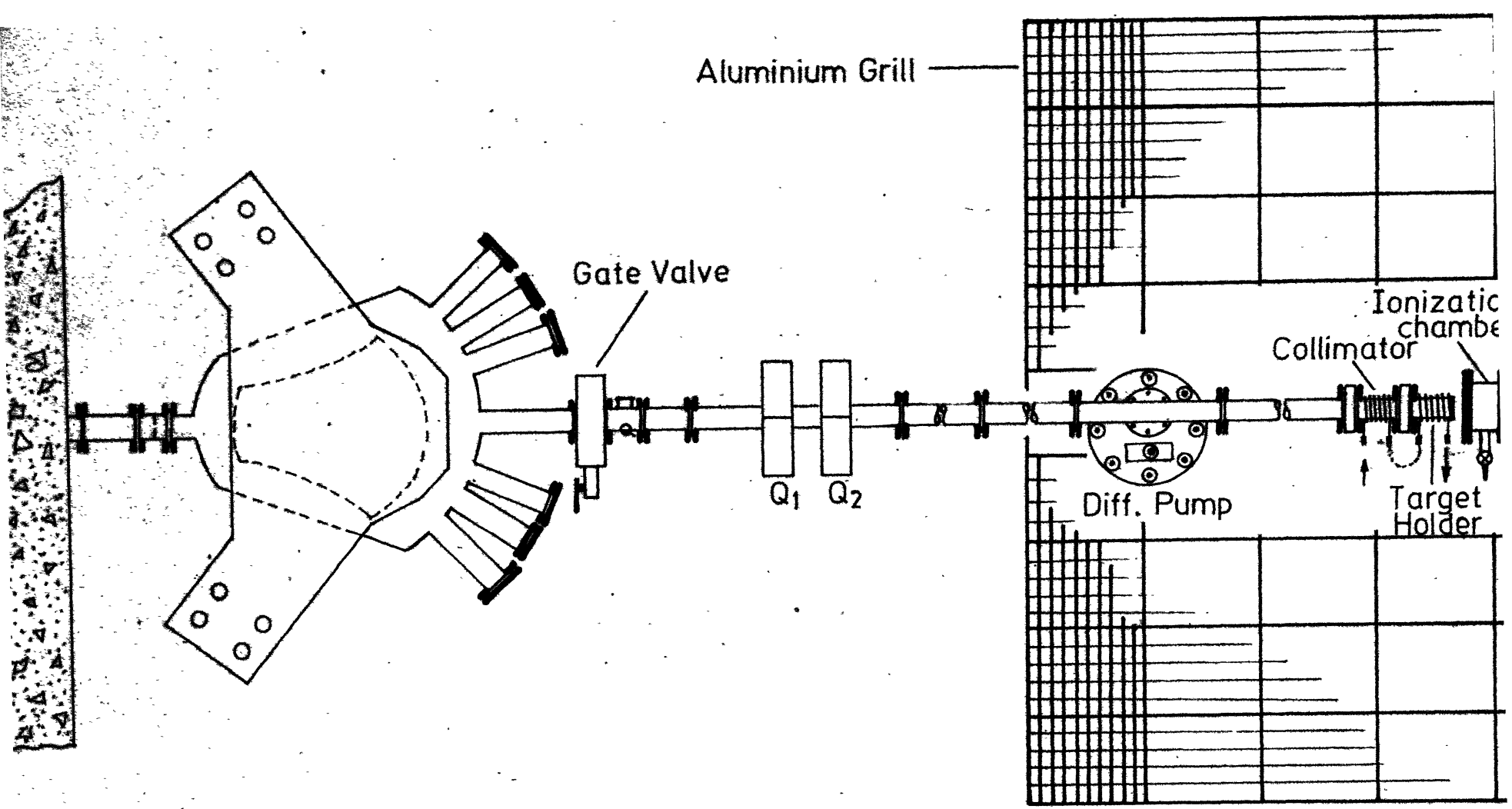

Fig. 3.6: Schematic diagram of beam transport system.

the scattered neutrons. On the contrary, the chilled water cooling of the target holder may enhance such a contamination. However, overall thermal neutron contamination in the fast neutron exposure was monitored by the neutron activation technique using indium target and estimated to be less than 0.01 %..

The neutron flux was monitored by a standard long counter. The detector had a fairly flat response over the neutron energies above 1 MeV while its efficiency falls to nearly 70 %. of the maximum as the neutron energy reduces to the thermal value. However, the main purpose of the neutron counter was to monitor the deterioration, if any, in the neutron target during the experiment.

3.2E The Fissile Source

The fissile source consisted of an uniform layer of enriched ^{235}U (93.7 %.) deposited over an area of ≈ 4 cm^2 on a thick nickel backing. The source thickness was ≈ 5 mg/cm^2 and was formed by using the spray technique in BARC, India.

3.3 Experimental Procedure

The ΔE and E detectors were tested for the energy resolution by using thin alpha-sources of ^{241}Am and ^{227}Ac and the initial leakage currents were measured. The detection chamber was tested for stability of the pressure of the

filled argon gas thus ensuring the stability in the fission pulse height. The electronic circuit was tested by providing the pulses in various preamplifiers to simulate the polar and the equatorial LCP events.

The ΔE and the E channels of the three parameter data acquisition system were calibrated by using a precision pulse generator (ORTEC Model 204). The pulse generator was previously calibrated for the ΔE and E detectors. The pulse generator was also used to check the linearity of the electronic system over the complete range of the possible LCP energies and to get the lower energy cutoff values for the ΔE and E channels. The stability of the electronic system was tested from time to time during the experiment with the help of the pulse generator.

The lower level cutoff in the LIC and the UIC channels were adjusted to cut the pulses arising due to natural alpha-particles. The lower energy cutoff values were 0.7 MeV and 1.5 MeV for the ΔE and the E channels respectively. The experiment was performed for the thermal and 600 keV neutrons. The typical count rates (singles) of the LIC, the UIC, the ΔE and the E pulses are indicated in the Table 3.1. Typical equatorial LPC count rate was $\approx$ 15/hour while the polar count rate was $\approx$ 0.5/hr. These numbers refer to the thermal neutron run. Count rate were less by a factor of 3-5 for the fast neutron run. Each fast neutron run was preceded and succeeded by a thermal run which provided a check on the

possible drifts.

TABLE 3.1

Typical count rates observed in the experiment for the thermal neutron run

The LIC pulse	The UIC pulse	The E det. pulse	The E det. pulse
7600/sec.	400/sec.	2.2/sec.	250/sec.

The leakage currents in the ΔE and E detectors were monitored regularly during the neutron exposure and the applied bias was adjusted to account for the fall in the voltage across the detectors resulting due to the increased leakage currents. This increase occurs because of the crystal defects introduced in the detectors due to the incident neutrons (damage being more severe for the fast neutrons) and causes a higher fall across the biasing resistance. The effect was more prominent for the E-detector due to its larger volume and so the biasing resistance in the preamplifier (ORTEC Model 142A) was reduced in this case.

3.4 Data Analysis

In the following, we shall be concerned with the details of the data analysis. The DEC-10 and IBM-1800

computer of I.I.T. Kanpur were employed in the calculations.

3.4A Particle Identification

Particle identification (PI) has been done by the PI signal generated from the ΔE and the E signals by using the following relation

$$PI = (E + \Delta E)^n - E^n$$

with n being nearly 1.76. The E and ΔE signals were derived from the corresponding channel numbers (stored event by event on a magnetic tape in the three parameter data acquisition system) and the calibration coefficients.

The principle of the above method is based upon experimental range-energy relations for the H and He isotopes in the detector medium(that is, the silicon), which is summarised by the following equation

$$R(E) = KMZ^2 E^n \qquad (1)$$

where R(E) is range of the particle with energy E, $n \approx 1.76$, M = Atomic mass, Z = Atomic number and K is a constant (for energy E < 3 MeV, K is observed to deviate from the constant value). If the incident particle deposits an energy ΔE in the thin detector of thickness T and gets completely absorbed by the thick detector depositing an energy E in it, then we may write

T = (Range of the particle with energy E + Δ E) - (Range of the particle with energy E)

or $$T = K MZ^2 [(E+\Delta E)^n - E^n]$$

Thus

$$PI = (E+\Delta E)^n - E^n$$

$$= \frac{T}{K} \cdot \frac{1}{MZ^2} .$$

The above equation brings out the independence of the PI signal upon the energy of the incident particle. The importance of the method used lies in the fact that the need of a very thin ΔE detector is avoided which was an indespensable requirement in the earlier methods[3] involving the measurement of E and (dE/dx). It is seen that the PI value depends upon the intrinsic characteristics (mass and charge) of the particle and thus is used for the particle identification.

3.4B Chance Coincidence Contribution

The present experiment is an extremely low counting rate experiment due to the rarity of the polar and the equatorial LCP emission. Thus care was taken to ensure a minimum of the contribution to the detected LCPs from those originating in nuclear reactions other than the fission reaction. This was done by imposing the three fold and four

fold coincidence conditions in the detection arrangement. The contribution owing to chance coincidence has been estimated to be < 1 % of the observed number of the polar and equatorial LCPs. Hence no correction was made to account for the chance coincidence contribution.

3.4C Detection Efficiency Calculation

Calculation of the detection efficiencies of the equatorial and polar LCPs have been performed using the Monte Carlo method. Such a method employs the concept of the random number and simulates the physical events by chosing proper random variables. Various events that are to be simulated should be of statistical origin, i.e., decay of the nuclei, absorption and scattering of the particles etc.

In the present calculations, the physical events of the production of the LCP and the fragments were simulated mathematically in the computer for their motion after the production. The direction of the motion were chosen by associating random variables having their probability distributions in accordance with the corresponding experimental distributions. Among a large number of such 'mathematical' events, in few the directions of the particles may be such that the conditions of the 'three fold' or the 'four fold' coincidences are satisfied. The fraction of such events provides a good approximation to the detection efficiencies of the equatorial and the polar LCPs. In the

following, the procedure adopted is described in detail.

1. Simulation of the Light Charged Particle Accompanied Fission (LCPF)

For simplicity, we shall consider a single collimator hole and the source area beneath it described by the shadow cone (Fig. 3.7).

(a) Chosing the Point of Emission

The point of occurence of the LCPF is chosen randomly within the shadow circle. For this purpose, we employ uniform unit random variable (to be denoted by RVU) which may have any value between 0 and 1 with uniform probability. Value of this random variable is supplied by the computer and we shall denote it by (RVU). If X and Y are coordinates of the emission point, then

$$X = R_s[2(RVU) - 1]$$

$$Y = R_s[2(RVU) - 1]$$

where R_s is radius of the shadow circle (Fig. 3.7) and (RVU) used twice in the above equations denotes two independent values taken by the random variable RVU.

Distance of the point of emission ($= \sqrt{(X^2+Y^2)}$) from the centre 'O' is calculated. In case this distance turns out to be more than R_s, the current value is rejected and

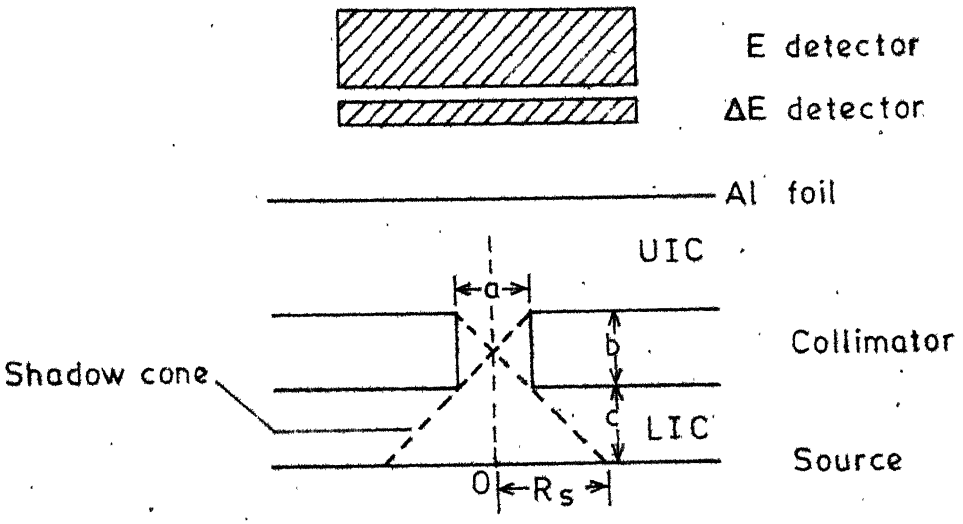

Fig. 3.7. Schematic diagram giving parameters used in detection efficiency calculation.

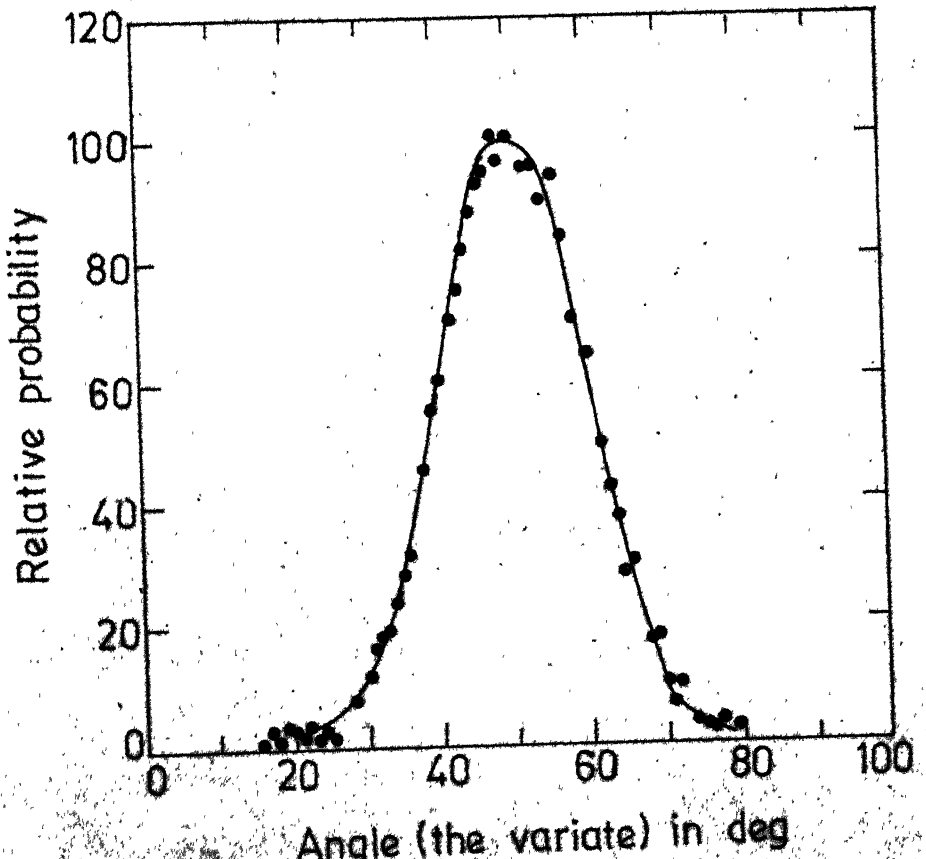

Fig. 3.8. Gaussian curve with standard deviation 10° and centered around 50° as generated by RVG (see text).

new values for X and Y are chosen till the point of emission lies within the shadow circle.

The uniform choice of the point of emission is justified only if the fission source is uniformly thick and the neutron flux and energy do not change significantly over the source area. Both of these conditions are satisfactorily met in the present experiment.

(b) Chosing the Direction of Emission of the Fragments

Direction of the fragment is specified by the spherical angle coordinates Θ_F, ϕ_F. The coordinate system chosen (to be called later as space fixed system) has its origin coinciding with the point of emission while the Z-axis is at right angles to the fission source. The experimental fragment angular distribution is isotropic in the thermal neutron induced fission while a small departure from isotropy occurs for the 600 keV neutron induced fission. However, this effect has been ignored and an isotropic emission of the fragments have been assumed. The angle Θ_F has been chosen by using a random variable with its probability distribution proportional to account for the Sin Θ - dependence of the solid angle described by the directions (Θ,ϕ), $(\Theta+d\Theta,\phi)$, $(\Theta,\phi+d\phi)$ and $(\Theta+d\Theta,d\phi)$. This random variable is given by inverse cosine of an uniform unit random variable[4]. The angle ϕ_F is chosen randomly within 0 and 2π with uniform probability.

(c) Chosing the Direction of Emission of the LCP

The direction of the LCP emission is correlated with the fragment direction. For accounting this, the direction of the LCP emission is specified by a proper choice of the spherical angle coordinates θ_α and ϕ_α defined in a coordinate frame with its Z-axis coinciding with the fragment direction (the origin coincides with the point of emission).

The angular distribution of the equatorial LCPs is peaked near 90° with FWHM (Full Width at Half Maximum) varying from 20° to 90°. The polar LCP angular distributions are not known accurately. They are found to be peaking along the fragment direction with FWHM of the order of 20° to 40°.

The shape of the angular distribution has been taken to be represented by a Gaussian curve. Thus the angle θ_α is chosen with the help of a Gaussian random variable (to be denoted by RVG). The RVG is derived from the RVU by a procedure described in Ref. 4. Figure 3.8 shows a typical spectrum as generated by the RVG. In addition, a weight factor equal to Sin θ_α is also associated with each LCP event when the LCP-angular distribution is given in terms of yield per unit solid angle. The angle ϕ_α is chosen randomly within 0 and 2π with uniform probability.

It is necessary to find the spherical angle coordinates of the LCP direction with respect to the space fixed system. This is achieved by using the rotational operator matrix. This matrix is obtained by taking the

inverse of the transformation matrix for the Euler rotations[5].

After chosing the above coordinates, we calculate the coordinates of the following points :

(i) Points where the fragment would have hit the lower and upper surfaces of the collimator.

(ii) Points where the LCP would have hit the lower and the upper surfaces of the collimator and the plane of the ΔE and E-detector.

Distances of these points from the axis of the collimator hole under consideration as well as from the axis of the ΔE and E detectors are calculated and the relevant distances are compared with the radii of the collimator hole and the ΔE and E-detectors. From these comparisons it is discerned whether the LCP produced in the mathematical event is detected or not and if detected, would it have given rise to a three-fold (an equatorial event) or a four-fold (a polar event) coincidence.

A large number of such mathematical events are generated by the computer. Number of the events which give rise to the detection of the equatorial or the polar LCPs are counted. If angular distribution used is given in yield per unit solid angle, a total 'weight' is evaluated for various types (equatorial or polar etc.) of events by adding the 'Sin Θ' weight factors. This number (or weight) when devided by the total number (or weight) of the events generated provides the relevant detection efficiency.

Calculations have been made on above lines by using the known angular distributions of the various LCPs. The experiment did not permit the identification of the light and the heavy fragment. In the efficiency calculations, this fact has been taken care of. The recoil of the fragments due to the LCP has also been included in the detection efficiency calculations. The detection efficiency depends upon the location of the collimator hole and the calculations have been done for different distances of the collimator hole from the common axis of the fission source and the LCP detectors. The distances of various holes in the collimator from this common axis are calculated and an average detection efficiency is evaluated.

The thick fission source causes a loss of the energy for some of the fragments. This loss is severe for the fragments emitted in directions close to the surface of the source and some of these may not get detected in the ionization chamber due to the lower level cutoff set in the experiment Such an effect has been simulated in the calculations of the detection efficiencies by setting a lower angle limit (θ_c) for the emitted fragments. The value of the θ_c is chosen so as to provide a value of the detection efficiency for the equatorial alpha-particles which gives the equatorial alpha-particle yield in agreement with the accepted value.

3.5 Results

3.5A Particle Identification

The particle identifier (PI) spectra for the LCPs in the thermal and the fast neutron induced fission are shown in the Fig. 3.9. A clear separation of the protons, tritons and alpha-particles is seen to occur in the PI spectra.

The collimator used in the present experiment reduces the spread in the angle of incidence of the LCP on the ΔE-E telescope resulting in a better resolution in the particle identification spectrum.

A simple Monte Carlo calculation of the PI spectra for the protons, tritons and alpha-particles has been performed for the geometry used. The angular spread of the LCPs, their energy losses in the gas and aluminium foil and the detector resolutions have been considered in the calculation. The calculated widths of the PI peaks agree with the corresponding values in the observed PI spectra.

The increase in proton yield for 600 keV neutron induced fission compared to the thermal fission is clearly seen in the PI spectra.

3.5B Energy Distributions of the LCPs

Figure 3.10 shows the energy distributions of the equatorial protons, tritons and alpha-particles corresponding to typical thermal and 600 keV runs. The energy

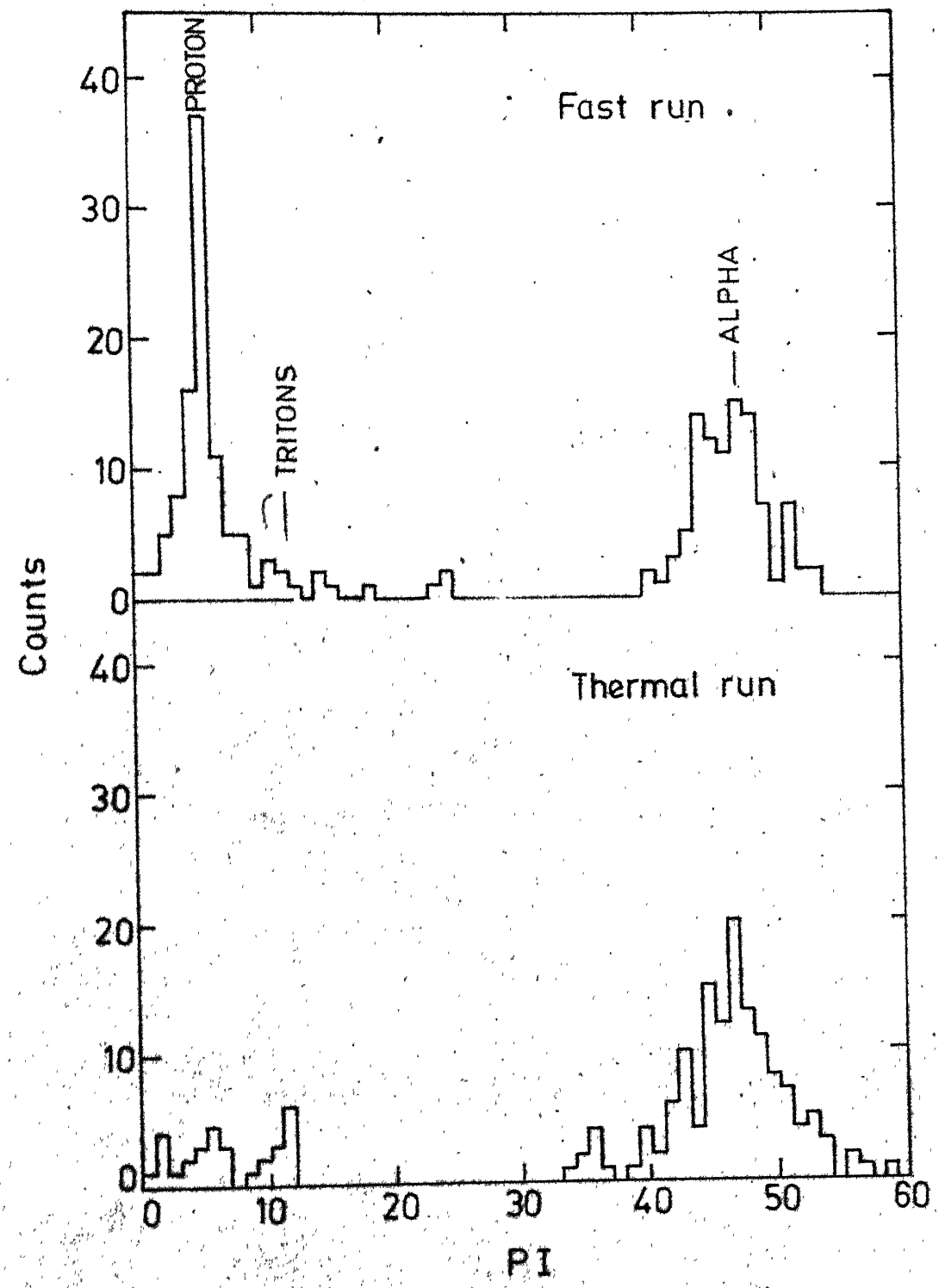

Fig. 3.9. Particle identifier spectra.

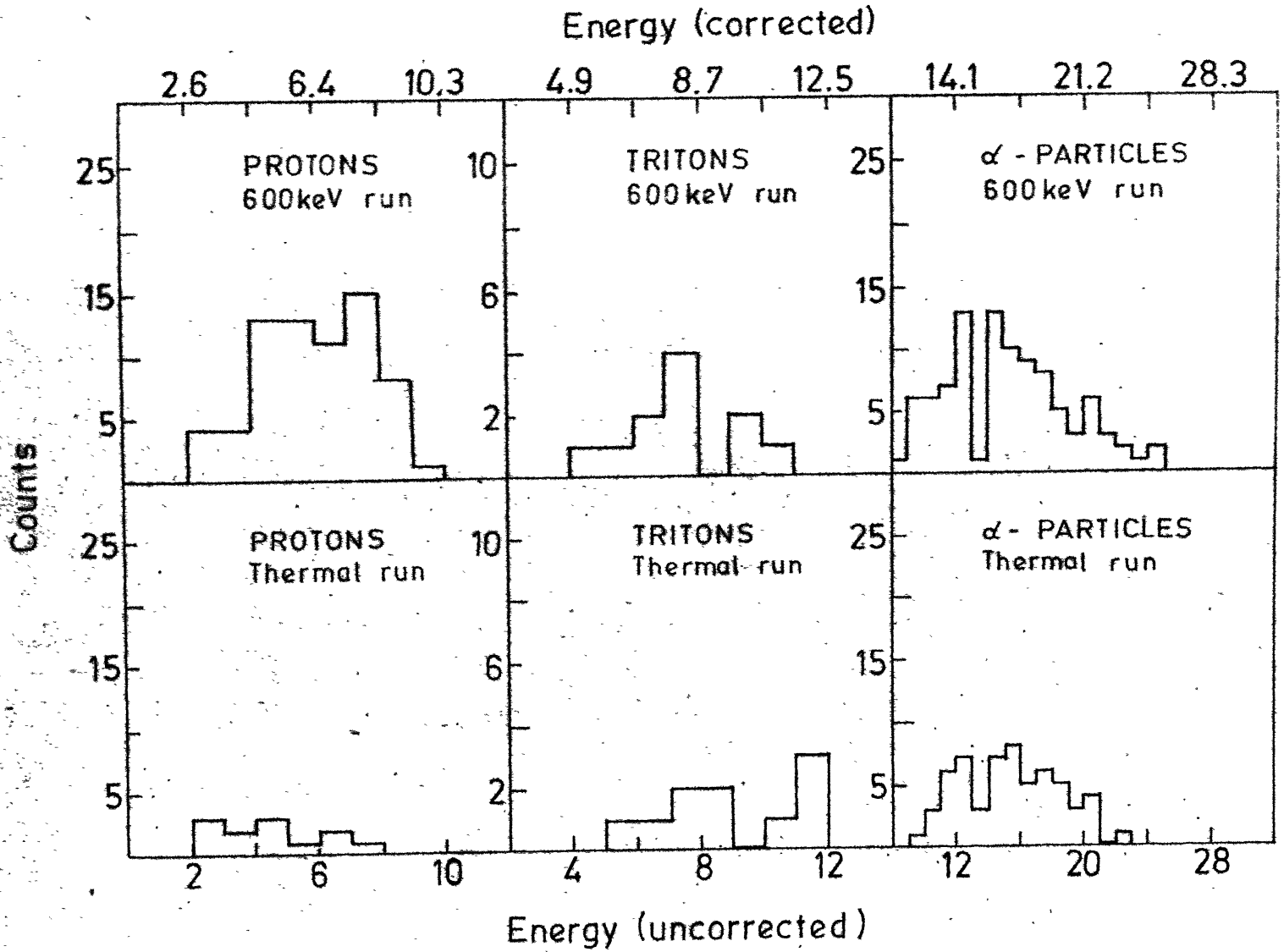

Fig. 3.10. Energy spectra of the equatorial light charged particles.

distributions of the polar LCPs have not been included due to their poor statistics.

The energy distributions for the equatorial LCPs agree resonably with those obtained in earlier works (see table 2.1 in Chapter II). However, a good quantitative comparison is not possible due to the low statistics in our experiment. The most probable energies of the equatorial protons and alpha-particles are nearly 8 MeV and 15 MeV respectively. A statistically significant value for the mean energy of the tritons could not be obtained.

The proton energy spectrum indicates a sudden fall in the energy region near 10 MeV. This is because of insufficient depletion depth of the E detector used in our experiment and thus for the protons incident on the telescope with energy more than $\approx$ 10 MeV, only partial absorption of the energy occurs. The alpha-particle energy distribution appears to be broader in comparison to the earlier results and indicates a somewhat double-humped structure. Such a shape of the energy spectrum is expected in our geometry due to (a) a lack of identification for the heavy and the light fragments and (b) discarding of the fission fragments emitted at grazing angle to the fission source. The effect arises essentially due to the angle-energy correlation for the alpha-particles. A Monte Carlo calculation of the alpha-particle energy distribution has been done

using the experimental results of Tsuji et al.[6] on the values of the mean and standard deviation of the energy distribution of the alpha-particles as a function of the angle of emission. Result of such a calculation is shown in Fig. 3.11. The calculated energy distribution is found to have a structure with double humped character similar to that in the experimental spectrum. The widths of the calculated and experimental spectra also agree reasonably well.

The energies of the polar LCPs were found to be consistent with the earlier results (see Table 2.3 in chapter II). The energy of most of the polar LCPs were found to be within twice the standard deviation from the accepted mean energies.

3.5C Relative Yields of the LCPs

Table 3.2 summarises the relative yields of the various LCPs. The yields of the equatorial and polar LCPs are normalised independently so as to give a value of 100 for the corresponding thermal alpha-particle yields. The yields shown are after correction for the detection efficiencies of various LCPs.

The detection efficiency is dependent upon the LCP angular distribution. Fig. 3.12 gives the calculated detection efficiency for the equatorial LCPs as a function of standard deviation of the angular distribution.

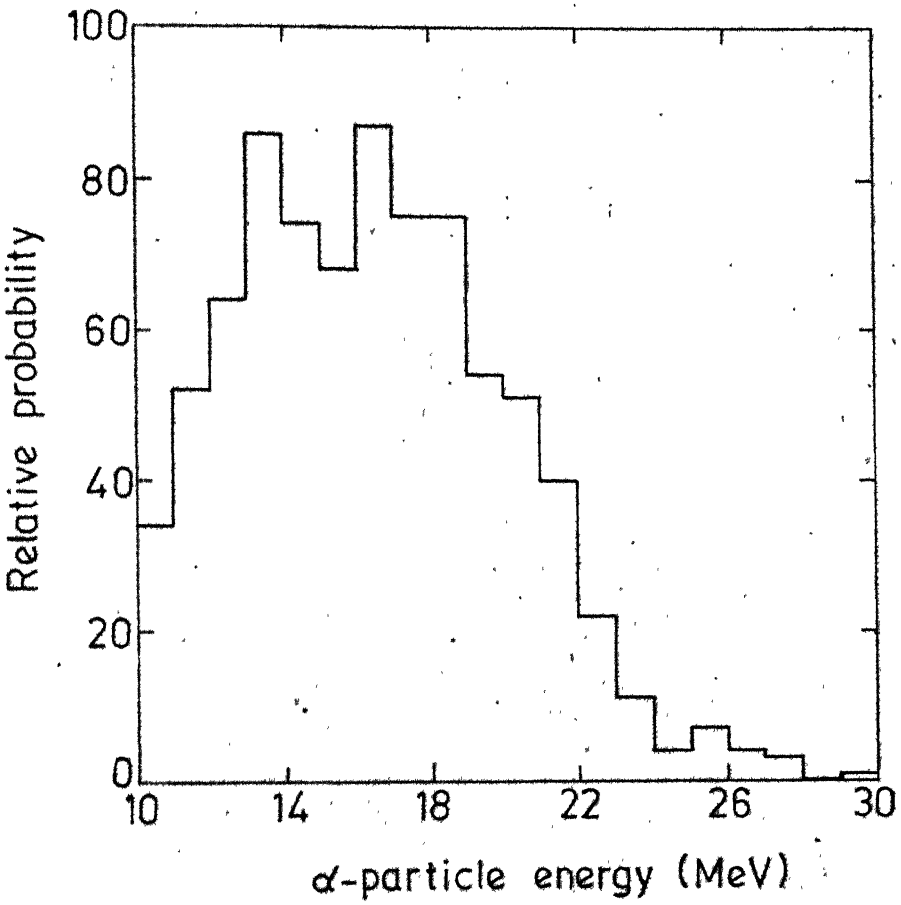

Fig. 3.11. Calculated energy spectra of the equatorial α-particles for the geometry used in the experiment.

Table 3.2

Relative yields of different equatorial and polar LCPs in the thermal and 600 keV runs

Particle	Equatorial Emission		Polar Emission	
	Thermal neutron fission	600 keV neutron fission	Thermal neutron fission	600 keV neutron fission
Proton	1.2 ± 0.4	6.7 ± .9	5.4 ± 3.5	25 ± 10
Triton	9.2 ± 3.0	10 ± 3	-	-
Alpha-particle	100 ± 9	88 ± 9	100 ± 33	80 ± 40

The angular distribution data have been taken from the work of Tsuji et al.[6] for alpha-particles while for protons and tritons work of Raisbeck and Thomas[7] was referred. The corresponding data for the fast neutron induced fission are not available. Hence, the detection efficiencies for the LCPs in the fast neutron induced fission have been calculated by taking the LCP angular distributions same as those in the thermal neutron induced fission.

The angular distributions of the polar LCPs are not accurately known. In the detection efficiency calculations for them, the angular distributions were taken from the

references given in the review paper of Piasecki et al.[8]. The dependence of the detection efficiency of the polar LCPs on their angular distribution is shown in the Fig. 3.13. The efficiency shown is normalized with respect to the fragments detected in the upper ionization chamber (in the case of the equatorial LCPs, the efficiency was normalized with respect to the fragments detected in the lower ionization chamber). The statistical errors associated with the calculated efficiencies are of the order of $\sim$ 10 %.

The errors shown in the table 3.2 are only statistical in nature. The possible errors arising due to the uncertainties in the detection efficiencies caused by the imprecise knowledge of the angular distributions are not included.

The data on the polar tritons have been omitted due to their poor statistics.

3.5D Comparison of Yields in Fast and Thermal Neutron Induced Fission

Table 3.3 contains the yields of the various LCPs in the fast neutron induced fission relative to the corresponding values for the thermal neutron induced fission. The errors indicated are only statistical as the errors due to uncertainties in the detection efficiency get cancelled out in the relative yield calculations.

Table 3.3

Yields of different equatorial and polar LCPs in the 600 keV run relative to that in the thermal run

Particle	Equatorial Emission	Polar Emission
Proton	5.6 ± 1.9	4.6 ± 3
Triton	1.1 ± 0.5	-
Alpha-particle	0.9 ± 0.1	0.8 ± 0.4

Underlying such an observation is our assumption that the angular distributions do not change substantially when the neutron energy increases to 600 keV from the thermal value. Another possible factor which may affect the relative yields is due to a change in the angular distribution of the fission fragments with neutron energy. A calculation of the detection efficiencies indicates that due to this effect, a maximum of about 7 % decrease might occur in the equatorial LCP detection efficiencies while the polar LCP detection efficiencies remain nearly unchanged.

It is observed that in fast fission, the yields of the equatorial and polar protons increases significantly while those of the equatorial and polar alpha-particles

remain nearly constant with a slight decreasing tendency. The yields of the equatorial tritons are nearly unchanged in the fast fission as compared to the thermal fission case. Corresponding data for the polar emission are not presented due to their poor statistics.

3.5E The Absolute Yields

From the observed yields of the equatorial and polar alpha-particles in the thermal neutron induced fission, their absolute yields are derived by using the calculated detection efficiencies. These calculations are intended to provide a check for the experiment and a comparison with earlier works. The equatorial alpha-particle yield comes out to be 0.20 ± 0.13 % of the binary fission rate†, which agrees reasonably with the experimental value[8] of 0.17 %. Cross-section for the polar alpha-particle accompanied fission is evaluated to be 24 ± 20 mb a number in reasonable agreement with the result of the earlier work[2,9]. Errors quoted include the contribution due to the uncertainties in in the detection efficiencies. The large errors in the evaluated cross-sections are mainly because of the uncertainties in the cut off value for the fission fragment pulses

---

† This value is obtained chosing an appropriate value of the lower angle limit 'θ_c' (see section 3.4C) which also reproduced the ratio of observed counts in the upper ionization chamber and the lower ionization chamber.

from the lower ionization chamber and the angular distributions.

3.6 Discussion

There is observed a marked increase in the yields of the polar and the equatorial protons for 600 keV neutron induced fission as compared to those for the thermal neutron induced fission (Table 3.3). The alpha-particle yield decreases slightly and the decrease is similar for the equatorial and polar emissions. The results on the equatorial alpha-particles and protons are similar to those obtained by Sharma et al.[10].

The most significant result of the present experiment is the observed similarity in the variations of the yield of protons and alpha-particles with neutron energy for the polar and the equatorial LCPs. The yield of the polar protons increases nearly five times for 600 keV neutron induced fission compared to the thermal neutron induced fission. An identical increase is observed for the equatorial protons. Similarly, the change in the yields for both the equatorial and polar alpha-particle is consistent. It may be emphasized that because of the simultaneous measurements of the polar and equatorial LCPs, these results are independent of normalization uncertainties connected with the neutron flux and detection efficiencies etc. Moreover, contamination to the data from the particles with non-fission origin is very

little. Reactions with the fission neutrons may result in particles emitted in coincidence with the detection of the fission fragments and thus cannot be discarded by the coincidence requirements set in the experiment. However, contamination due to fission neutrons (or even fission γ-rays) is seen to be insignificant as (i) the relative yields of the different LCPs agree well with the earlier measurements and (ii) the average number of the fission neutrons or γ-rays per fission do not increase substantially nor do their energy distributions change significantly when neutron energy changes by a small amount of 0.6 MeV to account for the observed changes in the yields.

Different models of the polar emission predict different dependences of the characteristics of the polar LCPs upon the excitation energy of the fissioning nucleus. In particular, nearly identical variations observed in the yields of the equatorial and the polar LCPs when the excitation energy changes by a relatively small amount of 0.6 MeV imply a similarity in the mechanisms for the production of the equatorial and the polar LCPs. The polar emission models, the nuclear orbitting model and the quantum mechanical diffraction model, possess this property and are thus favoured by the present experiment.

REFERENCES

1. E. Piasecki and L. Nowicki, Proc. of Symp. on Phys. and Chem. of Fission (Jülich, 1979), IAEA, Vienna (1980) p. 193
2. M.M. Sharma, A.K. Sinha, G.K. Mehta and D.M.Nadkarni, 'Angular distribution of polar light charged particles' to be presented in 'Silver Jubilee Physics Symposium', DAE, India, 1981
3. R. Chaminade, J.C. Faivre and J. Pain, Nucl. Instr. and Meth. 49 (1967) 217
4. I.M. Sobol, ''The Monte Carlo Method'', Mir Publishers, Moscow (1975)
5. H. Goldstein, ''Classical Mechanics'', Addison - Wesley Publishers (1980) p. 109
6. K. Tsuji, A. Katase, Y. Yoshida, T. Katayama, F. Toyofuku and H. Yamamoto, Proc. of Symp. on Physics and Chemistry of Fission, (Rochester, 1973), IAEA, Vienna (1973) p. 405
7. G.M. Raisbeck and T.D. Thomas, Phys. Rev. 172 (1968) 1272
8. P. D'hondt, C. Wagemans, A. Declercq, G. Barreau and A. Deruytter, Nucl. Phys. A346 (1980) 461
9. I. Wilhelm, R. Bayer, J. Cvanda and Z. Dlouhy, Nucl. Phys. A262 (1976) 301
10. S.C.L. Sharma, G.K. Mehta, R.K. Choudhury, D.M. Nadkarni
10. and S.S. Kapoor; Nucl. Phys. A355 (1981) 13.

CHAPTER IV

TRAJECTORY CALCULATIONS

4.1 Introduction

An experimental derivation of the configuration of a fissioning nucleus at the scission point (which essentially means the kinetic energies of the fragments and their relative separation) is one of the important problems before a fission physicist. If the fragments are found to have large kinetic energies at the scission point, adiabatic model will be more appropriate in describing the fission process beyond the saddle point. On the other hand, a statistical model will find support if the scission point kinetic energies turn out to be small.

Results on the binary fission have failed to provide a solution to this problem. Studies in the light charged particle accompanied fission (LCPF) indicate a possibility of obtaining the scission point configuration by using some characteristics of the LCPF. This is possible as there are strong evidences to conclude that the LCP is produced at an instant almost coinciding with the scission point. Also the characteristics of the LCPF and binary fission indicate that their scission point configurations are very similar to each other. The method based on classical mechanics to achieve thi end is known as the method of trajectory calculations.

The method of trajectory calculations essentially attempts to find a set of values of the dynamical coordinates (position-momentum) characterising the scission point configuration (SPC) which when time-developed results in an asymptotic distribution of the dynamical variables in agreement with the experimental results. The method has provided very useful information regarding the SPC. However, various trajectory calculations reported so far have not been able to provide an unambiguous picture of the SPC. Apart from the effects due to several simplifying assumptions made in calculation of the time development of the system, a formalism for reconstructing the SPC from the experimental results is not clearly laid yet. One of the most widely used method assumes a certain distribution in all or some of the SPC-variables as specified by a certain number of adjustable parameters. These parameters are adjusted so that the calculated asymptotic distribution in the dynamical coordinates reproduces the experimental distributions. The distribution characterised by the best fit values of the parameters is taken to correspond to the SPC. The method has obvious limitations due to use of a finite number of parameters in addition to the ambiguity associated with finding out the best set of values of the parameters as the search is made in a multi-dimensional space of the parameters. The second type of method attempts in some way to reconstruct the SPC directly by using the experimental distribution in the dynamical coordinates. The distribution in SPC-variables

is not specified a priori in these calculations. The method permits a search in the phase space of the dynamical coordinates specifying the SPC without introducing any 'artificial' bias for any part of the phase space which may come up in calculations of the first type (mentioned above) due to a priori specification of the distribution in the SPC-variables.

4.1A Phase Space Consideration

The experimental observables in the LCPF relevant to the trajectory calculations are the kinetic energies of the three particles and their relative directions of motion (which give their momentum coordinates). The SPC is essentially characterised by the initial momentum and position coordinates of the three particles. Among the experimental observables, it is the absence of knowledge of the position coordinates of the particles and the time elapsed from the scission point to the moment of the particle detection, which prohibits a calculation of the evolution of the three particle system backward in time to arrive at the SPC starting from the experimental distributions.

The momenta of the particles attain constant asymptotic values in contrast to the position coordinates. The position coordinates, in fact, keep changing even asymptotically at a rate decided by the velocity of the particle. Thus, in the phase space (momentum-position space) of the three particles, points corresponding to various

configurations of the scission point keep translating with different characteristic speeds along the axes corresponding to the position coordinates. To present a more clear picture, we may replace the position coordinates (viz., x coordinate of a particle) by a new set of coordinates obtained from the position coordinates by subtracting out a term consisting of a product of the time elapsed and the corresponding velocity components (viz., x-vt). The points in the phase space characterised by these modified position coordinates will now be stationary asymptotically. The coordinates '(x-vt)' are independent of the position and time of the experimental detection of the particle and bear a signature of the dynamics at the beginning of the motion when the forces were significant. It is clear that an experimental measurement with window on the momenta of the particles determines the integrated probability for various phase space points with same momentum coordinates but different position coordinates '(x-vt)'. Thus the experimental data do not provide any means to distinguish between points in the phase space with same momenta but different '(x-vt)' coordinates and in the present calculation as a first approximation, we have associated equal probability weight to all such points. This probability is decided by the energies of the particles which in turn are related to their momenta. The expressions used for the probability weight are given in Chapter V.

An additional problem of fundamental nature is associated with the method of trajectory calculations. Given a

distribution of initial variables consistent with the experimental data, we may find another distribution of the initial variables consistent with the experimental data by a time evalution of the former. This leads to an ambiguity in the proper identification of the distribution of the initial variables with the scission point configuration or equivalently in finding the proper time scale with reference to the scission moment.

4.2 Review of the Earlier Work

The pioneering work of Halpern[1] brought out the relevance of the method of trajectory calculations for the determination of the scission point configuration (SPC). The possibility of using such an approach was, however, already indicated by the work of Tsien[2], who attempted to investigate the SPC using the experimental velocity distribution of the α-particle in the LCPF of ^{235}U.

Till now, numerous attempts (atleast 24) have been made for reconstructing the SPC by the method of classical trajectory calculations. A large number of calculations start with a known distribution in some of the SPC-variables (while the others are held fixed). As a result of the ambiguity associated with this type of approach and due to the general problem of chosing the proper time origin (as discussed above), several mutually contradicting results have been reported regarding the SPC. A part of the

disagreement is also due to the errors in the earlier measurements on some of the characteristics (viz., the angular distribution of the α-particles) of the LCPF. Most of the calculations employ the experimental data on the α-particle accompanied fission only, as this is the most common mode of the LCPF. In the following, a chronological description of various trajectory calculations is presented.

Calculations by Tsien[2] were done with the initial momenta of the α-particle and the fragments taken as zero. He varied the fragment deformations and distance of the point of emission of the α-particle and could reproduce the experimental velocity distribution of the α-particle.

Halpern[1] worked out in detail the basic idea of trajectory calculations. He suggested that the use of classical mechanics in the time development of the three particle-system (α-particle and fragments) after the scission point could provide useful informations regarding the SPC and proposed the point charge model for the scissioning nucleus. His calculations indicated need of large kinetic energies of the α-particle (4.4 MeV) and the fragments at scission point for reproducing the experimental energy and angular distributions. He had taken a fixed value for the interfragment distance (27 fm) and a fixed point of emission for the α-particle. Thus he considered a variation in the momentum coordinates of the particles but ignored that for the position coordinates in ascertaining the SPC.

Geilikman and Khlebnikov[3] performed trajectory calculations to reproduce the energy and angular distribution of the α-particle under the framework of the droplet model. The magnitude of the initial momentum (whose direction was chosen isotropically) of the α-particle was varied for obtaining the best agreement of the calculated and experimental angular and energy distributions of the α-particle. The initial α-particle energy, uniformly distributed till a maximum value of 1 MeV, gave best agreement. However, the agreement was poor as far as the dispersion around the mean values (which were reproduced well) in the calculated distributions is concerned.

Boneh er al.[4], working under the point charge model, tried to reconstruct the scission point configuration by using the experimental data of Fraenkel[5] on the α-particle accompanied spontaneous fission of ^{252}Cf. Based upon arguments concerning the angular distribution of the α-particle and the anticorrelation between the final energies of the α-particle and fragments, they prescribed high values for the initial energies of the α-particle ($\sim$ 3 MeV) and the fragments ($\sim$ 35 MeV) at the instant of the emission of the α-particle. Under certain reasonable assumptions regarding the interdependence of various initial parameters characterizing the scission point configuration, they succeeded in reproducing the experimental angular and energy distributions of the α-particle. However, the arguments put forth by them were not conclusive. In addition, their conclusions would

have to be reconsidered in view of the disagreement between the result of Fraenkel[5] and the presently accepted data on the α-particle angular distribution.

Katase[6] calculated the α-particle trajectories under different initial conditions and obtained a parametric equation representing the final α-particle energy as a function of initial parameters for different values of the mass ratio and total final kinetic energy of the fragments. He attempted to find the scission point configuration by employing the method of least square for reproducing the experimental α-particle energy distribution with fixed values of the final angle of emission of α-particle, mass ratio and energy of the fragments. The results indicated large values for the interfragment distance ($\approx$ 27 fm) and energies of the fragments ($\approx$ 60 MeV). He used a certain functional form of distribution in the interfragment distance and initial α-particle energy. Apart from the approximations made in the calculations, the result may not be taken as conclusive because of the limitations arising due to a specific choice of the functional forms and possible ambiguities in the method of least squares.

Strictly speaking, trajectory calculations aim at reconstructing the configuration of the scissioning nucleus at the instant of emission of the α-particle, which is expected to be very close to the actual scission point. This fact was explicitly taken into account in the calculations of Raisbeck and Thomas[7]. They assumed that the α-particle

emission occurs a time interval 't_o' after the scission point (at which the fragments are formed with zero velocity). At the instant of emission of the α-particle (with 't_o' as 0.4×10^{-21} sec), the average energies for the α-particle and the fragments were determined as ≈ 2 MeV and 8 MeV respectively with interfragment distance equal to 21.5 fm. The calculated energy distribution agreed with the experimental one while the calculated angular distribution was found to be narrower. In a later calculation by Rajagopalan and Thomas[8], a simple modification in the initial position distribution of the α-particle was done to remove the discrepancy regarding the angular distribution. They extended their point charge model calculations for other light charged particles, viz., protons, tritons and ^{6}He and met partial success in explaining their characteristics with a single set of initial conditions.

Blocki and Krogulski[9] carried out computations for the light charged particle emission in the fission of $^{236}U^{*}$. They suggested that the experimental results are not sufficient to pin point whether the scission point configuration is compact or loose. Under the assumption of sudden approximation, they considered the fragments to be at rest at the moment of scission. In addition to the α-particle, their calculations attempted to reproduce the energy distributions of the ^{1}H, ^{2}H, ^{3}H, ^{6}He and some heavier isotopes. In a subsequent publication[10], they reported the results of their trajectory calculations for the light charged particles

emitted in the spontaneous fission of ^{252}Cf. These results included predictions regarding the energy and angular distributions of the particles. They concluded that the initial conditions for the emission of α-particle, tritons and ^{6}He were quite similar. However, an extremely elongated configuration was needed for the emission of protons and deuterons, which led them to conclude that the emission mechanism for these particles was different from that of α-particles, e.g., emission from the surface of the fragments instead of from the neck.

Nardi et al.[11] carried out trajectory calculations for the light charged particles (^{1}H, ^{2}H, ^{3}H, ^{4}He, ^{6}He and ^{8}He) emitted in spontaneous fission of ^{252}Cf. They attempted, for each of these light charged particles, to derive initial conditions that best fit the experimental results. The basic method of obtaining the initial conditions was similar to the one used by Boneh et al.[4]. The results indicated that both the initial distances between the fission fragments at scission and the initial kinetic energies of the particles tend to decrease as the mass of the light particle increases. The interfragment distance in the proton accompanied fission was found to be unusually large. They suggested that a different mechanism may be responsible for proton emission.

Trajectory calculations by Ertel[12] could successfully reproduce the experimental results on the angular correlation of the α-particle in the spontaneous fission of ^{252}Cf. Values of $\approx$ 0.5 MeV and $\approx$ 1.0 MeV were obtained for the kinetic

energy of the α-particle and fragments respectively.

In the trajectory calculations by Vitta[13] and Fong[14], the initial conditions were taken directly from the predictions of the statistical theory of fission. They could reproduce some of the characteristics of the α-particles.

Gazit et al.[15] used trajectory calculations to complement their measurements on thermal neutron induced fission of ^{235}U. The method adopted was similar to that of Boneh et al.[4]. The calculations indicated a value of 24 fm for the interfragment distance with initial kinetic energies of the α-particle and the fragments as 3.4 MeV and 31 MeV respectively.

Musgrove[16] carried out trajectory calculations for different fixed values of the initial kinetic energy of the fragments and interfragment distance. He permitted variations in the position and momentum coordinates in accordance with the uncertainty principle. Value of interfragment distance equal to ≈ 23.7 fm was found necessary for reproducing the experimental energy and angle correlations for the α-particle. Mean initial α-particle kinetic energy was found to be ≈2.75 MeV.

Tsuji et al.[17] complemented their elaborate experiment on the energy and angular distribution of α-particles in the fission of ^{252}Cf by performing trajectory calculations to derive the scission point configuration. A value of about 22 fm for the interfragment distance was seen to be most consistent with their experimental results. The initial

kinetic energies of the fragments and α-particle were estimated to be ≈ 10 MeV and ≈ 1 MeV respectively.

Calculations by Cavallari et al.[18], Fossati and Pinelli[19] and Krishnarajulu and Mehta[20] attempt to achieve the initial conditions for the scission point configuration from the experimental measurements without any fitting or iterative procedure.

Cavallari et al.[18] used a range of values for the initial parameters. These ranges were divided into a number of intervals. The trajectories were calculated for a fixed mass ratio using different sets of initial values selected from these intervals and for five values of the initial fragment energy. Using the experimental α-particle energy distribution, they assigned a probability weight to each trajectory provided the final kinetic energies of the fragments and final angle of α-particle emission fall within a specified most probable range. The initial conditions calculated by them indicate low values for the kinetic energies of the fragments and the α-particle.

Fossati and Pinelli[19] presented results of their extensive trajectory calculations based on the formulation presented earlier[18]. The reconstructed scission point configuration for the most probable mode of fission showed a douple peaked structure in the initial α-particle kinetic energy. The lower energy peak was situated near 0.5 MeV and corresponded to the prediction of the statistical theory of fission.

Krishnarajulu and Mehta[20] working under the assumption of point charge model, attempted to reconstruct the distributions in the parameters characterising the scission point configuration by using the experimental kinetic energy distributions for the α-particle and the fragments. The input parameters took values distributed over a wide range. By using the statistical weight factor derived from the experimental energy distributions, they obtained the initial distributions. The calculated distributions of initial energies of the fragments and the α-particle are broad and cover the predictions of both the statistical as well as the dynamical theories.

Gavron[21] has done an extensive calculation to determine scission point parameters which fit experimental data on light particle emission from ^{252}Cf. The parameters were given Gaussian distributions. In calculating the standard deviations, care was taken of the Heisenberg's uncertainty relations. Trajectories were calculated for different sets of values of the initial parameters chosen randomly in accordance with their assumed distributions employing the Monte Carlo method. Apart from the energy and angle correlations for the α-particle, data of Cheifetz et al.[22] on the emission of particle unstable ^{5}He were reproduced satisfactorily, with interfragment distance fixed at 21.6 fm. The relevance of ^{5}He data was brought out for getting over a basic ambiguity associated with the trajectory calculations which arises due to the fact that any set of scission point parameters can be

extrapolated to later times to yield larger initial kinetic energies and distances. He extended his calculations to explain the characteristics of other light particles, viz., ^{1}H and ^{3}H. Triton accompanied fission could be fitted by using scission point parameters similar to those for the α-particle accompanied fission. Such a thing could not be achieved for the proton accompanied fission.

Choudhury et al.[23] carried out the trajectory calculations in a three point charge model for the α-particle accompanied spontaneous fission of ^{252}Cf. By using the method of multivariate analysis and assuming the initial α-particle energy to be zero to find the earliest set of scission point parameters, they succeeded in reproducing various energy and angle correlations for the ternary fission of ^{252}Cf. The scission configuration obtained by them corresponded to low kinetic energies of the fragments and α-particle and a interfragment distance of ≈ 20 fm.

Trajectory calculations discussed so far do not consider the effect of the remnant nuclear interaction between the particles after scission. However, few of them have taken some account of this effect in so far as the α-particle was assumed to be absorbed by the fragments if the distance between them falls below a certain value. Incorporation of fragment deformation is also done in some of the works while calculating the Coulomb force. Recently, a critical survey of the point charge model of the scissioning nucleus is given by Dakowski et al.[24]. They suggested that

the inclusion of the nuclear forces among the three particles in the ternary fission plays significant role in the determination of scission point configuration. Their calculations on the lines of Gavron[21] indicate that due to inclusion of nuclear forces the interfragment distance is to be increased from 21.6 fm to 24 fm to reproduce the energy and angular distributions in the ternary fission. They emphasized a need of a more realistic model of the scissioning nucleus than the point charge model.

In a recent publication, Guet et al.[25] have performed trajectory calculations with some account taken for the nuclear forces among the particles after the scission point using the experimental results in the thermal neutron induced ternary fission of ^{235}U of Guet et al.[26]. Their calculations indicated that the experimental correlations in the energy and angle of the α-particle and fragment energy can be successfully reproduced with a compact scission point configuration with interfragment distance around 21 fm and fragment kinetic energy $\gtrsim 8$ MeV.

Apart from the present review, reader is also referred to the review articles by Feather[27], Asghar et al.[28] and Vandenbosch and Huizenga[29].

REFERENCES

1. I. Halpern, CERN Report 6812/P, 1963 (unpublished)
2. S.T. Tsien, J. Phys. Radium 9 (1948) 6
3. B.T. Geilikman and G.I. Khlebnikov, Atomnaya Energiya 18 (1965) 218
4. Y. Boneh, Z. Fraenkel and I. Nebenzahl, Phys. Rev. 156 (1967) 1305
5. Z. Fraenkel, Phys. Rev. 156 (1967) 1283
6. A. Katase, J. Phys. Soc. Jap. 25 (1966) 933
7. G.M. Raisbeck and T.D. Thomas, Phys. Rev. 172 (1968) 1272
8. M. Rajagopalan and T.D. Thomas, Phys. Rev. C5 (1972) 2064
9. J. Blocki and T. Krogulski, Nucl. Phys. A122(1968) 417
10. T. Krogulski and J. Blocki, Nucl. Phys. A144(1970) 617
11. E. Nardi, Y. Boneh and Z. Fraenkel, Proc. of Symp. on Physics and Chemistry of Fission, (Vienna, 1969), IAEA, Vienna (1969) p. 143
12. J.P. Ertel, M.S. Thesis (1968), Emory University, also in ''Statistical Theory of Nuclear Fission'' by P. Fong, Gordon and Breach, New York (1969) p. 191
13. P.B. Vitta, Nucl. Phys. A170 (1971) 417
14. P. Fong, Phys. Rev. C2 (1970) 735
15. Y. Gazit, A. Katase, G. Ben-Devid, R. Moreh, Phys. Rev. C4 (1971) 223
16. A.R. de L. Musgrov, Austral. J. Phys. 24 (1971) 129

17. K. Tsuji, A. Katase, Y. Yoshida, T. Katayaina, F. Toyofuku and H. Yamamoto, Proc. Symp. of Chemistry and Physics of Fission, (Rochester, 1973), IAEA, Vienna (1974) p. 405

18. F. Cavallari, F. Fossati and T. Pinelli, Lett. Al Nuovo Cimento 2 (1971) 1217

19. F. Fossati and T. Pinelli, Nucl. Phys. A249 (1975) 185

20. B. Krishnarajulu and G.K. Mehta, Pramana 4 (1975) 74

21. A. Garvon, Phys. Rev. C11 (1975) 580

22. E. Cheifetz, B. Eylon, Z. Frankel and A. Gavron, Phys. Rev. Lett. 29 (1972) 805

23. R.K. Choudhury and V.S. Ramamurthy, Phys. Rev. C18 (1978) 2213

24. M. Dakowski, E. Piasecki and L. Nowicki, Nucl. Phys. A315 (1979) 370

25. C. Guet, H. Nifenecker, C. Signarbieux and M. Asghar, Proc. of Symp. on Physics and Chemistry of Fission, (Julich, 1979) IAEA-SM-241/F13

26. C. Guet, C. Signarbieux, P. Perrin, H. Nifenecker, M. Asghar, F. Caitucolli and B. Leroux, Nucl. Phys. A314 (1979) 1

27. N. Feather, Proc. of Symp. on Physics and Chemistry of Fission (Vienna, 1969), IAEA, Vienna (1969) p. 143

28. M. Asghar, R. Chastel and T.P. Doan, Journees d'Etudes sur la fission, Cadarache (1971)

29. R. Vandenbosch and J.R. Huizenga, ''Nuclear Fission'', Academic Press, New York and London (1973) p. 385.

CHAPTER V

THE PRESENT CALCULATIONS

5.1 Motivation

Importance of the light charged particle accompanied fission (LCPF) lies in the possibility of studying a large number of intercorrelations among the various characteristics of the LCPs and the fragments. These data are used by the method of trajectory calculations to reconstruct the scission point configuration (SPC) which plays a crucial role in understanding of the fission process. The trajectory calculations attempt to find a set of values of the parameters specifying the SPC which can reproduce the experimental intercorrelations between the various characteristics of the three particles. The configuration, specified by this set actually corresponds to the instant of the light charged particle (LCP) production. The experimental characteristics indicate that the LCP is emitted at (or very close to) the scission point and thus the calculated configuration provides a good description of the scission configuration.

The energy distributions of the LCP and the fragments and the angular distribution of the LCP relative to the fission axis have been studied for different values of the mass ratio for the fragments in the LCPF of several nuclei.

The LCP angular distribution is found to be peaked at nearly right angles to the fission axis (refer to Chapter II). It is, in fact, this important characteristic of the angular distribution which indicates that LCP emission coincides with the scission point. Several workers have studied the angular distribution of the LCPs, mostly concentrating on the alpha-particles. Initial measurements[1] indicated a large width of the angular distribution while the recent experiments with refined techniques prescribe an angular width (FWHM $\approx 18^{\circ}$) nearly half of the initial estimate. Trajectory calculations demonstrated the sensitive dependence of the calculated angular distribution upon the degree of compactness of the scission configuration. This led to more elaborate measurements. The angular distribution has been studied for some judiciously selected LCP events with the objective of narrowing down the position-momentum spread of the SPC. For example, the LCP-angular distribution has been studied by selecting LCPF events with the LCP energy restricted within narrow range[2]. The results indicated lesser focussing of the more energetic LCPs. Such a result has provided an additional clue to the SPC. Recently, a finer selection of the fission events has been made by Guet et al.[3] by imposing the restriction on the fragment kinetic energy and studying the LCP angular distribution. They have also studied the LCP angular distribution with a window on the LCP-energy alongwith that on the fragment kinetic energy. They found that the mean

value of the angular distribution of the alpha-particle remains nearly constant with an increase in the total fragment kinetic energy while the angular width shows a decrease with increasing fragment energy. The restriction on the fragment kinetic energy is expected to narrow down the variations in the initial position-momentum coordinates of the fragments. Keeping this in view, we have performed the conventional trajectory calculations with particular attention to the angular distribution results of Guet et al.[3].

In trajectory calculations, several approaches have been used in ascertaining the SPC (refer to Chapter IV also). Most of the present techniques start with a given distribution in the values of the initial position-momentum coordinates of the three particles in LCPF. Such a distribution is characterised by a certain number of parameters and is assumed to correspond to the SPC. A distribution in the values of the final dynamical variables of the particles is obtained by solving the relevant equations of motion for different sets of values of the initial position-momentum coordinates. These sets are formed by a random selection of the initial coordinates so that the ensemble of such sets has a frequency distribution matching with the assumed distribution in the initial coordinates. The final distribution so calculated is brought in agreement with the experimental results by adjusting the values of the parameters characterising the initial distribution. The distribution characterised by

these adjusted parameters is taken to correspond to the SPC of the fissioning nucleus. The other mode of attack uses the experimentally determined distributions to provide a probability - weight for various combination of the values of initial dynamical variables possible for the SPC. The distributions in the initial values of the dynamical variables (assumed to correspond to the scission point) are obtained with the help of these weights.

The later method appears more general and provides a search over the whole phase space possible for the position-momentum coordinates corresponding to the SPC. However, both of these methods suffer from the basic ambiguity regarding the fixation of the moment of the scission on the time scale chosen in the calculations. Assumption is normally made that the origin of the time scale corresponds to the scission moment. The wide and double humped distributions of the initial kinetic energies obtained by Krishnarajulu et al.[4] and Fossati et al.[5] possibly reflect the effect of this ambiguity as pointed out by Fong[6]. In addition, several approximations are made in solving the equations of motion of the three particle, i.e., the point charge approximation and ignoring nuclear forces among the particles after scission. Moreover, there is also a need of refining the overall method of trajectory calculations so as to arrive at an unique and possibly final description of the SPC.

We have made some efforts towards an improvement in the method of trajectory calculations. The calculations have been performed for the alpha-particle accompanied spontaneous fission of ^{252}Cf.

5.2 Point Charge Model Calculations

In this model, the fragments and the alpha-particles are substituted by point particles and their motion is followed classically under pure Coulomb interaction. A consideration of the de Broglie wavelengths of the particles involved indicatesthat they are small in comparison with the dimensions of the fissioning system. It implies that the classical dynamics should provide to a first approximation a good description of the motion of the three particles.

5.2A Specifying the Initial Configuration

For fixing the initial configuration of the three particles, a total of eighteen position-momentum coordinates need be specified. Here we ignore the internal coordinates of the particles as we are working within the framework of the point charge model. This implies a coverage of initial phase space region in an eighteen dimensional space. However, the specification of the positions of the three particles does not really require nine coordinates in view of the fact that we have to specify their relative positions only. We

need only define three variables to achieve the specification of the relative positions, because the relative positions are fixed once the triangle formed by joining the particles is specified. Thus we need only three variables for an unique definition of the relative positions. In the present calculations, the coordinates chosen are (i) two coordinates to specify the relative position of the alpha-particle and (ii) the distance between the fission fragments. Thus the number of the required coordinates gets reduced form 18 to 12.

Furthermore, the assumption of planar motion implies that the components of momenta of the three particles at right angles to the plane through them are zero. Such an assumption may not be valid, for example, in case the alpha-particle has some rotational motion about the fission axis or the fragments have some rotational motion about the direction of the alpha-particle emission at the scission moment. The bending vibration of the fragments at right angles to the plane of the three particles may also invalidate this assumption. The first possibility can be discarded as this may imply a rotation about the symmetry axis (along which the imminent fragments separate) which is forbidden quantum-mechanically. The effects due to the rest of the possibilities are expected to be insignificant if the associated angular momenta are small. In addition, earlier calculations[7] have indicated that the assumption of the planar motion is a good approximation. Thus, we assume the planar

motion to be valid and the number of the required momentum-coordinates reduces to six from nine. The fissioning nucleus conserves its total linear momentum which is zero in the present case concerning with the spontaneous fission. Thus the total linear momenta of the three particles is zero which provides two equations of constraint for the momentum-components in the plane through them. This brings down the number of the required momentum variables to four. In the present calculations, we take two momentum variables to specify the velocity of the alpha-particle. The other two are to specify the velocity of the fragments. To achieve this, only the total kinetic energy of the two fragments is specified and the individual velocities are obtained by ensuring that the fragments have equal and opposite momenta. Such a procedure ignores the small perturbation due to the recoil of the fragments from the comparatively light alpha-particle. Thus the number of the required momentum-coordinates has been reduced to three.

The parameters chosen to specify the scission point configuration are elaborated in Fig. 5.1 and described below:

i) The coordinates X and Y fix the position of the alpha-particle. The coordinate-system has its X-axis along the fission axis and the origin coincides with the point on the fission axis where the resultant electric field due to the two fragments vanishes.

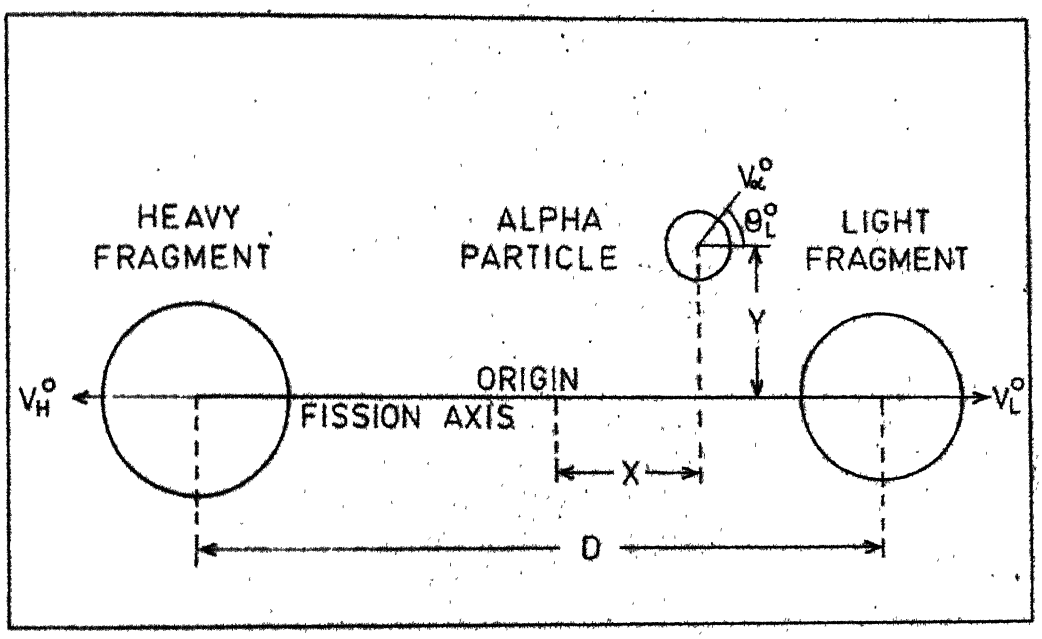

Fig. 5.1. Schematic diagram of the SPC-parameters used in the calculation.

ii) The distance 'D' between the fragments.

iii) The kinetic energy E_α^o and the angle of emission θ_L^o of the alpha-particle.

iv) The total initial kinetic energy of the fragments (E_F^o).

The values of the various parameters mentioned above were varied over a wide range except for the coordinates Y and θ_L^o. The coordinate Y was given a fixed value equal to zero while θ_L^o was chosen isotropically between 45^o and 135^o. As earlier calculations[4,7] indicate that the final values of the dynamical variables are not affected significantly for a reasonable large change in the value of Y and because of limitations imposed on the computer time, such an assumption on the value of Y has been made.

The range of the other coordinates were kept large to cover the values expected on the basis of the statistical and adiabatic assumptions regarding the saddle to scission motion. The values of the parameters are chosen so that any combination of their values has a total energy (kinetic + potential) within the (three sigma) range of the experimentally observed distribution in the total kinetic energy of the three particles. Table 5.1 gives the ranges of the initial parameters.

Table 5.1

The input-parameters and their ranges of values.

Parameter	Symbol	Range of values
Mass Ratio	R	1.0 to 1.8
Interfragment distance	D	17 fm to 28 fm
Initial distance of α-particle from zero field point	X	-7.0 fm to 6.5 fm
Initial distance of α-particle from fission axis	Y	0.0 fm (fixed)
Initial α-particle energy	E_α^o	0.4 to 4.0 MeV
Initial fragment energy	E_F^o	0.5 to 40 MeV
Initial angle of emission of α-particle	θ_L^o	35^o to 145^o

5.2B Mass and Charge Specification of the Fission Fragments

Calculations have been done for several values of the fragment mass ratio. The charges of the fragments are calculated from their masses according to the equation[8] :

$$Z_H = M_H/2.587 \text{ and } Z_L = Z_T - Z_H$$

where Z_H, Z_L represent the mean charges of the heavy and light fragments and Z_T corresponds to the charge of the fissioning nucleus minus the charge of the alpha-particle. M_H is the

mass of the heavy fragment.

Effect of the experimentally observed spread in the fragment charge is estimated to be small and has been ignored in the present calculations. The estimated spread in total potential energy due to this factor is less than 1 %. The emission of prompt neutrons occurs after full acceleration of the fragments and its effect on the fragment kinetic energies is small. In the present calculations, the prompt neutron emission is ignored.

5.2C The Forces Among the Particles and the Equations of Motion

After specifying the initial position-momentum coordinates of the fragments and LCP, the classical equations of motion are solved to get the values of the final kinetic energies of the three particles and their relative directions.

The forces among the particles are taken to be purely electromagnetic, ignoring the effects of the nuclear forces acting in the initial stages of the post-scission motion.

The dominant force among the particles is due to the Coulomb interaction among them. The charge distribution in the fragment volume is not spherically symmetric as the fragments are deformed at the scission point. This implies that the electrostatic force contains contributions due to quadrupole and higher order interactions in addition to the dominant monopole interaction. Moreover, under the mutual

Coulomb field, the fragments may get polarised and resulting dipole moment interaction may also influence the motion. However, their contribution to the total potential energy is estimated to be less than ≈ 4 %.[4,9]. Hence only monopole interaction has been considered to keep the computation simple.

The time taken for the full acceleration of the particles is of the order of $\approx 10^{-20}$ sec. During this motion the electronic configuration in the atom remains unaffected and the fragments move in a stationary electron cloud. The electron cloud provides a force towards the centre of the atom on the fragments and the LCP. This effect is estimated to reduce the total energy of the three particlesonly by 0.02 %. and so it has been ignored. Force due to magnetic interaction among the moving charged particles is smaller by a factor of $(v_1 v_2/c^2)$ as compared to the mutual Coulomb force. In the present case, this factor is nearly 3×10^{-4} and hence the magnetic force is not considered in the present calculations.

The equations of motion to be solved are given by

$$M_i \frac{d^2 X_{ij}}{dt^2} = F_{ij} ; \qquad i = 1, 3 \qquad j = 1, 2$$

where M_i - mass of the i^{th} particle

X_{ij} - j^{th} position coordinate of the i^{th} particle

F_{ij} - j^{th} component of the force acting on the i^{th} particle.

These equations are integrated numerically on a computer with the help of following equations[7]:

$$\Delta t^{(n+1)} = \Delta t^{(n)} \; e^{a}$$

$$\hat{U}_{ij} = U_{ij}^{(n)} + \frac{F_{ij}^{(n)}}{M_i} \frac{\Delta t^{(n+1)}}{2}$$

$$X_{ij}^{(n+1)} = X_{ij}^{(n)} + \hat{U}_{ij} \; \Delta t^{(n+1)}$$

$$U_{ij}^{(n+1)} = \hat{U}_{ij} + \frac{F_{ij}^{(n+1)}}{M_i} \frac{\Delta t^{(n+1)}}{2}$$

where Δt : represents time interval

a : is a constant

U_{ij} : represents j^{th} component of the velocity of the i^{th} particle

$\hat{U}_{ij}$: gives the mean velocity during the $(n+1)^{th}$ step of the integration.

The superscripts on U_{ij}, X_{ij}, F_{ij} and Δt correspond to the integration steps.

The time interval has been chosen so as to be small in the initial stages when the forces are large and increase after each integration step. Such a choice saves computation time.

The forces F_{ij} are related to the position coordinates by the following equation

$$F_{ij} = e^2 Z_i \sum_{k=1}^{2} Z_k \frac{(X_{ij} - X_{kj})}{\left[\sum_{\ell=1}^{2} (X_{i\ell} - X_{k\ell})^2\right]^{3/2}}$$

The subscript k refers to the particles other than the i^{th} one.

The initial values (corresponding to the first step in the numerical integration) of the X_{ij} and U_{ij} are provided by the specified initial configuration. Initial time interval $\Delta t^{(o)}$ is chosen to be 10^{-23} sec. while the constant 'a' is given a value equal to 0.1.

The calculation was terminated after 81 time intervals, that is, after 3.3×10^{-19} sec., by which time the potential energy reduced to less than 1 %. of its initial value.

The final energies are given by

$$E_i = \frac{1}{2} M_i \sum_{j=1}^{2} [U_{ij}]^2$$

and the angle the alpha-particle makes with the direction of light fragment ($\theta_{\alpha L}$) is given by inverse tangent of the ratio of the Y and X components of the velocity of the alpha-particle.

A simple consideration of the difference equations used for integrating the equation of motion indicates that

alpha-particle. The experimental distributions have been assumed to be of Gaussian shape.

Distribution in a SPC-parameter is obtained by summing up the weights of all trajectories with specific values of the parameter. This procedure removes the possibility of any artificial bias for any particular region of the initial phase space of the three particles. By using the statistical weight factor alone a selection of the initial phase space is achieved which describes the SPC.

(ii) Restriction on the Interfragment Distance

Different assumptions regarding the coupling coefficient among various degrees of freedom during the saddle-to-scission descent of the fissioning nucleus essentially predict different kinetic energies of the fragments at the scission point. This, in turn, implies different values of the inter-fragment distance because of the constraints introduced by the experimental kinetic energy distributions. Trajectory calculations have been performed to test the validity of various assumptions regarding the saddle-to-scission motion by restricting the interfragment distance D within a range of ± 0.5 fm at values varying from 19.5 fm to 26.5 fm. The range of variation of D chosen accounts for nearly 60 %. of the variation in the final kinetic energies of the fragments. All other SPC-parameters are allowed to have their normal statistical distributions as demanded by

the experimental kinetic energy distributions used for assigning weights to the trajectories.

We found that the trajectory calculations with all the SPC-parameters having their normal statistical distributions could not reproduce the angular distribution results of Guet et al.[3]. The experimental anticorrelation between the final kinetic energies of the fragments and alpha-particle could be reproduced[4] with value of D restricted in the narrow range. These observations have further prompted us to make a detailed trajectory calculations with values of D restricted within a reasonable range around mean values lying between the limits set by the adiabatic and the statistical assumptions.

5.2E Results and Discussions

Figure 5.2 gives the angular distribution of the alpha-particle for mass ratio R equal to 1.4 with two windows on the total kinetic energy E_F of the fragments and permitting a free variation in all the SPC-parameters. Mean value of the angle of emission of the alpha-particle with respect to the light fragment $\theta_{\alpha L}$ is unchanged for the two E_F windows while the FWHM is more for the higher values of E_F. The result on $\bar{\theta}_{\alpha L}$ agrees with the result of Guet et al.[3] while the variation in the calculated FWHM with E_F is in opposite direction than observed in the experiment. In addition the calculated widths are higher than the experimental value of FWHM $\approx 20^{\circ}$. Similar results have been obtained for other values of the

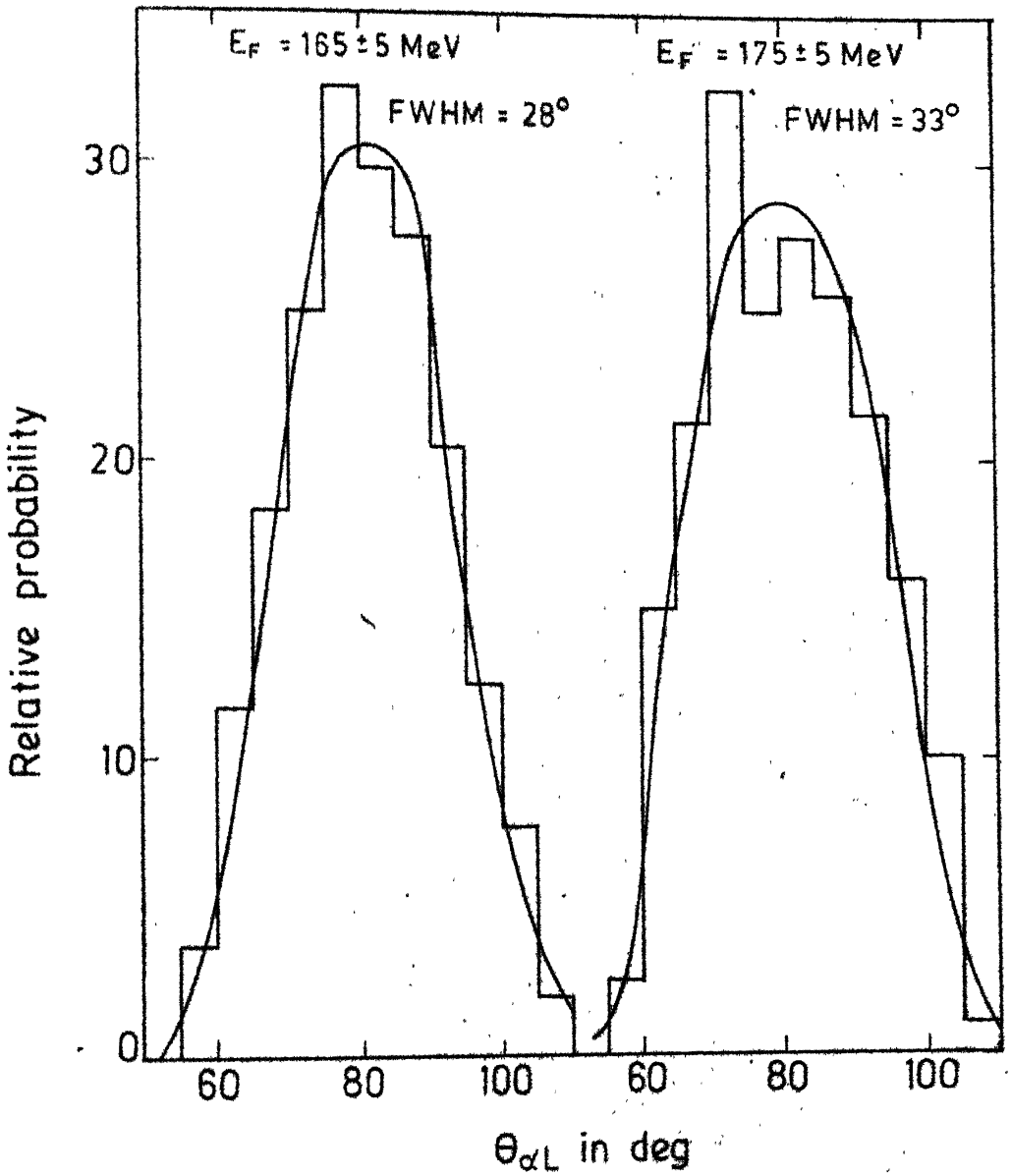

Fig. 5.2. Angular distributions for R=1.4 with no restriction on the value of interfragment distance (D) for different fragment energy (E_F). (Lines are visual fits)

mass ratio.

In our calculations, we have taken an isotropic distribution for the direction of emission of the alpha-particle. So the width of the angular distribution is expected to be more if E_F^o increases as then the Coulomb field responsible for the focussing of the alpha-particles diminishes at a faster rate. The effect of the interfragment distance on the angular width is essentially due to the subsequent limitations on the spread in the position X of the alpha-particle along the fission axis. At lower values of D, the spread in the position of the alpha-particle is expected to be less which should result in a reduced value for the angular width while the opposite effect might be expected for the higher values of D. The change in the calculated angular width with different value of E_F is mainly due to a combination of two opposite effects arising due to changes in the values of D and E_F^o. Higher E_F value corresponds to a reduced D and/or an increased E_F^o. An increase in the calculated angular width with increasing value of E_F implies that the enhancement in the angular width due to increased E_F^o value is higher than the decrease expected on account of reduced D value. A possible reason for this may lie in the approximations made in the calculation. The selection of the spread in the X-value by the weight factor chosen may not be sufficiently realistic due to these approximations. It may be, for example, due to ignoring the nuclear interaction which

may cause more severe limitation on the spread in the position of the alpha-particle (thus narrowing the angular distribution more effectively) for the lower values of D.

Krishnarajulu et al.[4] found that other energy-angle intercorrelations among the fragments and alpha-particle, viz., variation of the $\bar{\theta}_{\alpha L}$ with R, dependence of mean energy of the alpha-particle E_α on $\theta_{\alpha L}$ etc. can be successfully reproduced without any restrictions on D. The experimental anticorrelation could be reproduced only after a restriction in the variation of D is imposed.

We present results of the trajectory calculations performed by fixing the interfragment distance at values lying between 19.5 fm and 26.5 fm in steps of 1.0 fm and allowing a variation of $\pm$0.5 fm around each value. Relations among the E_α, E_F, $\theta_{\alpha L}$ for various values of R have been obtained for different values of D and compared with the experimental results.

It is found after a detailed comparison of the calculated results with the experimental data that only when the value of the interfragment distance is restricted below 21 fm, the calculations reproduce all the experimental correlations.

The calculations indicate that the observed narrowing of the angular distribution with higher E_F values and the anticorrelation between E_F and E_α provide a sensitive check for finding the correct value of the interfragment distance.

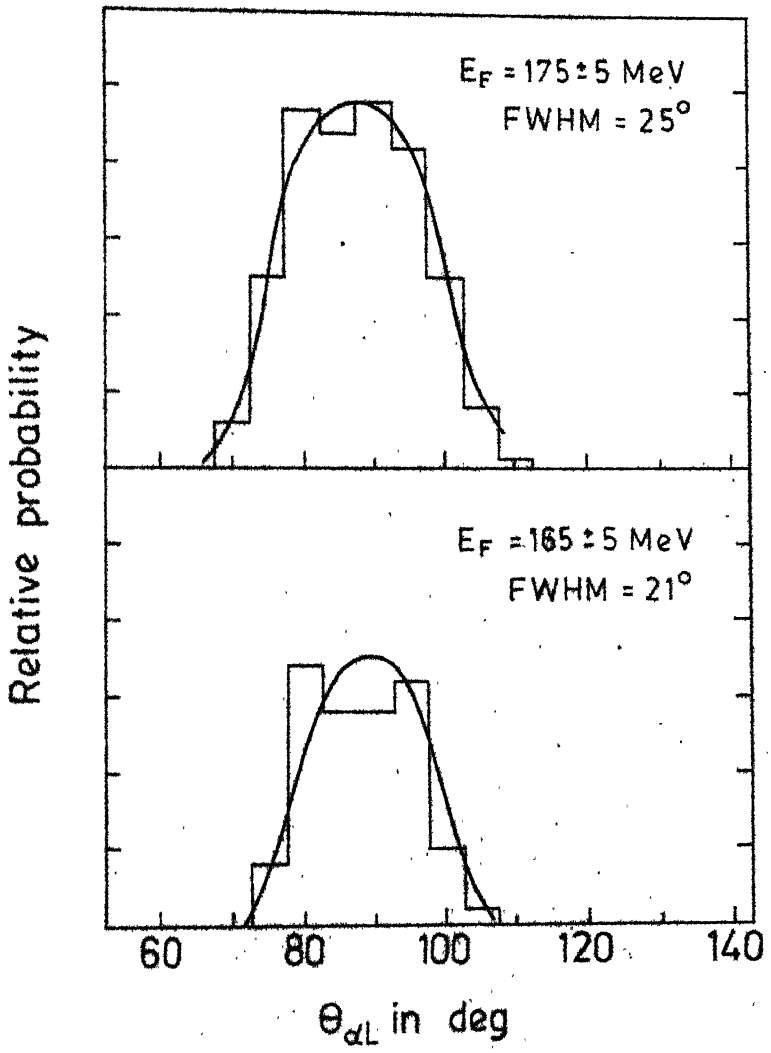

Fig. 5.3. Angular distribution for two windows on E_F. Mass ratio is 1.2 and D = 21.5 ± 0.5 fm. (lines are visual fits)

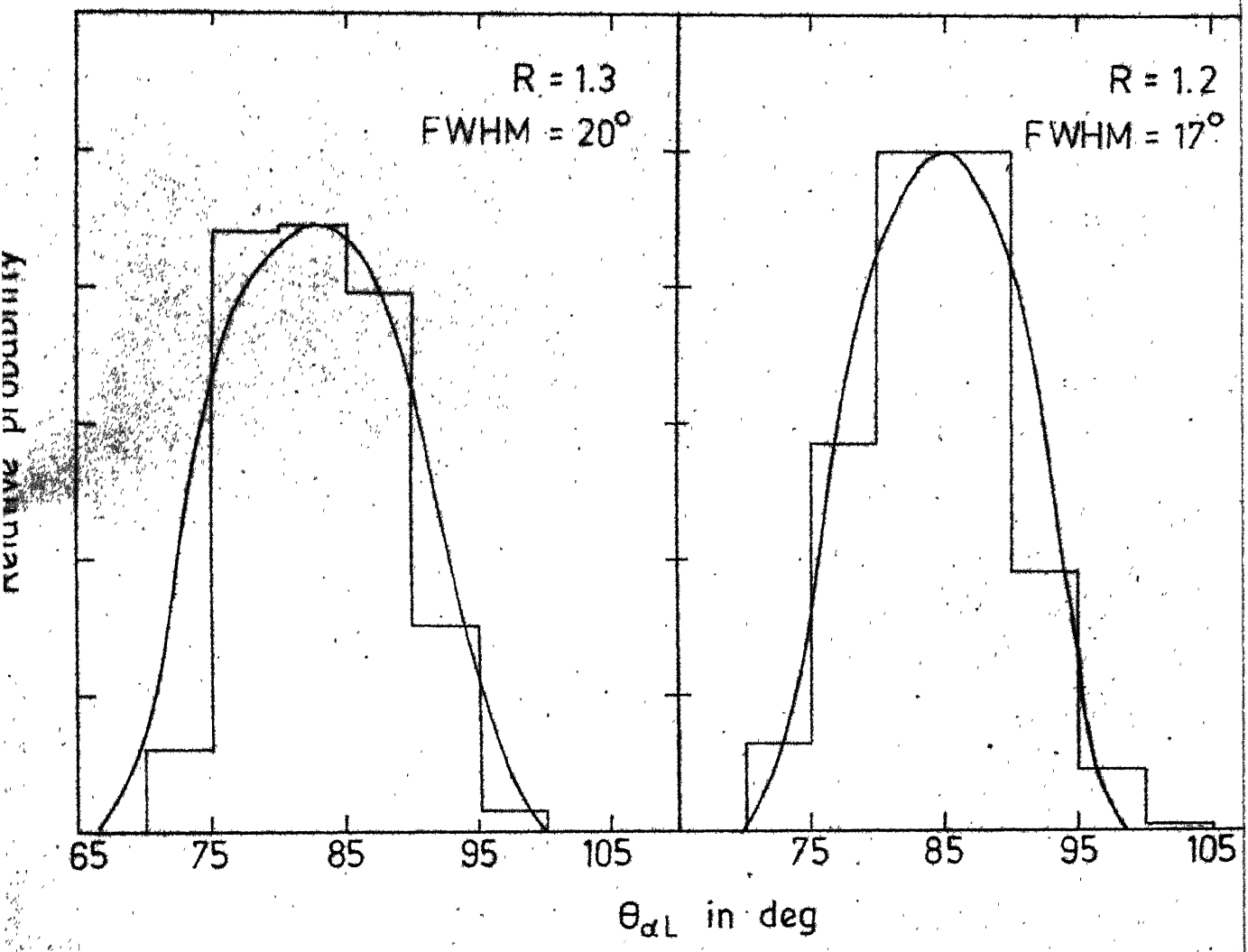

Fig. 5.4. Angular distribution of the alpha-particle. (Lines are vi
fits).

The angular distribution of the alpha-particle for different values of the mass ratio has been found to be reproducible for more than one D-values studied. Similarly, the dependence of the $\bar{E}_\alpha$ upon $\theta_{\alpha L}$ could be reproduced for more than one D-value. Thus these correlations seem to be comparatively less effective in deciding upon an estimate of the actual interfragment distance.

Figure 5.3 shows the angular distribution of the alpha-particle for values of D restricted around 21.5 fm with two windows on the value of E_F. The result for D restricted at 21.5 fm are observed to be contrary to the experimental trend. This indicates the significance of the results of Guet et al.[3] in obtaining the SPC by the help of trajectory calculations.

In the following we shall be describing various experimental correlations that have been reproduced by our trajectory calculations with D restricted below 21 fm.

(i) The Angular Distribution

Figure 5.4 gives the angular distribution of the alpha-particles for R = 1.2 and R = 1.3. Similar results have been obtained for other values of the mass ratio. The calculated angular widths are in excellent agreement with the experimental results[2,10].

Figure 5.5 shows the dependence of the mean angle of emission $\theta_{\alpha L}$ on the mass ratio. Also shown are experimental results of Fraenkel[1] and Fluss et al.[10]. Our results

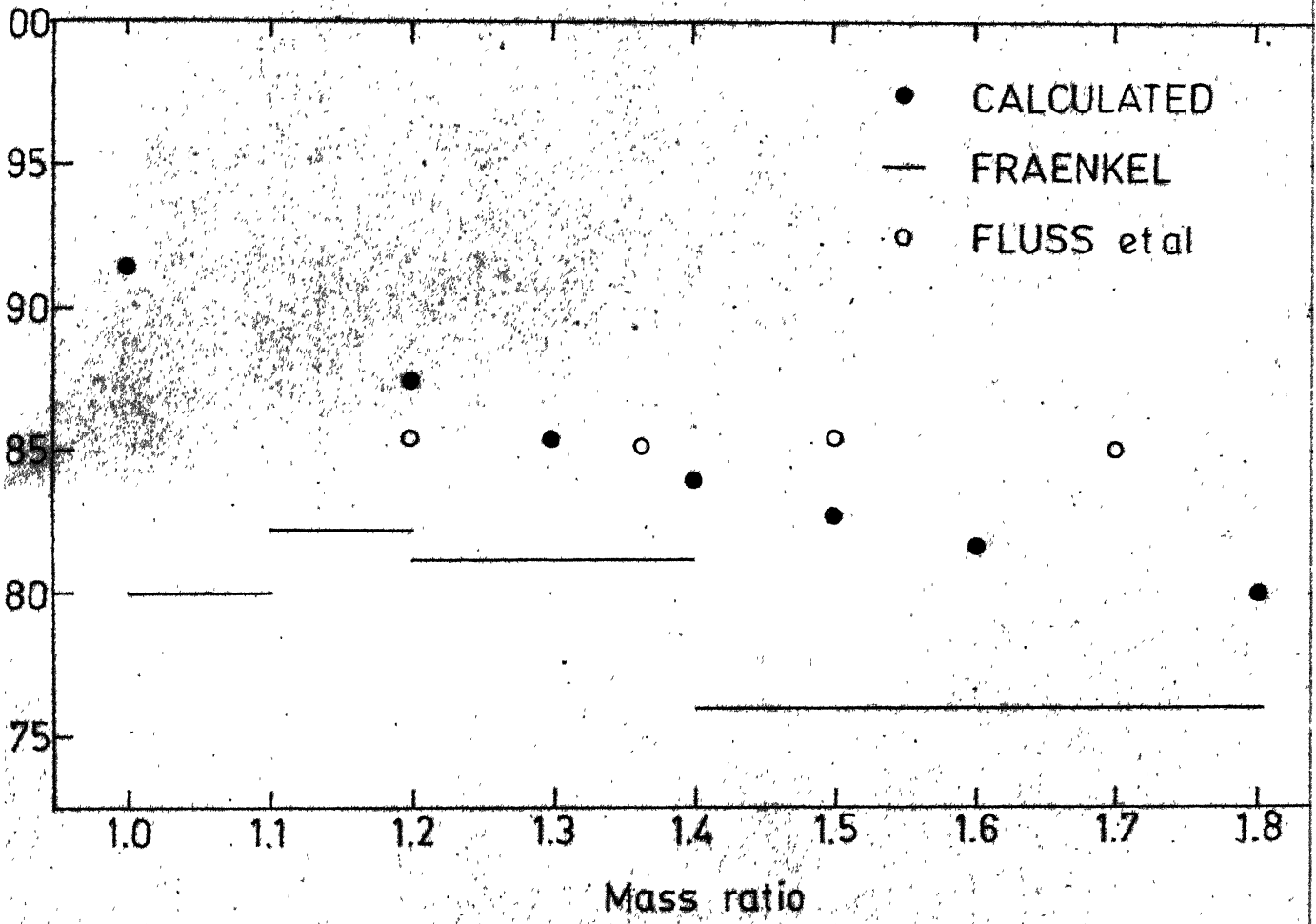

Fig. 5.5 Variation of the average angle of emission of the alpha-particle ($\bar{\theta}_{\alpha L}$) with mass ratio. Also shown are experimental results of Fraenkel [1] and Fluss etal. [10]

lie in between the two experimental results for asymmetric mass division while for near symmetric region, the calculated values are above the experimental result. This disagreement might be partly due to experimental inaccuracies associated with less probable symmetric fission. In addition, it might be a reflection of the approximation made regarding the deformation of the fragments. Light fragment in near symmetric fission is known to be highly deformed as seen by their enhanced prompt neutron yields. In our calculations without including the fragment deformations a value of $\approx 92^{\circ}$ is expected for $\bar{\theta}_{\alpha L}$ near symmetric division due to the symmetry of the electrostatic field of the fragments (in absence of the fragment-recoil, it would be expected to be 90°). A deformed light fragment will exert lesser deviating force upon the alpha-particle as compared to the undeformed heavy fragment. This may cause a decrease in the value of $\bar{\theta}_{\alpha L}$ from 92° making the agreement with the experimental result better.

(ii) Angular Distribution with Window on the Fragment Energy

The calculated mean angle $\bar{\theta}_{\alpha L}$ and the angular width for two windows on the fragment energy E_F are presented in Table 5.2. Fig. 5.6 gives the angular distribution for the mass ratio 1.4 with two windows on the E_F. The value of $\bar{\theta}_{\alpha L}$ remain nearly constant with an increase in E_F while the angular width shows a definite decrease with an increase in E_F. These results are in good agreement with the experimental

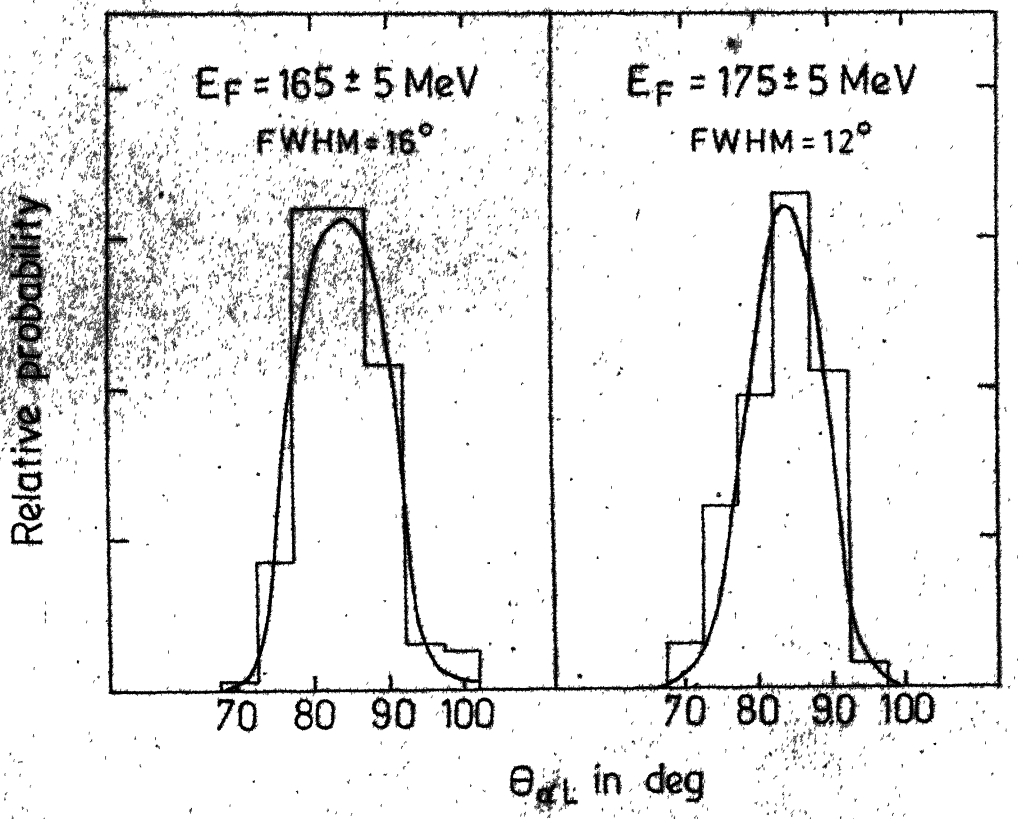

Fig. 5.6. Angular distributions for R = 1.4 with two E_F windows. D is restricted below 21 fm (lines are visual fits).

results of Guet et al.[3].

Table 5.2

Calculated angular distributions for various values of the mass ratio (R) and the kinetic energy of the fragments (E_F).

E_F	165 ± 5 MeV		175 ± 5 MeV	
R	$\bar{\theta}_{\alpha L}$	FWHM	$\bar{\theta}_{\alpha L}$	FWHM
1.2	88.9°	15°	87.4°	12°
1.3	85.5°	17°	85.3°	14°
1.4	84.3°	16°	84.2°	12°

Guet et al.[3] inferred that their experiment favours a SPC with low initial kinetic energies. In such a case the experimental spread in the fragment kinetic energy E_F will be primarily due to variations in the interfragment distance D. In our calculations, the contributions to the spread in E_F are possible due to fluctuations in D as well as in E_F^o. Both of these variables are allowed a free variation over a reasonable range except for the restrictions arising due to the statistical weight factor. As discussed earlier, the change in the angular width with increasing E_F arises due to a combination of a focussing effect caused by a possible reduction in D and a defocussing effect caused by a possible increase

in E_F^o. Our calculations could reproduce the result of Guet et al. only with lower D values inspite of the fact that all values of D were checked in an identical fashion. This may be expected as the focussing effect associated with D-variation becomes relatively dominant for lower D values as compared to the defocussing effect associated with E_F^o variation. Moreover, it must be pointed out that the necessity of taking low D-value for reproducing the results of Guet et al. may become less critical once we remove the approximations of ignoring the fragment deformations and the nuclear interaction.

(iii) Average Energy of the Alpha-particle ($\bar{E}_\alpha$) as a Function of its Angle of Emission ($\theta_{\alpha L}$)

Figure 5.7 shows the variation of the average energy of the alpha-particle as a function of its angle of emission. Also plotted are the experimental results of Tsuji et al.[11]. The position of the minima in the calculated and the experimental curves are in good agreement with each other. The calculated and experimental $\bar{E}_\alpha$ values agree within 0.5 MeV for different values of $\theta_{\alpha L}$.

(iv) Dependence of $\bar{E}_\alpha$ on E_F and $\bar{E}_F$ on E_α

Figure 5.8 shows the correlations among the fragment energy E_F and alpha-particle energy E_α for the mass ratio of 1.3. A linear relation is observed between average fragment

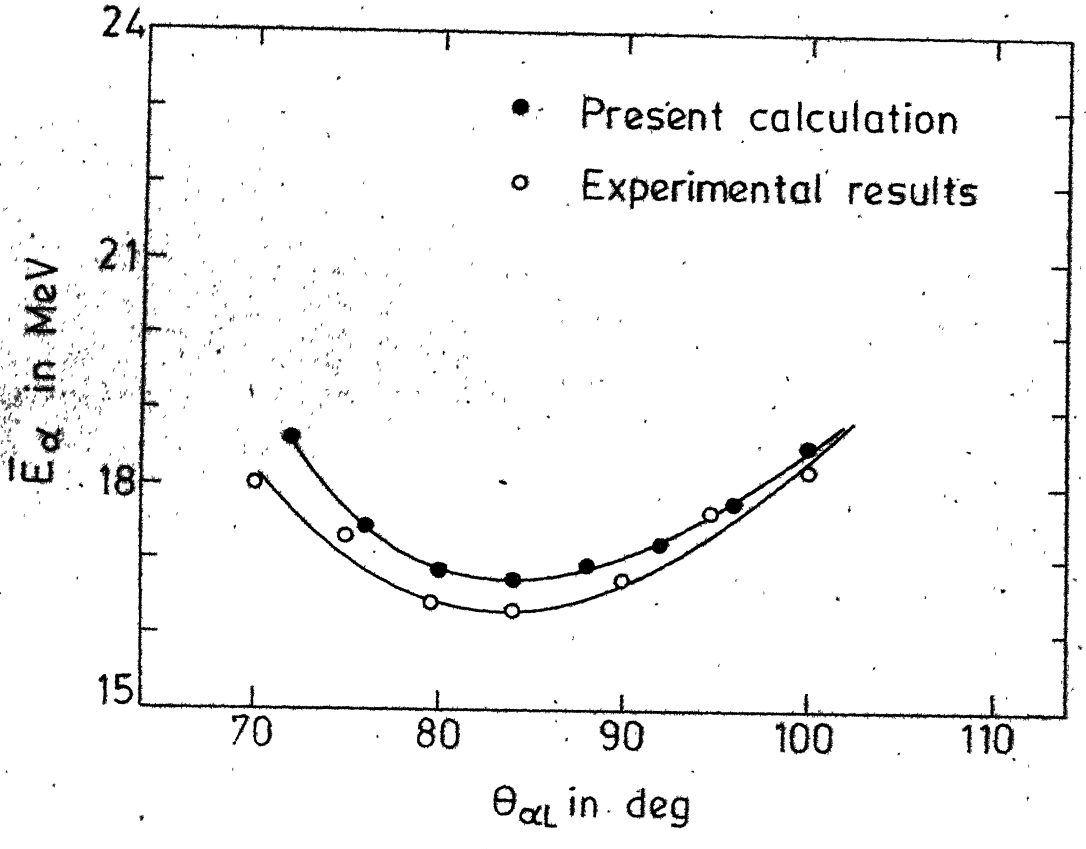

Fig. 5.7. Average energy of the alpha-particle $\bar{E}\alpha$ as a function of its angle of emission $\theta_{\alpha L}$. Also shown are the experimental results of Tsuji et al [11]. (Lines are visual fits).

energy $\bar{E}_F$ and E_α (Fig. 5.8a). The slope of this line comes out to be -0.4 in excellent agreement with the experimental value of -0.44 obtained by Mehta et al.[12]. The relation between average alpha-particle energy $\bar{E}_\alpha$ and E_F turns out to be nonlinear (Fig. 5.8b) in agreement with the experimental result[12].

These correlations have been calculated for different values of R. Figure 5.9 gives the calculated anticorrelation ($\partial \bar{E}_F / \partial E_\alpha$) as a function of the mass ratio R. Also shown are the experimental results of Mehta et al.[12]. The agreement between the two is seen to be satisfactory. Boneh et al.[7] suggested that the anticorrelation between $\bar{E}_F$ and E_α can be reproduced only by chosing high initial kinetic energies ($\approx$ 20 %. of their final values). On the other hand Chaudhury et al.[13] could reproduce the anticorrelation condition with smaller values of the initial kinetic energies. The calculations of Krishnarajulu et al.[4] covering lower as well as higher values for the initial kinetic energies indicated that the correct anticorrelation is reproducible if the D-variation is limited in a narrow range. Necessity of limiting the D-variation is attributed[4,7] to a possible positive correlation between E_α^o and E_F^o arising with D-variation which gives rise to a positive correlation between E_α and E_F. In the present calculations, the permitted variation in D is reasonably wide accounting for nearly 60 %. of the observed spread in E_F. With this much

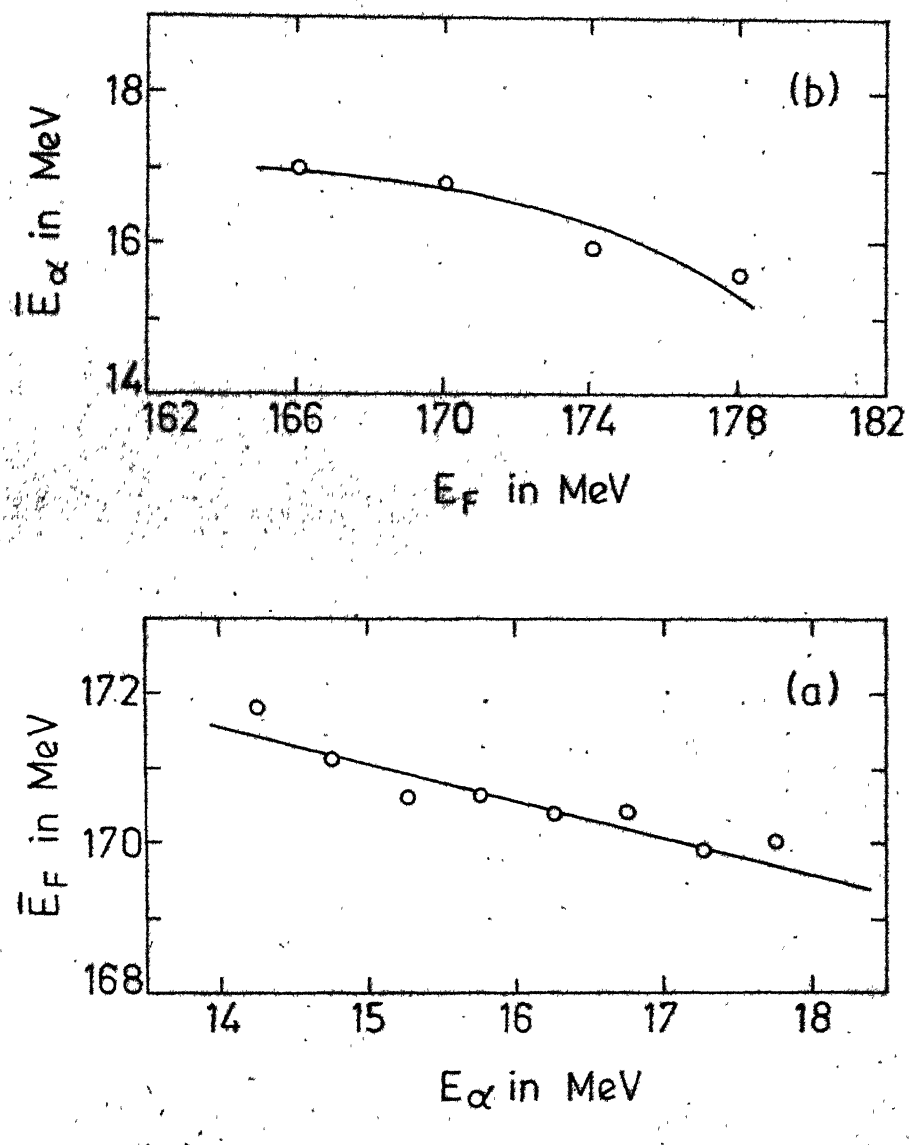

Fig. 5.8. (a) Dependence of average fragment energy $\bar{E}_F$ on the alpha-particle energy E_α.
(b) Dependence of the average alpha-particle energy $\bar{E}_\alpha$ on the fragment energy E_F. Mass ratio is 1.3. (Lines are visual fits)

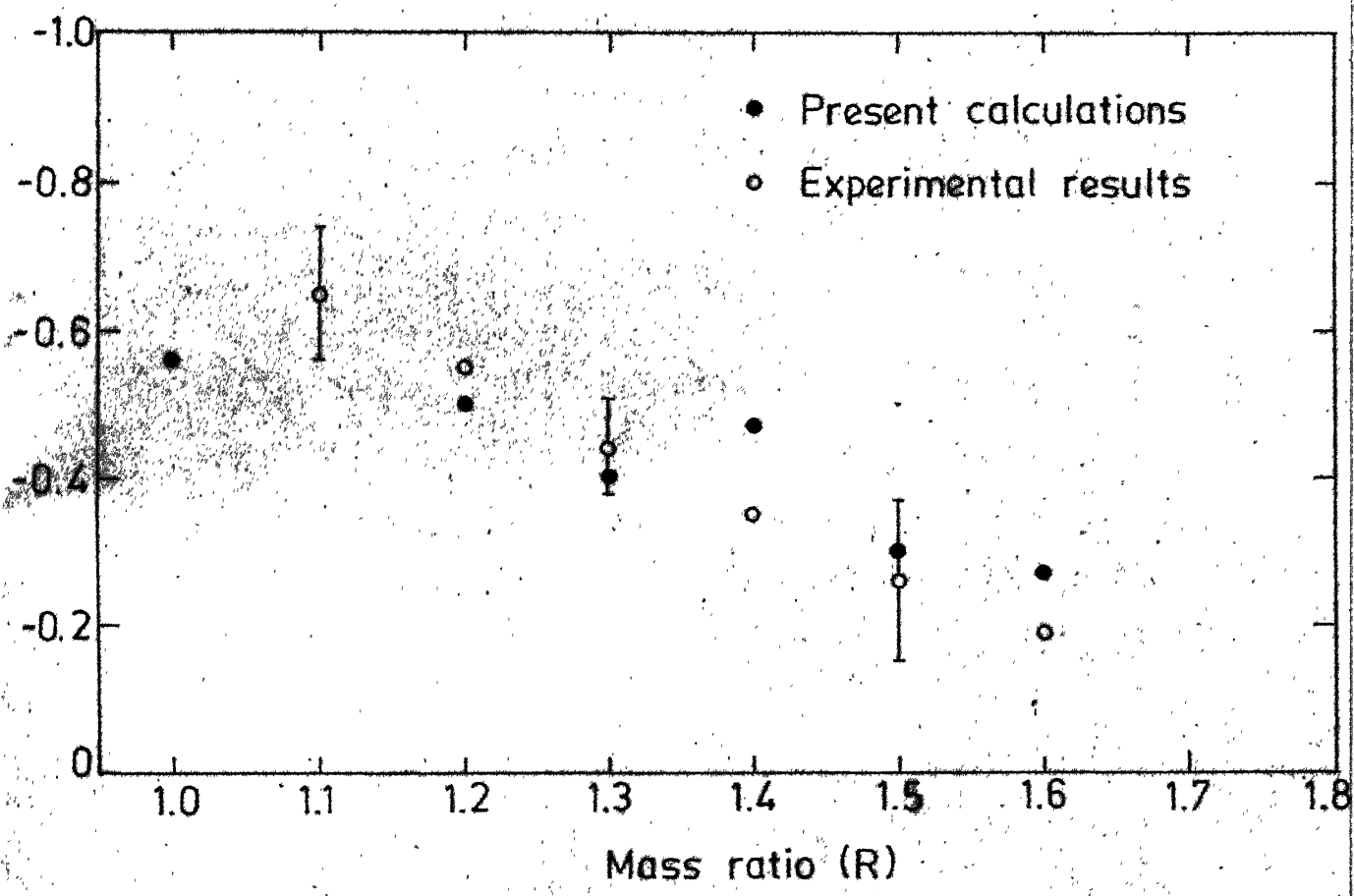

Fig. 5.9. Anticorrelation ($\partial \bar{E}_F / \partial E_\alpha$) as a function of the Mas ratio (R). Also shown are experimental results of Mehta et al [12].

of variation in the D-value, the anticorrelation condition could not be reproduced for higher D-values. At lower D-values, the interplay between the various SPC-parameters in deciding the asymptotic energies and angles becomes fairly strong. This makes any qualitative reasoning for searching the source of the observed anticorrelation rather difficult and less reliable and emphasizes the need of an accurate and unbiased approach for ascertaining the SPC.

(v) Distributions in the Fragment Kinetic Energies (E_F) and the Alpha-particle Energy (E_α)

We used experimental E_F and E_α distributions for assigning the weights to the trajectories. As a cross check for the procedure used, we have calculated the final fragment energy and α-particle energy distributions. Mean values of E_F and E_α are quite accurately reproduced for all the values of mass ratio. The width of the E_F distribution agreed quite satisfactorily with the one used in assigning the weights. However, the width of the alpha-particle energy distribution was low (about 0.6 times the width used in assigning the weights). This might be a reflection of the approximations involved with the point charge model calculations.

(vi) Distributions in the SPC-parameters

Figure 5.10 (a) and (b) give the distributions in the initial α-particle energy and the total fragment kinetic

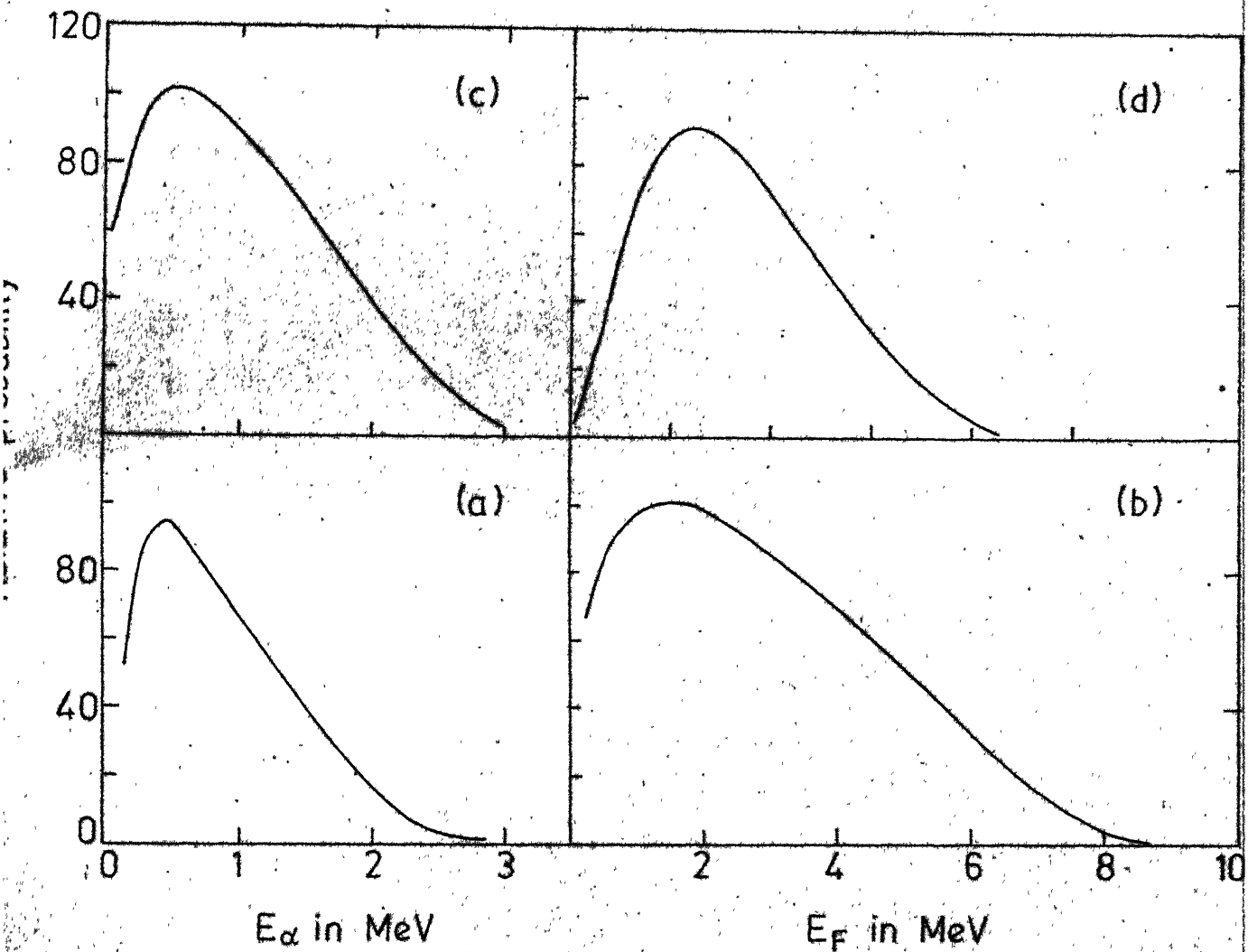

Fig. 5.10. (a) and (b) are the calculated distributions in the initial α-particle energy (E_α) and fragment kinetic energy (E_F) (c) and (d) are the distributions in E°_α and E°_F as obtained by assuming Maxwellian energy distributions for the α-par light fragment and the heavy fragment with temperature 0.5

energy obtained from our calculations. The calculated distributions of the E_α^o and E_F^o are sharply peaked at about 0.5 MeV and 1.2 MeV respectively, with high energy tails. They seem to resemble very closely the Maxwellian distributions shown in Fig. 5.10(c) and (d). They have been obtained by assuming a Maxwellian energy distributions for the α-particle, light fragment and the heavy fragment with temperature 0.5 MeV. Distribution in E_F^o, the sum of the energies of the two fragments, is obtained from individual distributions by using the Monte Carlo method. Such a shape of the initial kinetic energy distribution for the light charged particle was used by Blocki et al.[14] and might be expected under statistical equilibrium.

The distribution in the position of the alpha-particle (the X-coordinate) is shown in Fig. 5.11. It is found to be peaked at about 1 fm towards the light fragment from the zero field point with a full width at half-maximum (FWHM) of about 5 fm. This distribution actually represents distribution of the projection of the actual emission point on the fission axis. It may be inferred that this spread in the X-coordinate contributed most dominantly to the angular width in the present calculations.

5.2F Conclusions

The experimental correlations between the energies of the three particles and the angle of alpha-particle

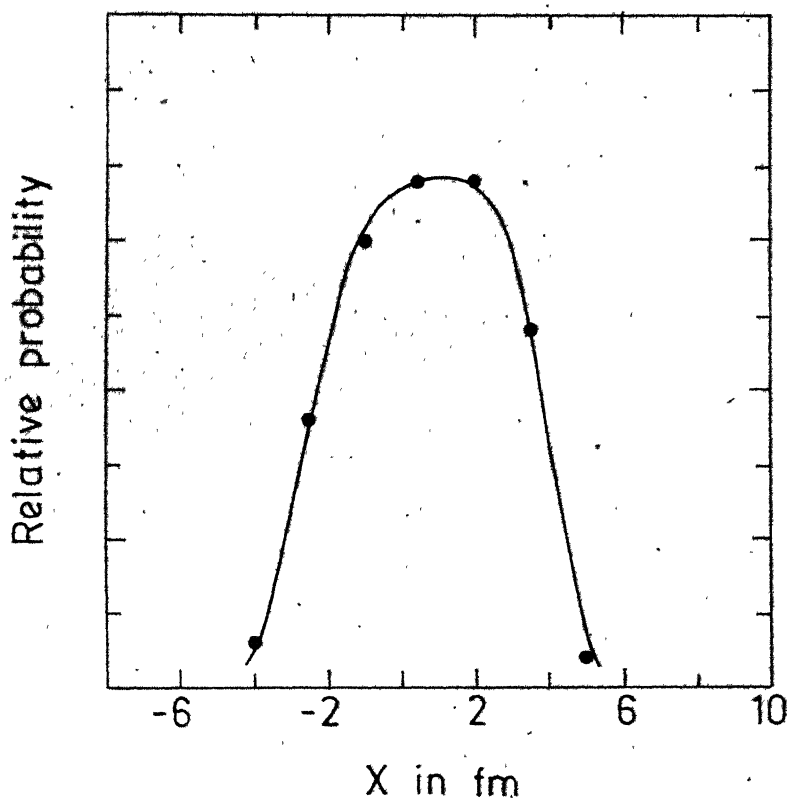

Fig. 5.11. Distrbution of the point of emission (X) of the alpha-particle. The point with X_o=0 fm corresponds to the point of zero coulomb fields of the fragments. Line is a visual fit.

emission could be successfully reproduced by our trajectory calculations. Within the errors due to approximations made in the point charge model, a compact scission point configuration with low initial energies is favoured by our calculations. However, as pointed out earlier, there is a basic ambiguity in determining the SPC using trajectory calculations. During the time evolution of the trajectory, any time along the trajectory can be taken as the scission point. However, we find that for a typical trajectory characterised by E_α^o = 0.5 MeV, E_F^o = 1.2 MeV, Y_o = 0 fm and D = 20.5 fm (these are the most probable values as determined by our calculation), distance of the alpha-particle from the fission axis, exceeds 3 fm when the fragment separation becomes more than 23 fm. Davies et al.[15] give an estimate of the neck radius of about 2 fm at scission. Taking 3 fm as a limiting value of the neck radius at scission, we see that for D > 23 fm, the configuration of the three particles is nonphysical for the scission point (assuming that the α-particle emission coincides with the scission and occurs in the neck region). Considering the fact that the scission point parameters can be extrapolated to later times which will yield larger values for the initial kinetic energies and the fragment separation, we can get estimates of the range of variations in the initial parameters by imposing the condition that Y at scission point should be < 3 fm. We find that under this restriction, upper limits of the possible values of E_α^o, E_F^o and D would be $\approx$ 1.4 MeV, 16 MeV and 23 fm

respectively.

5.3 Improvements in the Point Charge Model

We have, so far, discussed the results of the trajectory calculations by using the point charge model for describing the post scission motion of the fragments and alpha-particle. We could reproduce various energy-angle correlations among the three particles when we restricted the interfragment distance (D) around 20.5 fm.

A simple consideration of the fragment sizes and range of the nuclear force indicates that the effect due to the nuclear forces may be significant for the alpha-particle emission points lying close to the fragments. The X-distribution obtained by the point charge model calculations (Fig. 5.11) shows a spread of nearly 5 fm. This spread plays a significant role in reproducing the width of the angular distribution as trajectories with emission angle away from the most probable direction start mainly from the points with X-values away from the mean value. Upon the inclusion of the nuclear interaction, such trajectories might undergo substantial changes resulting in a modified angular distribution. The fraction of trajectories thus affected may be pretty large in the present case of compact SPC. This may demand alterations in the SPC obtained by the point charge model. Once we incorporate the correct nuclear deformations at the scission point, the above mentioned

effect can cause substantial changes in the predictions of the trajectory calculations based on point charge model even with higher D-values.

We have performed trajectory calculations with an improved model incorporating the nuclear interaction. The calculations include the effects of the fragment deformations.

The restriction on the Y-coordinate of the alpha-particle (Fig. 5.1) has been removed and all the SPC-parameters have been allowed a free variation.

The weight factor used in selecting the SPC from the phase space covered by the calculations, has been modified to provide a proper time scale with its origin coinciding with the instant of scission. For this purpose the data of Cheifetz et al.[16] on the ^{5}He emission in fission has been used.

5.3A Specifying the Initial Configuration

The parameters defining the SPC are the same as used in the point charge model calculation (Fig. 5.1). Rotational and vibrational degrees of freedom are ignored. The fragment deformations at the scission point have been approximated by their ground state values. The heavy fragment is taken to be spherical as it is having a nearly closed shell while the light fragment has been taken to be of ellipsoidal shape. The deformation of the light fragment is specified by the ratio of axes along and at right angles to the symmetry axis, which is given a value equal to 1.3.

Values of the parameters E_F^o (initial total kinetic energy of the fragments), E_α^o (initial kinetic energy of the alpha-particle), D (the distance between the centres of mass of the fragments) and X (the position of the alpha-particle along the fission axis) have been varied over a wide range in uniform steps. Values of E_α^o and E_F^o were chosen randomly within narrow ranges around their mean values, which were varied in uniform steps. Such a smearing of the values of initial kinetic energies is done to provide an uniform and unbiased coverage to the initial phase space of the three particles. The parameters Y (the distance of the alpha-particle from the fission axis) and θ_L^o (the angle of emission of the alpha-particle) are allowed values between 0.0 fm to 3.6 fm and 45^o to 135^o respectively. These values are chosen randomly for each set of values of parameters E_F^o, E_α^o, D and X.

The range of variation of D is calculated for each set of values of E_F^o and E_α^o, using the constraint due to the experimental distribution in the total kinetic energy of the three particles.

As described later, for certain configurations of the fragments and alpha-particle, the latter may get trapped by the fragments due to the remnant nuclear attraction. In particular alpha-particle gets absorbed when the initial position of the alpha-particle is very close to one of the fragments. Range of the parameter X has been calculated

for different D-values as a function of Y for typical E_F^o and E_α^o values by finding the closest distance from the fragments to which the alpha-particle can be placed without getting absorbed by the fragments. The range of X, thus determined, is found to be dependent on the interfragment distance, being more for larger D values. (However, it might be pointed out that this dependence may become milder, once we include the correct deformations at the scission point).

5.3B The Forces Among the Particles and the Equations of Motion

Apart from the monopole term in the Coulomb force among the particles, quadrupole interaction has been included, which is derived from the quadrupole interaction potential due to a nucleus with ellipsoidal deformation. The potential is given in terms of the coordinates (r,θ) by the following equation :

$$V_{quad}(r,\theta) = \frac{Ze\ (c^2-a^2)}{5r^3} P_2(\cos\theta)$$

Here c and a are respectively the values of the semi-axes along and at right angles to the symmetry axis of the ellipsoid. The symmetry axis is taken to lie along $\theta = 0$. Ze represents the charge of the nucleus.

The nuclear force between the alpha-particle and the fragments is calculated from the potential obtained by the energy density formalism. The nuclear interaction among the

fragments has been ignored. The formula given by Ngo et al.[17] was used for calculating the nuclear potential $V_N(S)$ which is given below for the spherical nuclei :

$$V_N(S) = \frac{A_1^{1/3} \cdot A_2^{1/3}}{(A_1^{1/3} + A_2^{1/3})} U_N(S)$$

where $U_N(S) = -V_o \exp(-0.27\ S^2)$; $S > 0$

$= -V_o + 6.3\ S^2$; $S < 0$

with $V_o = 27$ MeV

and $S = R - r_o\ (A_1^{1/3} + A_2^{1/3})$

where R = Distance between the centroids of the two nuclei

r_o = 0.98 fm

A_1, A_2 = Atomic masses of the nuclei.

In case of the light fragment, the necessary corrections were made in the expression for $V_N(S)$ to account for the deformation. The coefficient of $U_N(S)$ in the expression for $V_N(S)$ is modified to include the effect of position dependent curvature of the nuclear surface. For a given position of the α-particle, point 'P' on the surface of the light fragment lying closest to the it is determined (see appendix for the method of calculation). If (r,θ) are

the coordinates of this point then the coefficient is given as

$$\frac{A_1^{1/3} \cdot A_2^{1/3}}{A_1^{1/3} + (A_2^{1/3}/F)}$$

with

$$F = \left[\frac{\beta^4 \tan^2\theta + 1}{\beta^2 \tan^2\theta + 1} \right]^{3/2} \beta^{1/3}$$

where $\beta = c/a$ for the light fragment and A_2 refers to its mass.

The value of 'S' is calculated by using this point 'P' on the surface of the light fragment so as to get the shortest distance between the surfaces of the nuclei. The equationsof motion are similar to those used in the point charge model calculations. The procedure for numerical integration is same as described in section 5.2C except that the time interval for the steps of integration is made 10^{-23} sec. , moment the nuclear force between the nuclei becomes significant. This ensures a good computation accuracy. The energy conservation during the entire trajectory was better than 1 %. .

5.3C Procedure of Obtaining the Scission Point Configuration (SPC)

The general method for obtaining the SPC is based on the arguments presented in Chapter IV and similar to the one used

in the point charge model calculations.

The experimental results of Cheifetz et al.[16] on the emission of the particle unstable ^{5}He are used in the selection of the proper time origin (which coincides with the acual scission point). The particle ^{5}He decays into ^{4}He and a neutron with half life of $\tau_{1/2} = 8\times10^{-22}$ sec. The decay half life is small compared to the time needed for the full acceleration of the particles. Thus the decay occurs while the light particle still experiences the Coulomb field of the fragments. From the neutron energy, the energy of the particle ^{5}He at the time of its decay was deduced by Cheifetz et al. This provides an independent means to put a constraint on the SPC as it demands that the light particle should have an energy of 6.3 ± 0.8 MeV after an average time of $\tau_{1/2}$ from the scission point. As the energy of the ^{5}He at the instant of its decay is essentially calculated from the neutron energy, in the present calculations we have calculated energy of the neutron emitted from the ^{5}He decay.

For each set of the SPC-parameters along with the alpha-particle trajectory, a ^{5}He trajectory was calculated. The ^{5}He trajectory was followed for about twice the half life of ^{5}He-decay. The energy of the neutron from the ^{5}He was calculated by assuming the emission angle to lie within $\pm 5^{o}$ (in the centre of mass frame) at ten equal time intervals. An average energy of the neutron $\bar{E}_n$ was evaluated for the exponential decay of ^{5}He. Under the assumption that the SPC

is identical for the ^{4}He and ^{5}He accompanied fission, a weight factor W was assigned to the corresponding alpha-particle trajectory, which is given as

$$W = P_{E_F} . P_{E_\alpha} . P_{E_n}$$

where P_{E_F}, P_{E_α}, P_{E_n} represent the probability factors corresponding to the experimental distributions in the energy of the fragments (E_F), the alpha-particle (E_α) and the neutron (E_n) from the ^{5}He breakup respectively.

5.3D Results and Discussions

Figs. 5.12 and 5.13 provide a typical illustration of the effects of incorporating the nuclear forces. The drastic effects on the final values of the dynamical variables are found due to the presence of the nuclear interaction. However, this occurs for certain initial configurations only. For some initial configurations, the alpha-particle trajectory does not approach the fragments close enough and the resulting asymptotic values of the dynamical variables are very close to the values obtained from the calculations without nuclear forces. In addition, some initial configurations result, due to nuclear attraction, in the reabsorption of the fragments (see Fig. 5.13). In the absence of the nuclear interaction, the very same configurations result in the emission of the alpha-particle with reasonable asymptotic values for the dynamical variables.

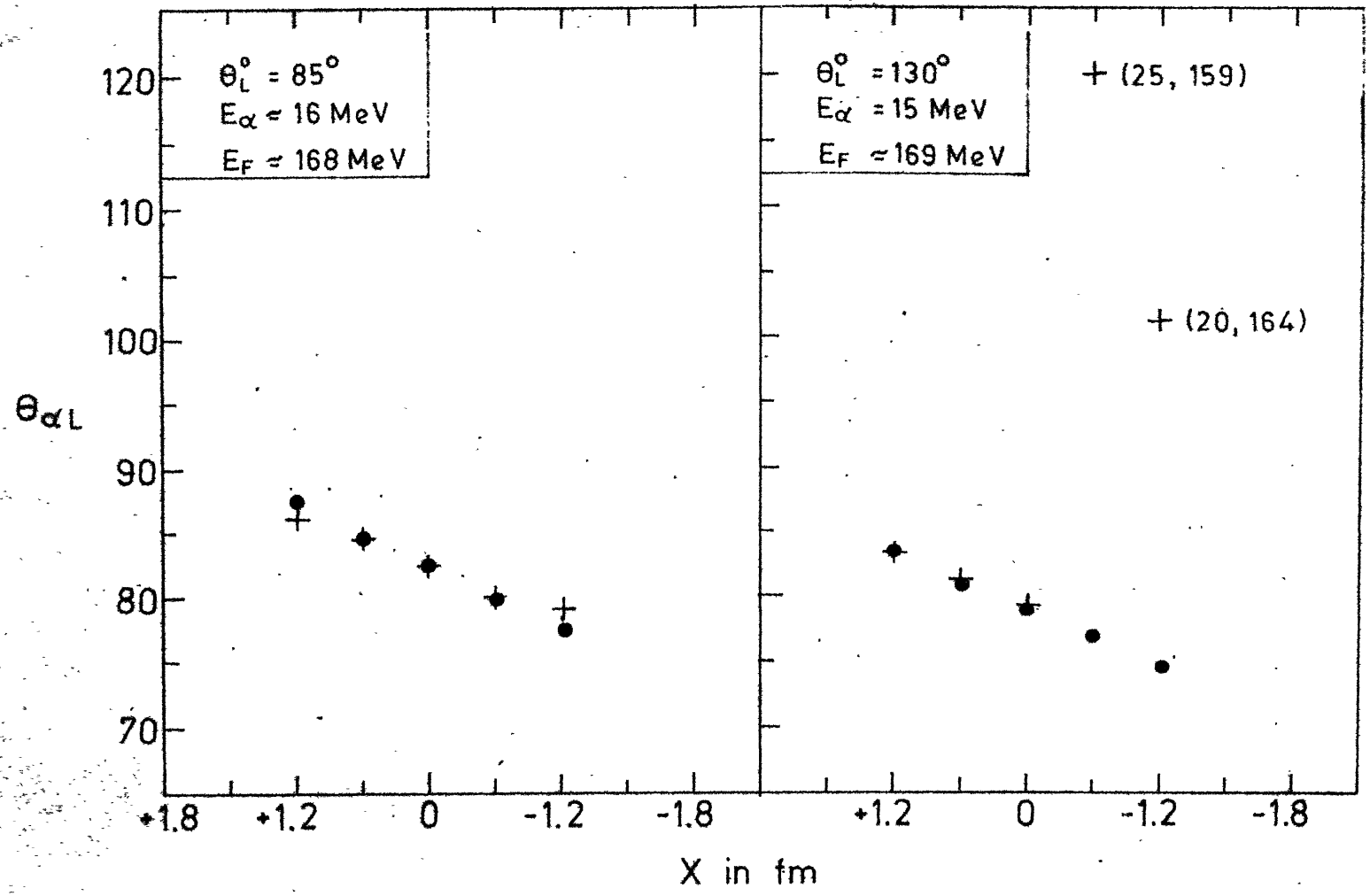

Fig. 5.12. The asymptotic angle $\theta_{\alpha L}$ of the alpha particle for two values of θ_L° as a function of coordinate X. Values of D = 23.5 fm, E_α° = 1.8 MeV, E_F° = 19 MeV, Y = 0.0 fm. Values of the E_α, E_F are nearly constant and are given in the insets except for the two points on the right hand top corner. • - Corresponds to calculations without nuclear interaction while + corresponds to calculations

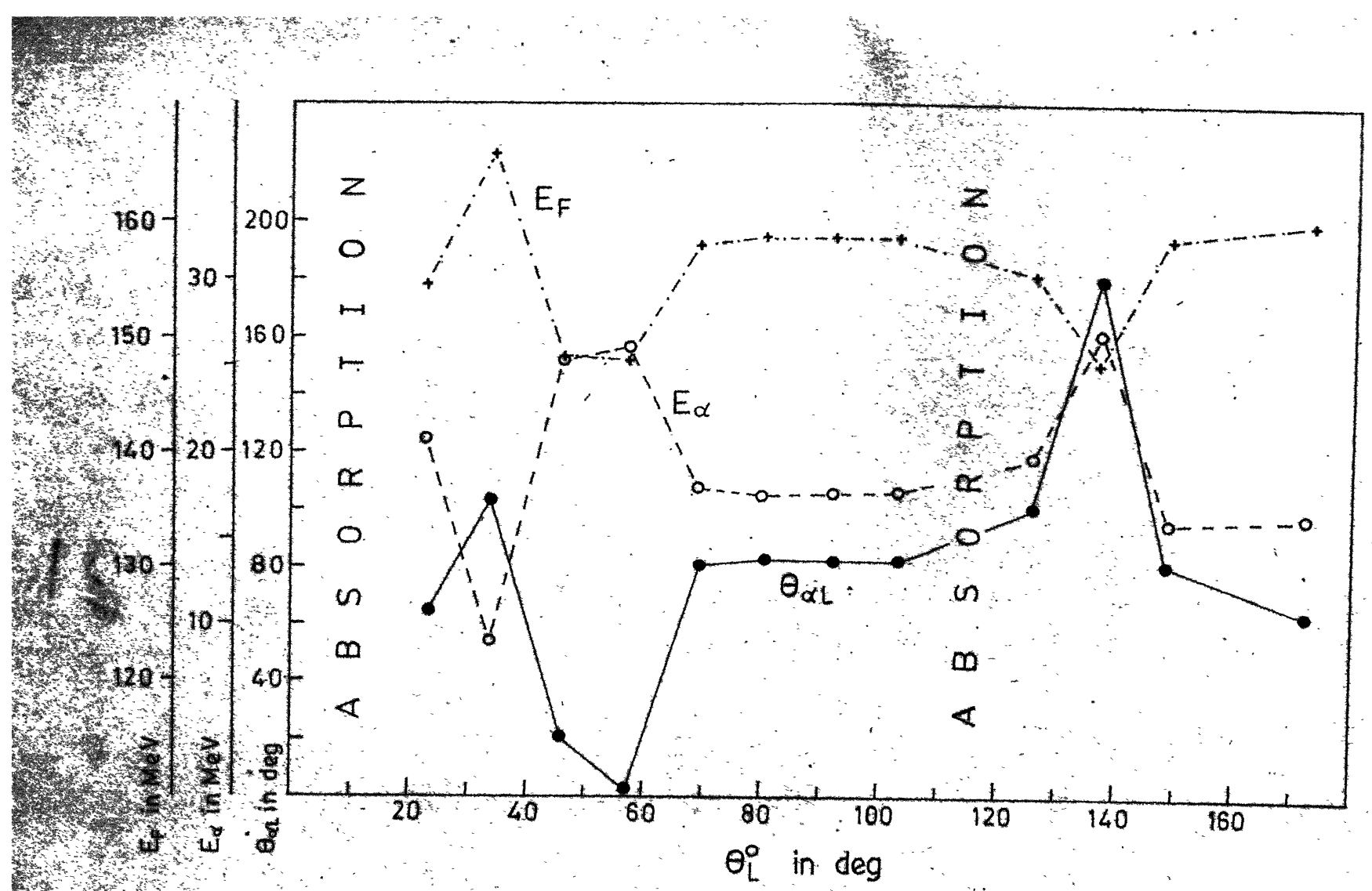

Fig. 5.13. The angle of emission ($\theta_{\alpha L}$), energy of the α-particle (E_α) and the total fragment kinetic energy as a function of the initial angle of emission (θ_L°). D = 22 fm, E_α° = 1.0 MeV, E_F° = 4.0 MeV, X = 0, Y = 0. Lines are drawn only to guide the eye.

This indicates that the approximation, such as ignoring the nuclear interaction, erroneously permits inclusion of non-physical parts of the initial phase space of the three particles in the trajectory calculations. Further illustrations of the effects on the final values of dynamical variables due to inclusion of the nuclear force are provided later in the discussions of the tarjectories that result in the polar emission of the alpha-particle.

In the following, we shall be first presenting the results obtained by allowing all the SPC-parameters to have their normal distribution as demanded by the experimental E_α, E_F and E_n distributions used for assigning the probability weight. The modifications in the results due to inclusion of ^{5}He data in providing the probability weight factor have been discussed. Later the results obtained by imposing restrictions on the variation of the interfragment distance and some results on polar emission will be presented.

5.3D-I Results With Free Variation in all the SPC-Parameters and Discussion

(i) Angular Distribution and its Correlations with the Energy

Fig. 5.14 gives the calculated angular distribution of the alpha-particle by using (E_α, E_F) weight as well as (E_α, E_F, E_n) weight. Inclusion of the 'E_n-term' in the weight factor results in the narrowing down of the angular distribution. Both the weightsprovide satisfactory agreement

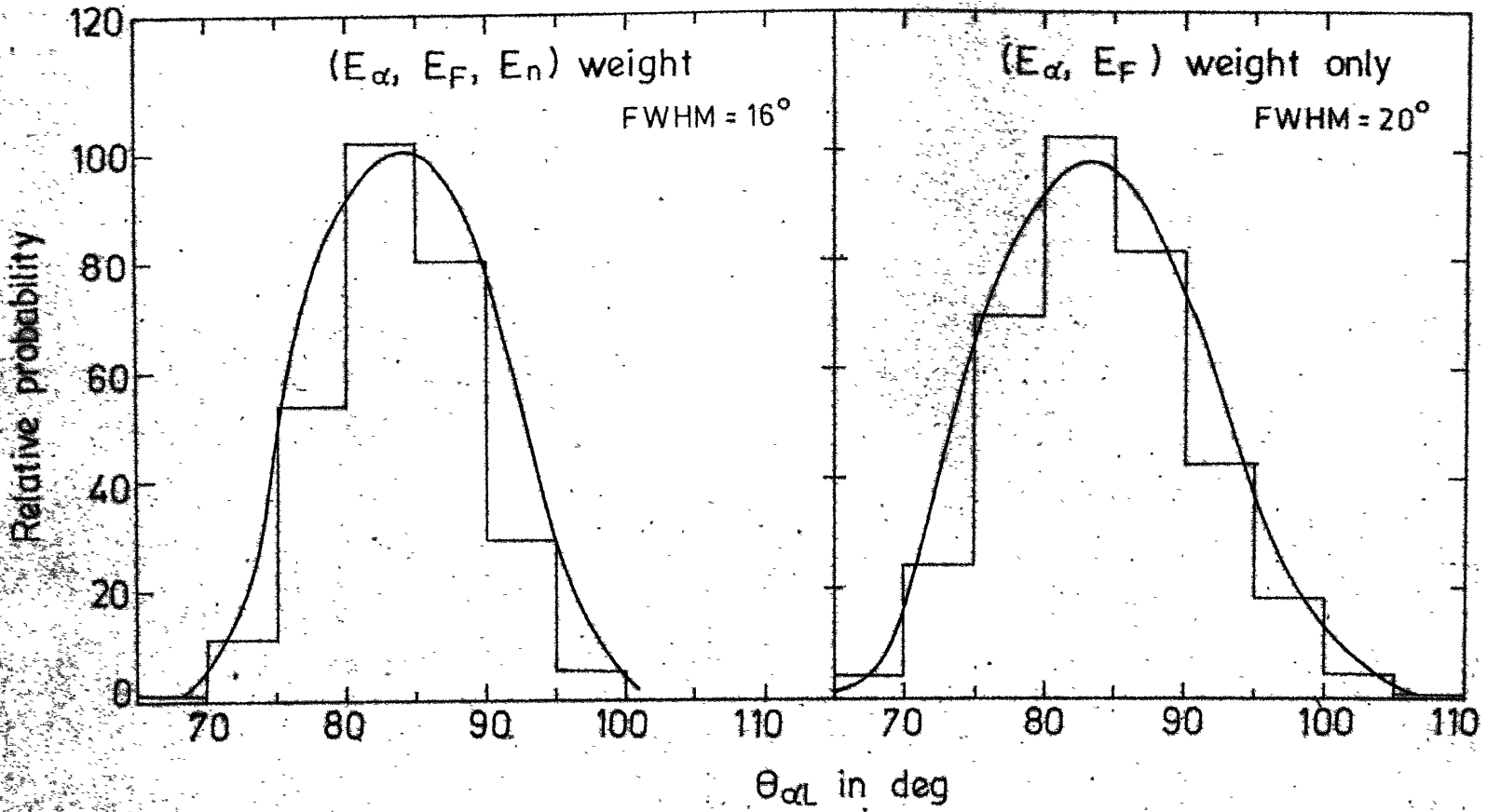

Fig. 5.14. Angular distribution of α-particles calculated by using (E_α, E_F, E_n) weight and (E_α, E_F) weight. (Lines are visual fits)

as regards the width and the mean value for the angular distribution of the alpha-particle with the corresponding experimental values. However, (E_α, E_F, E_n) weight provides a width in better agreement with the results of the latest measurement[2] which give a FWHM $\approx 17^\circ$.

Fig. 5.15 gives the calculated average energy of the alpha-particle ($\bar{E}_\alpha$) as a function of its angle of emission ($\theta_{\alpha L}$). The variation of $\bar{E}_\alpha$ with $\theta_{\alpha L}$ corresponding to both weights show a minimum around the most probable angle of emission as is also observed experimentally. However, the minimum value of $\bar{E}_\alpha$ obtained by using (E_α, E_F, E_n) weight is 16 MeV, in agreement with the accepted value. While the corresponding value as obtained by using (E_α, E_F) weight is nearly 1 MeV above the accepted value. This brings out the effectiveness of the 'E_n-term' in the weight factor for selecting proper volume in the phase space. Figure 5.16 gives the mean value of $\bar{\theta}_{\alpha L}$ as a function of E_α. It is found to be very mildly dependent upon E_α with a small increasing tendency with E_α. This result agrees well with the experimental observation[10]. However, the Guet's result[3] of decreasing angular width with an increase in fragment energy (E_F) could not be reproduced by using (E_α, E_F) or (E_α, E_F, E_n) weights (Fig. 5.17). This probably reflects the relatively lesser effectiveness of the 'E_n-term' in selecting the proper values of the dynamical coordinates of the fragments as compared to those of the alpha-particle as the neutron energy depends more sensitively on the energy of light

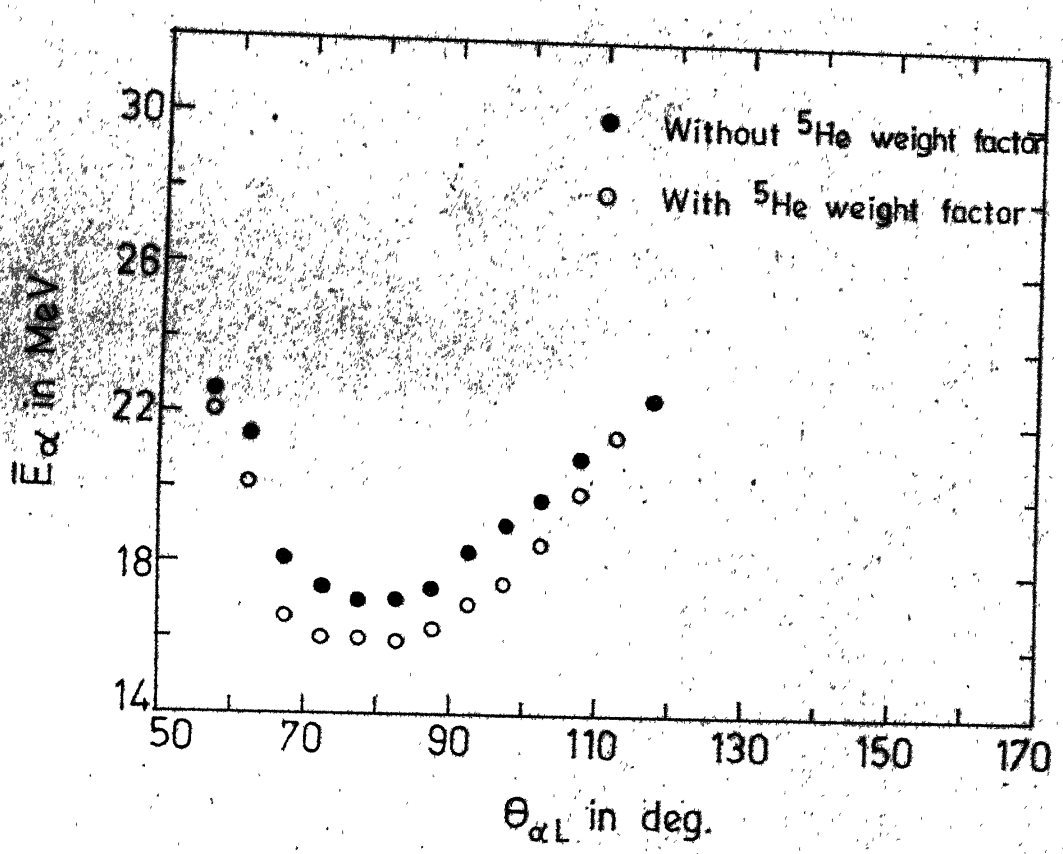

Fig. 5.15. Average alpha-particle energy ($\bar{E}_\alpha$) as a function of the angle of emission ($\theta_{\alpha L}$) with no restriction on D. Mass ratio = 1.4.

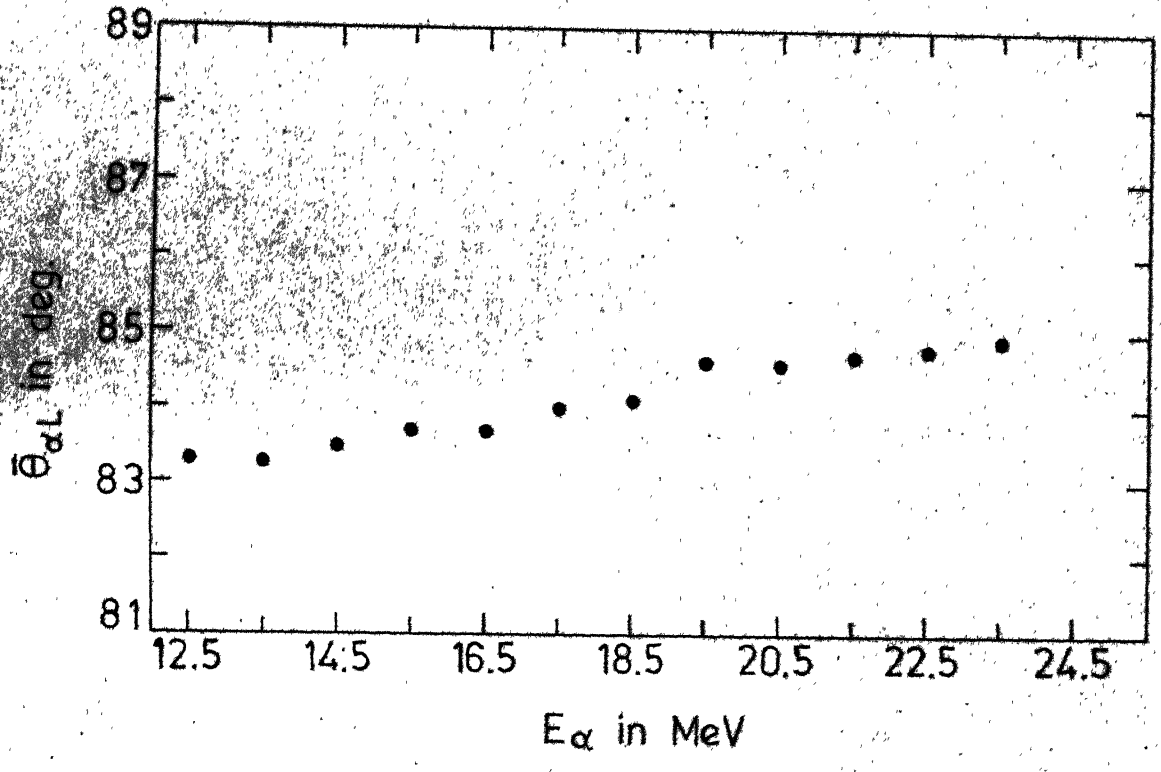

Fig. 5.16. Average angle of emission as a function of the alpha-particle energy. Results are obtained by (E_α, E_F, E_n) weight and with no restriction on D.

particle as compared to the energy of fragments.

(ii) Dependence of $\bar{E}_\alpha$ on E_F and $\bar{E}_F$ on E_α

Fig. 5.18 displays the calculated dependence of average alpha-particle energy ($\bar{E}_\alpha$) on the fragment kinetic energy (E_F). Also shown is the calculated relation between $\bar{E}_F$ and E_α. It is seen that the calculated results are not in agreement with the experimental ones. It might be recalled that the point charge model calculations allowing a free variation in all the SPC-parameters also failed to reproduce the experimental anti-correlation between $\bar{E}_F$ and E_α.

(iii) Distributions in E_α and E_F

Fig. 5.19 gives the calculated distribution in the energy of the alpha-particle. The width and the mean values are in excellent agreement with the experimental values, which are used in calculating the weight factor.

The calculated distribution in the total kinetic energy of the fragments is shown in Fig. 5.20. The calculated width are found to agree reasonably with the experimental results while the calculated mean value is about 1 MeV less than the experimental value. Some asymmetry is discernible in the calculated E_F-distribution. The source for such an asymmetry possibly lies in the approximations made in the calculations. For instance, it might be due to larger values of the interfragment distance being erroneously more favoured

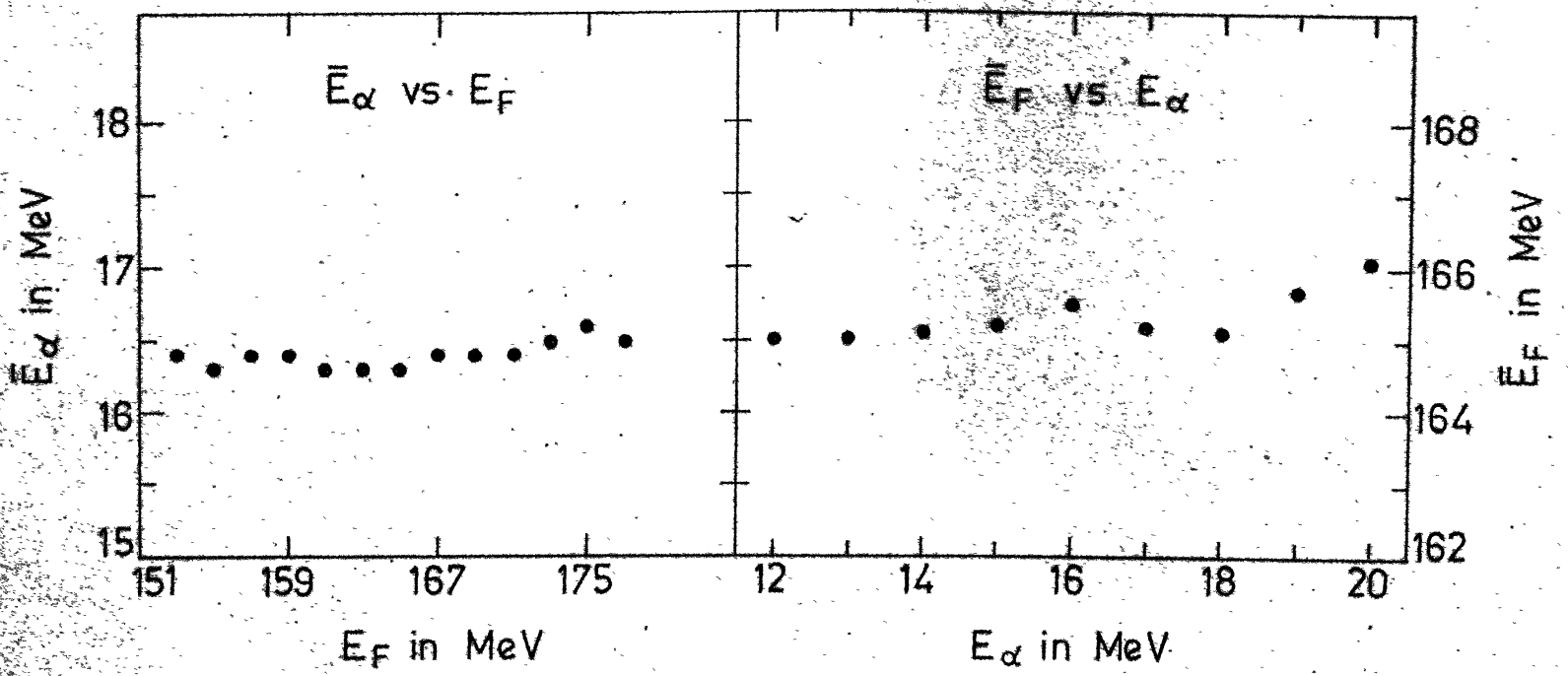

Fig. 5.18. Dependence of average alpha particle energy ($\bar{E}_\alpha$) on fragment kinetic energy (E_F) and dependence of $\bar{E}_F$ on E_α. Results are obtained by using (E_α, E_F, E_n) and without any restriction on D.

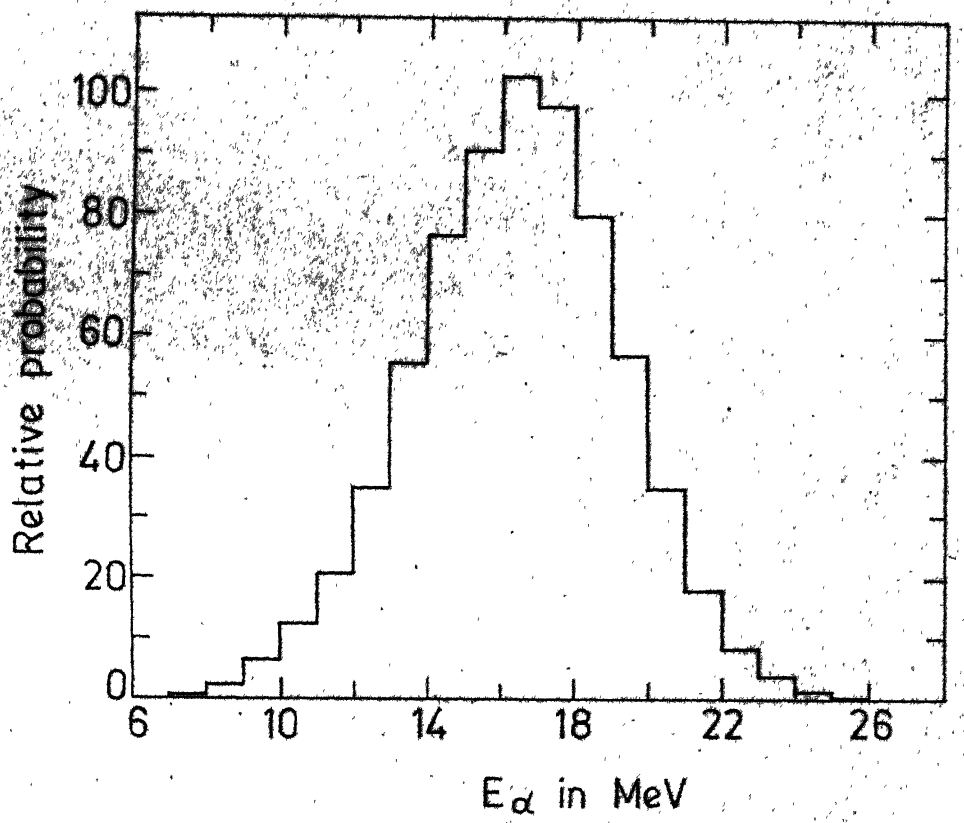

Fig. 5.19. Calculated α-particle kinetic energy ($E\alpha$) distribution. Results are obtained by using ($E\alpha$, E_F, En) weight and with no restriction on D.

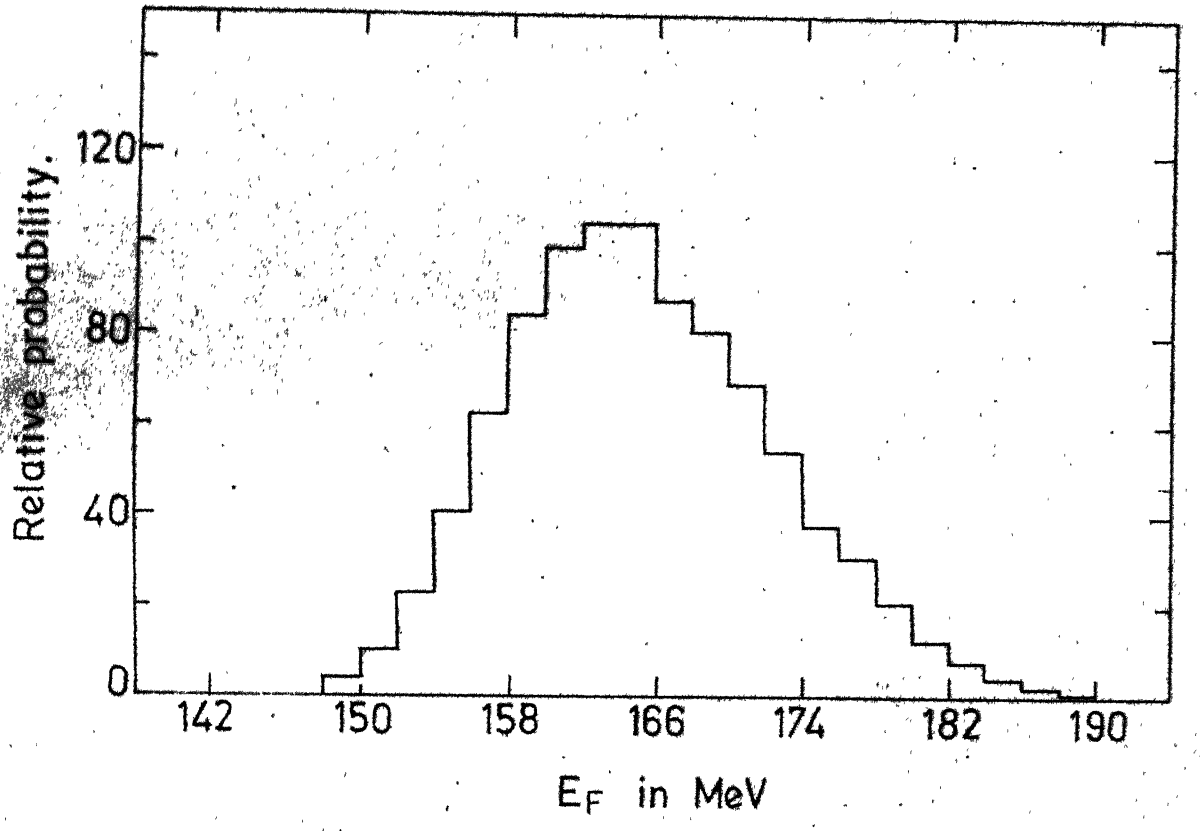

Fig. 5.20. Calculated distribution in the total fragment kinetic energy (E_F). Results are obtained by using (E_α, E_F, E_n) weight and with no restriction on D.

in comparison to the lower ones. This happens in the present calculations as we have approximated the fragment deformations corresponding to the scission point by their ground state values. This results in the availability of relatively higher volume of the initial phase space for the trajectories (with larger D-values) that result in lower values of E_F.

The above argument emphasizes the caution to be observed in chosing the phase space volume for different interfragment distances.

(iv) Distributions in the SPC-Parameters

Fig. 5.21 gives the distribution in the initial kinetic energy of the alpha-particle. The distribution is peaked at about 1.5 MeV with a high energy tail. The distribution in the initial fragment kinetic energy is shown in Fig. 5.22. The distribution is peaked around 28 MeV with a tail in the high energy region. The interfragment distance (D) is distributed as shown in Fig. 5.23. The distribution in D is seen to be fairly wide (FWHM $\approx$ 5 fm) and centered around 24.6 fm.

5.3D-II Results with Restricted Variation of Interfragment Distance and Discussion

We performed calculations with the interfragment distance (D) restricted within a range of $\pm$ 0.5 fm around

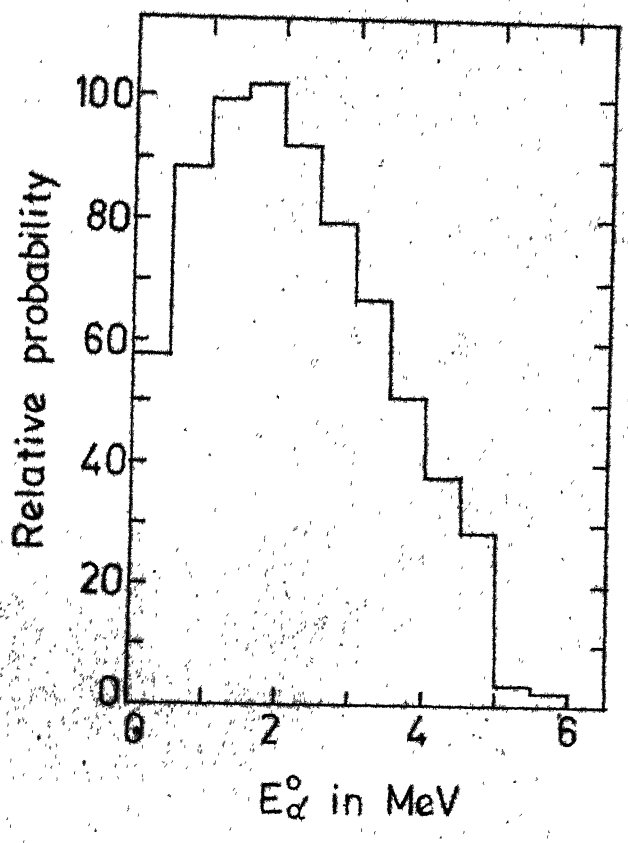

Fig. 5.21. Distribution in the initial α-particle energy obtained by using (E_{α}, E_F, E_n) weight and with no restriction on D.

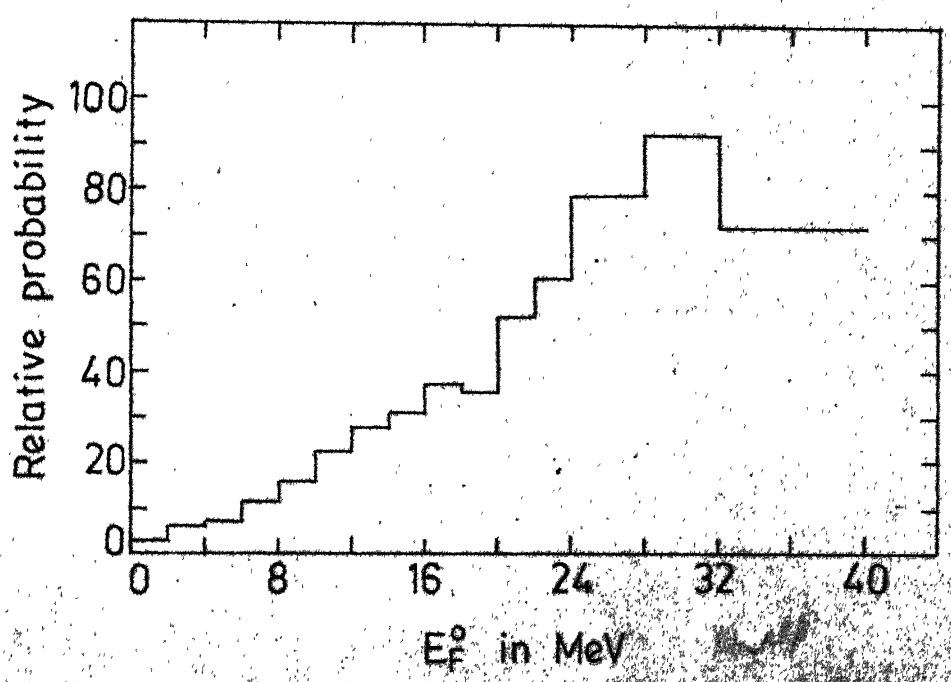

Fig. 5.22. Distribution in the initial total fragment energy (E°_{F}). Obtained by using (E_{α}, E_F, E_n) weight and with no restriction on D.

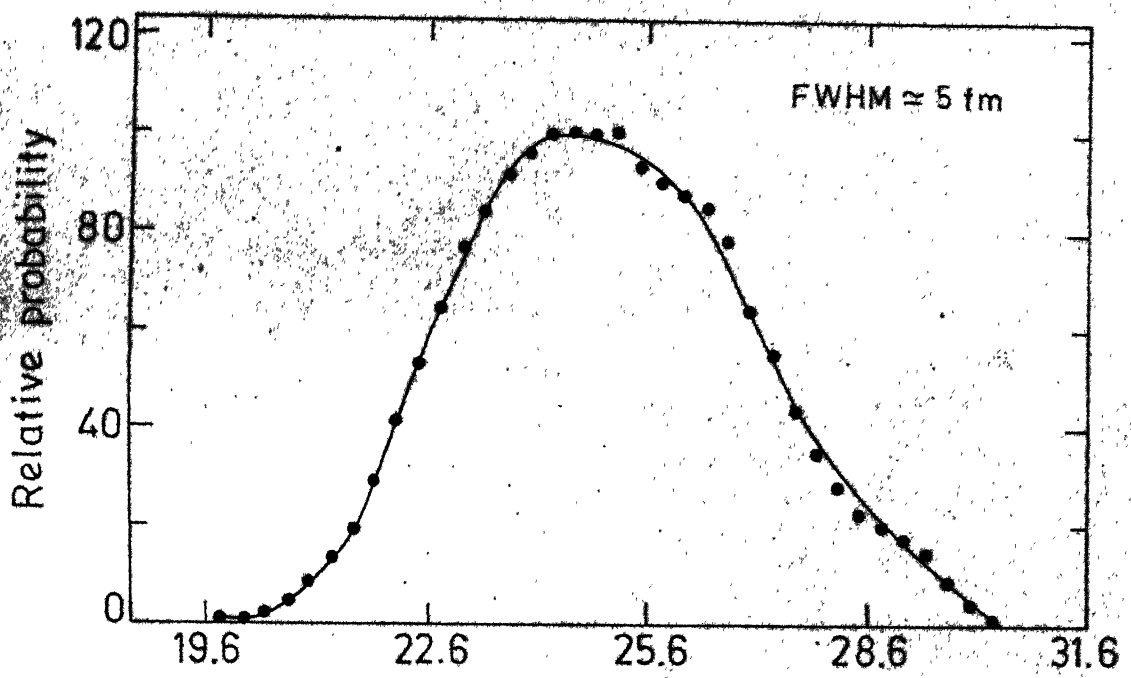

Fig. 5.23. Distribution in the interfragment distance (D). Obtained by using (E_α, E_F, E_n) weight. (Line is only a visual guide).

values varying from 20 fm to 29 fm. The results indicate that a fairly reasonable agreement with the experimental data can be obtained if the value of D is restricted around 24.9 fm.

(i) Angular Distribution and Energy Angle Correlations

Fig. 5.24 gives the calculated angular distribution of the α-particle for different ranges of the interfragment distance. The calculated angular distribution for 'D' around 20.4 fm is seen to be narrower (FWHM $\approx 12^{\circ}$) as compared to the experimental angular distribution (FWHM $\approx 18^{\circ}$). On the other hand, calculations with higher 'D' value around 28.5 fm yield a bit too wide angular distribution (FWHM $\approx 30^{\circ}$). The calculated angular distribution is seen to be of right width (FWHM $\approx 20^{\circ}$) when 'D' is restricted around 24.9 fm. Unlike the variation in the calculated angular width with 'D', the mean value of the angular distribution is nearly unchanged for different 'D' values and agrees with the experimental results.

Fig. 5.25 gives the calculated angular distribution for 'D' restricted around 24.9 fm for two windows of the total fragment kinetic energy (E_F). The mean value of the angular distribution is nearly constant while the distribution becomes narrower for the higher values of the E_F in agreement with the experimental results of Guet et al.[3].

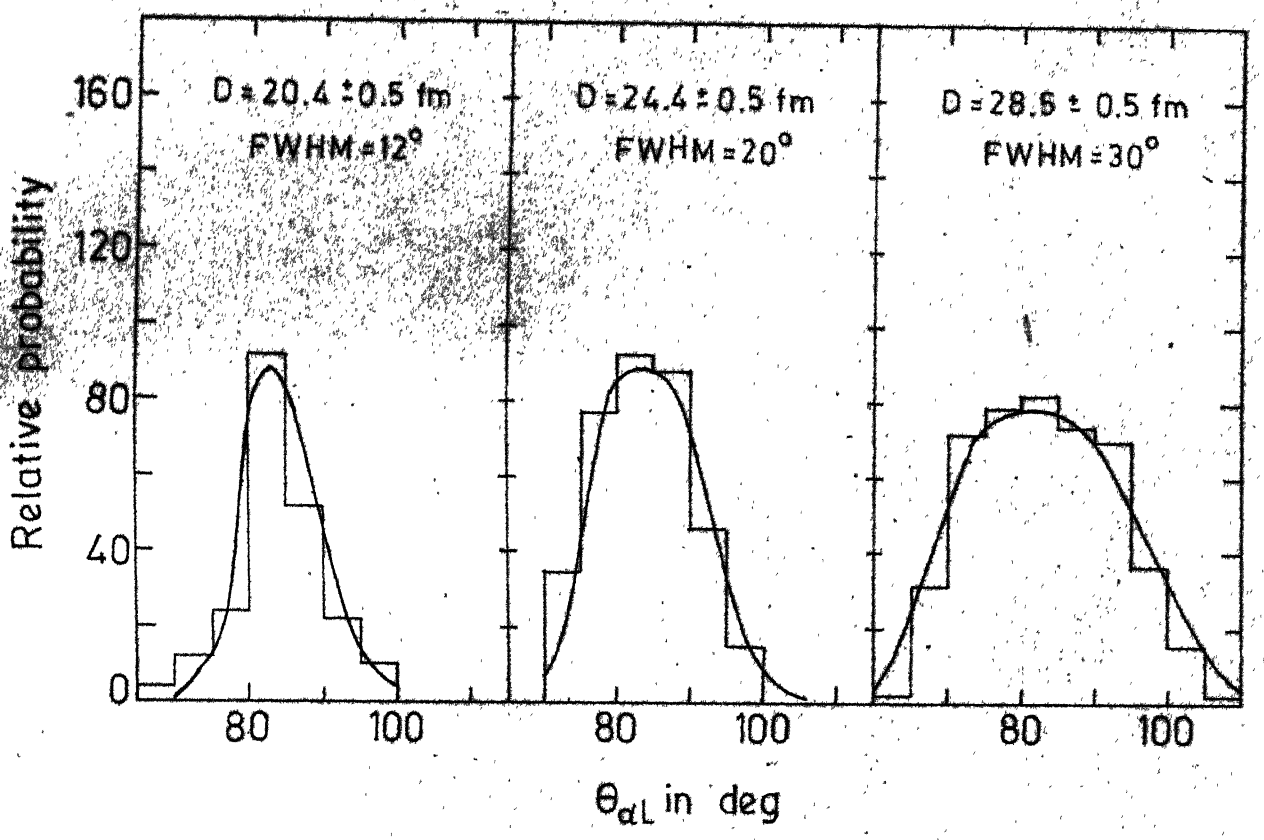

Fig. 5.24. Angular distribution of alpha-particle calculated for different ranges of the interfragment distance (D). (Lines are visual fits).

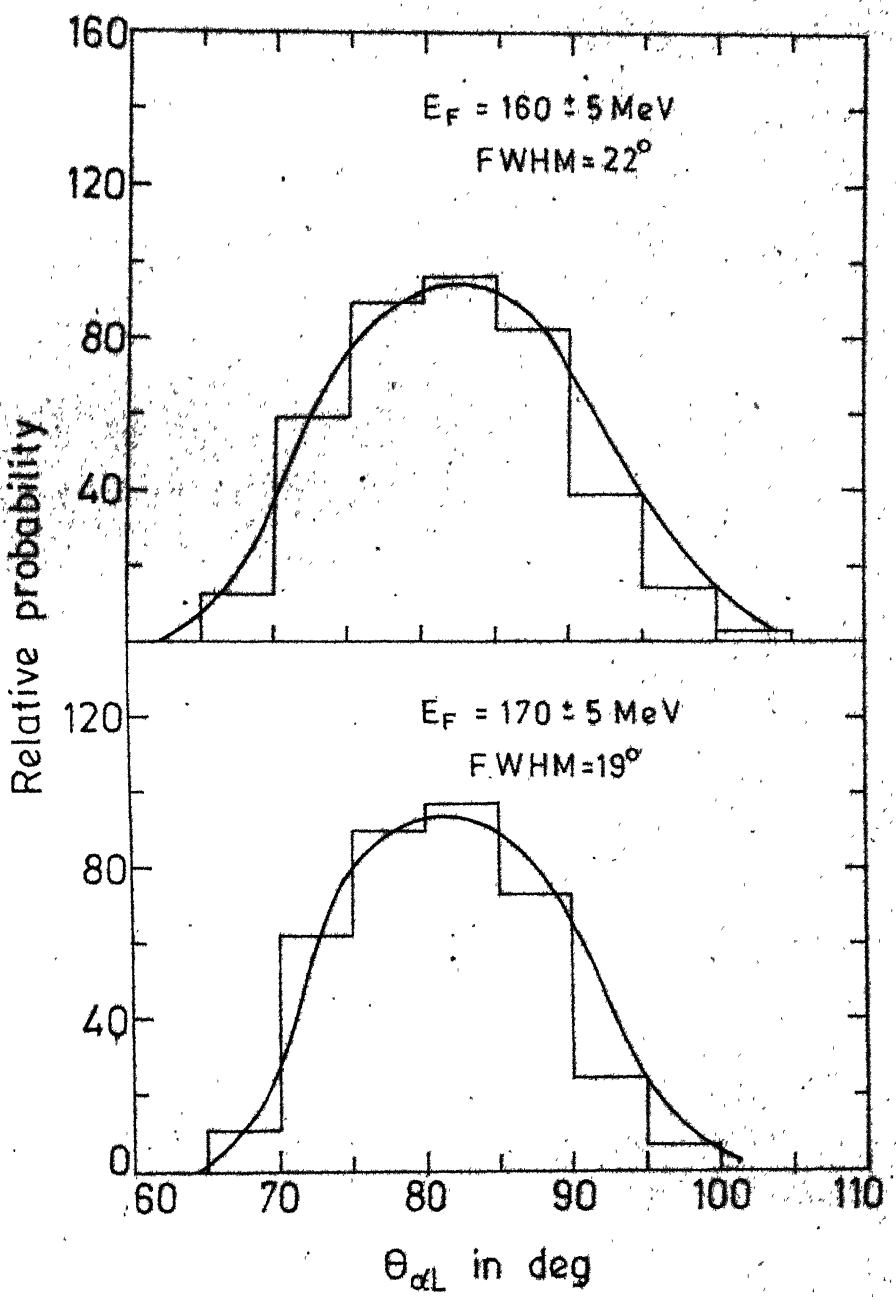

Fig. 5.25. Calculated angular distribution for different windows on the fragment kinetic energy (E_F).

Fig. 5.26 shows the dependence of the average alpha-particle energy as a function of its angle of emission for 'D' restricted around 24.9 fm. The minima observed in the value of $\bar{E}_\alpha$ occurs around the most probable angle of emission in agreement with the experimental results. In addition the minimum value of $\bar{E}_\alpha$ (= 15 MeV) is also in agreement with the experimental value.

(ii) Energy Distributions and Correlations

Fig. 5.27 shows the calculated distributions in the total fragment energy (E_F) and the alpha-particle energy (E_α). The results shown are for 'D' restricted around 24.9 fm and are in nice agreement with the experimental data used in calculating the weight factor. Fig. 5.28 gives the calculated relationship between average alpha-particle kinetic energy $\bar{E}_\alpha$ and the fragment kinetic energy E_F for 'D' restricted around 24.9 fm. The observed fall in the value of $\bar{E}_\alpha$ with E_F and its non-linear nature agree reasonably with the experimentally observed trend. The dependence of average total fragment kinetic energy ($\bar{E}_F$) upon 'E_α' is shown in Fig. 5.29. The observed anti-correlation between $\bar{E}_F$ and E_α comes out to be -0.5 in reasonable agreement with the experimental value (-0.3 ± 0.1) of Mehta et al.[12].

(iii) Distribution in the SPC-Parameters

Fig. 5.30 gives the distributions in the initial total fragment kinetic energy (E_F^o) and alpha-particle

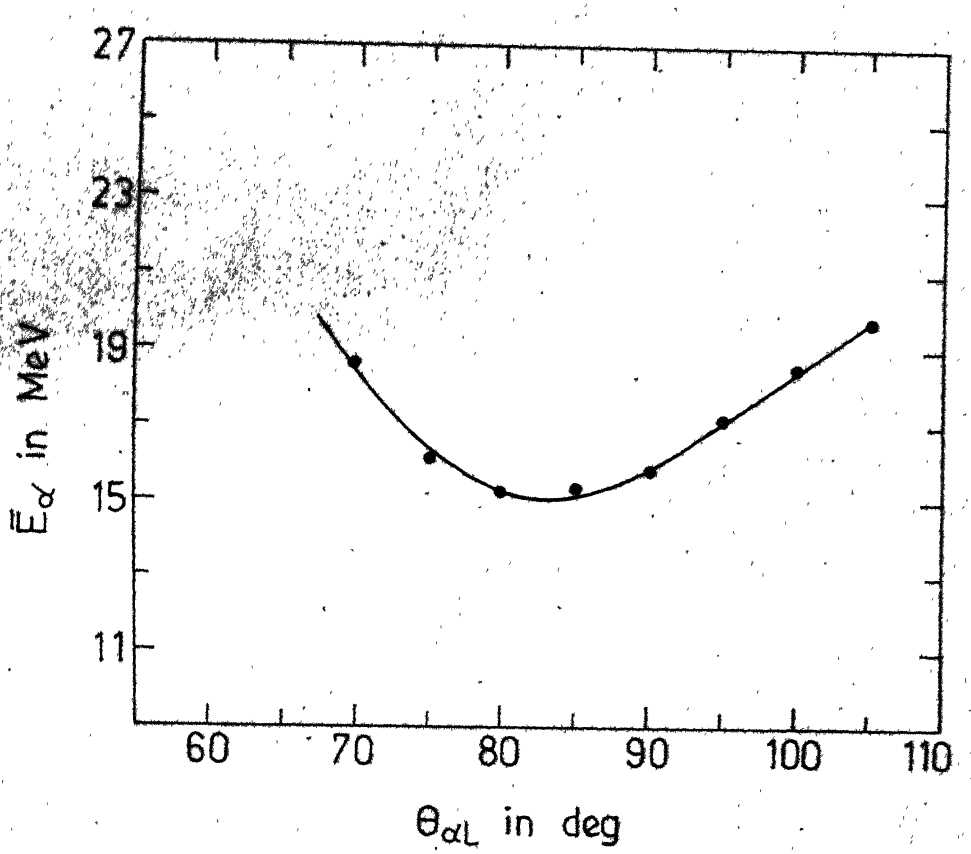

Fig. 5.26. Calculated average alpha-particle energy ($\bar{E}_\alpha$) as a function of the angle of emission ($\theta_{\alpha L}$).

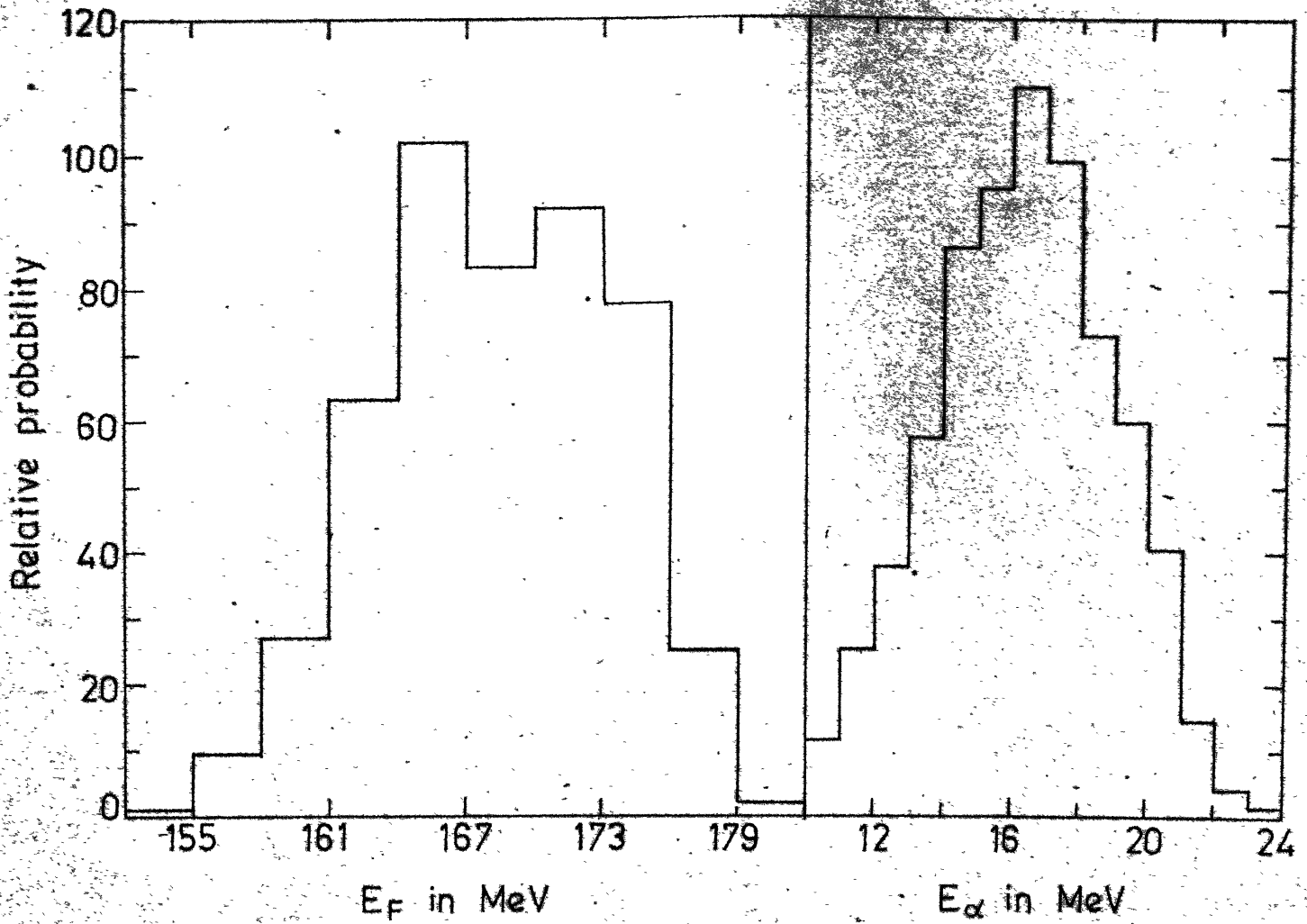

Fig. 5.27. Calculated distributions of the total fragment energy (E_F) and the alpha particle energy (E_α).

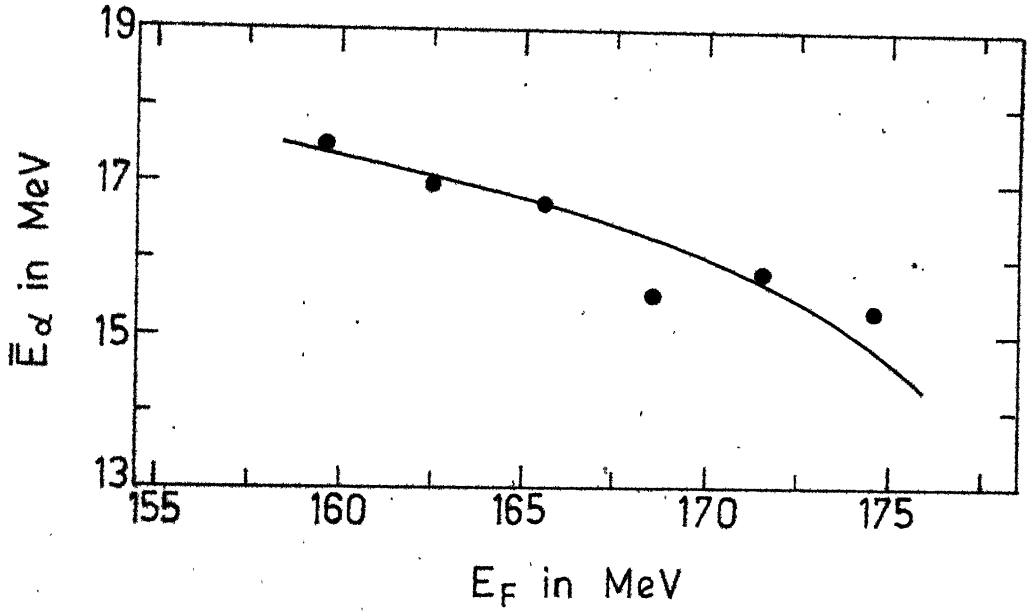

Fig. 5.28. Calculated average alpha-particle energy ($\bar{E}_\alpha$) as a function of the fragment kinetic energy (E_F).

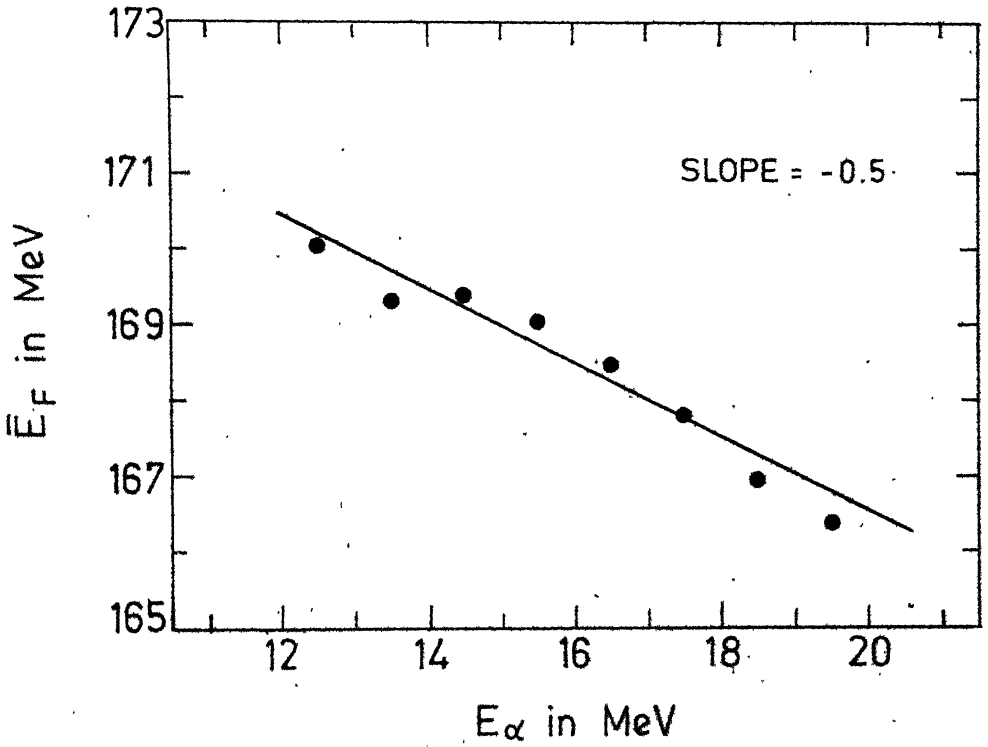

Fig. 5.29. Average fragment energy ($\bar{E}_F$) as a function of alpha-particle energy (E_α).

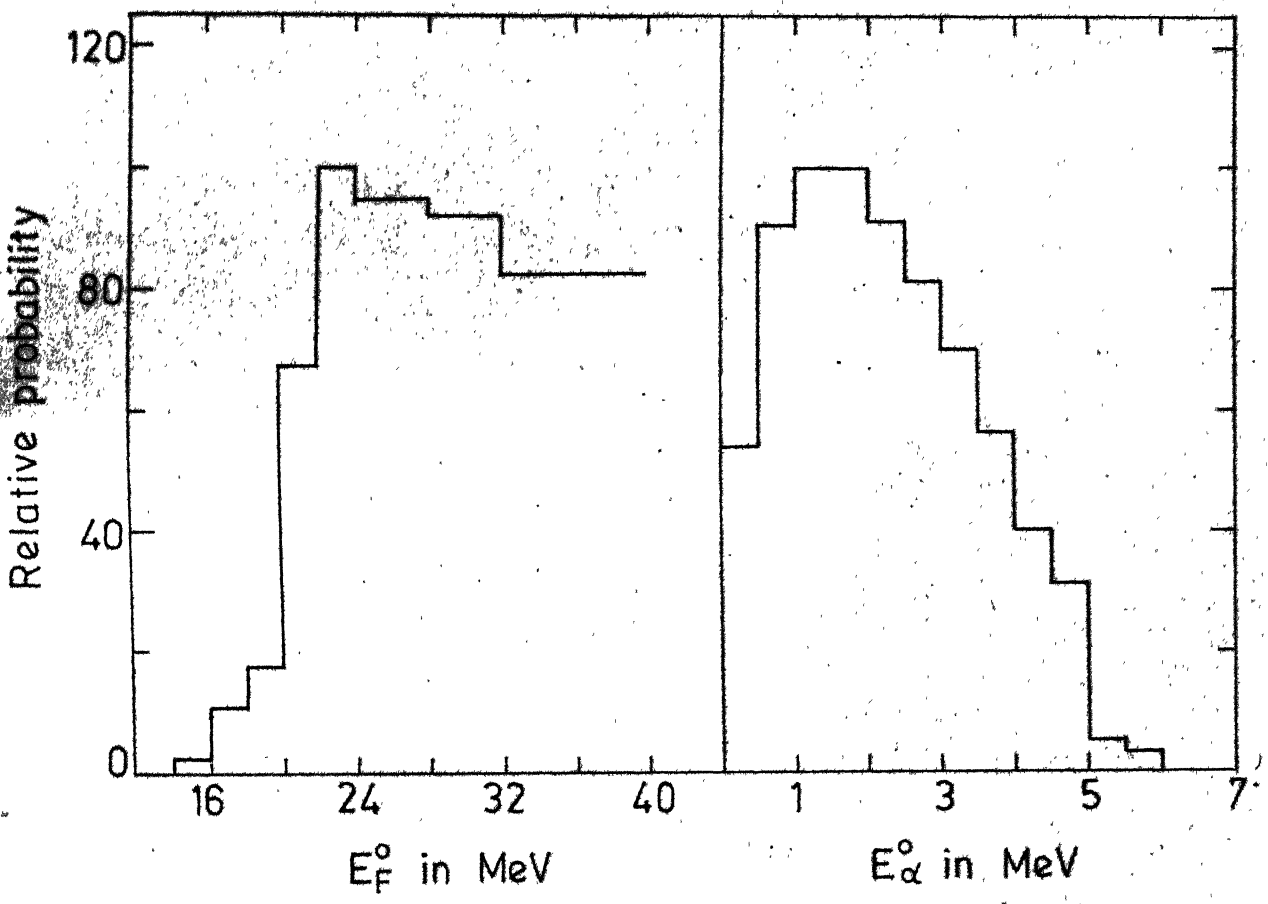

Fig. 5.30. Distributions in the initial fragment kinetic energy (E_F°) and alpha particle kinetic energy (E_α°).

energy (E_α^o) for 'D' restricted around 24.9 fm. Distribution in E_α^o is peaked around 1.5 MeV with a high energy tail. Distribution in E_F^o shows a peak around 24 MeV with a high energy tail, an observation similar to that seen in Fig. 5.22. In the present calculations E_F^o was initially varied upto a maximum of 30 MeV which was extended by about 10 MeV to check the falling trend in E_F^o distribution. Further extension of this range may seem desirable by looking at the calculated distribution. It might be mentioned here that the number of trajectories added in the calculation become fairly large when we include higher E_F^o. This happens as higher E_F^o imply higher 'D' values, requiring more number of points of emission as the distance of the point of emission is varied in uniform steps of 0.1 fm. Even in calculations for extending the range of E_F^o from 30 MeV to 40 MeV, the number of trajectories increased from nearly 40,000 to 70,000. It is seen that this does not affect the main conclusions drawn from the present calculations.

Fig. 5.31 gives the distribution in the distance of the point of emission along the fission axis from the centre of the light fragment. It is peaked around 14 fm with a full width at half maximum of about 5 fm. Distribution in the distance of point of emission from the fission axis is found to be nearly uniform. This reflects the relative insensitivity of the final variables on the coordinate Y.

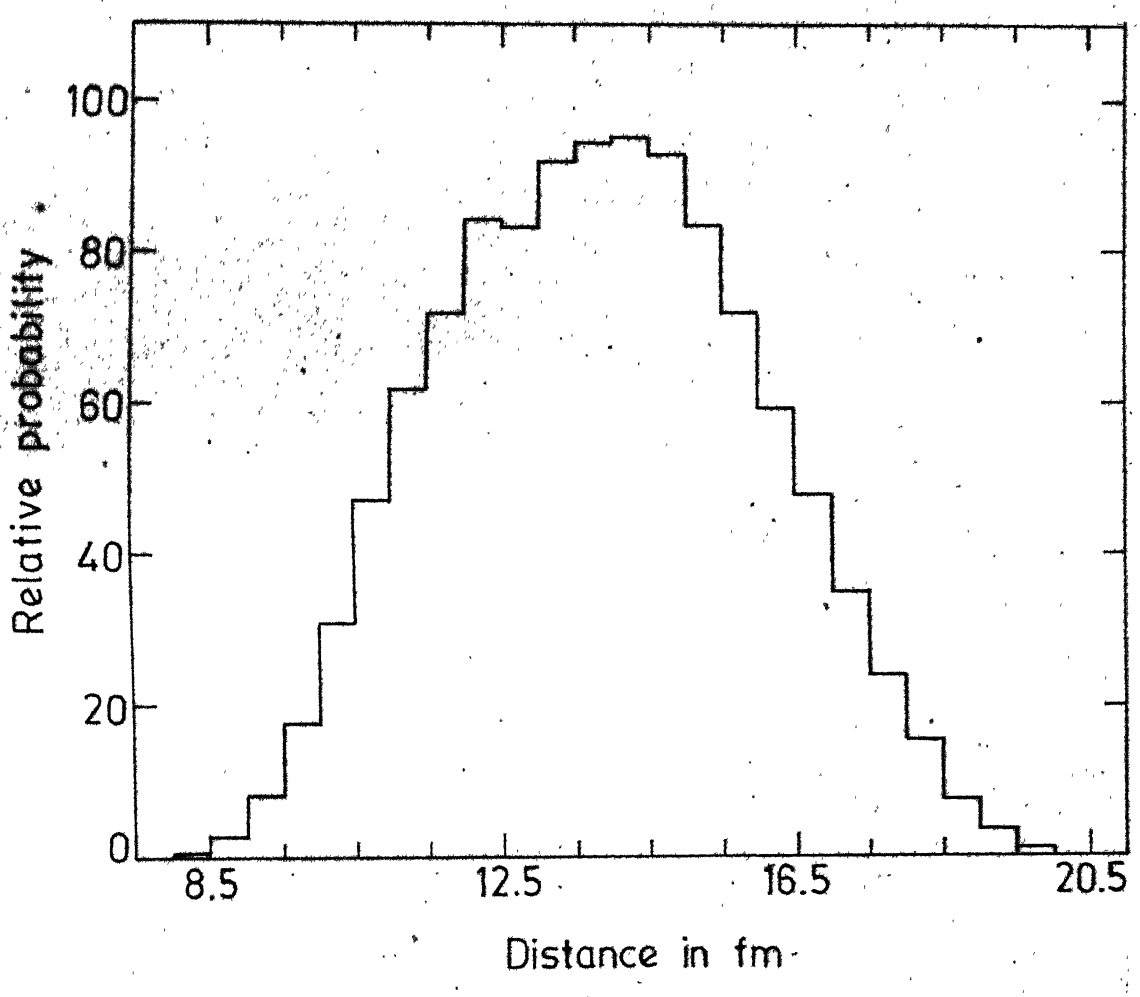

Fig. 5.31. Distribution in the distance of the point of emission along the fission axis as measured from the centre of light fragment.

5.3D-III Results on the Polar Alpha-Particles and Discussion

Due to presence of attractive nulcear forces, some of the alpha-particle trajectories are bent in the polar direction (which is conventionally taken as within 25^{o} from the fission axis). In pure Coulomb force calculations, the Coulomb repulsion of the fragments prohibits the alpha-particle to emerge in the polar direction (refer to Chapter II, section 2.2).

In the present calculations, we have used a fairly fine grid to cover the phase space characterising the SPC. A significant fraction of the total number of trajectories is found to be bent in the polar region. We associate an additional term in the weight factor for the equatorial alpha-particles to take account of the polar alpha-particles. The equatorial term consisted of a product of normalised Gaussian functions corresponding to the distributions of the alpha-particle energy and total fragment energy in the equatorial emission. To this equatorial term was added the polar term obtained by taking product of normalised Gaussian functions corresponding to the distributions of the alpha-particle energy and total fragment energy in the polar emission. With this weight factor we calculated the angular distribution of the alpha-particle over the range covering the equatorial and polar directions. Figure 5.32 gives the calculated relative yield per unit solid angle as a function of the angle of emission ($\theta_{\alpha L}$) of the alpha-particle

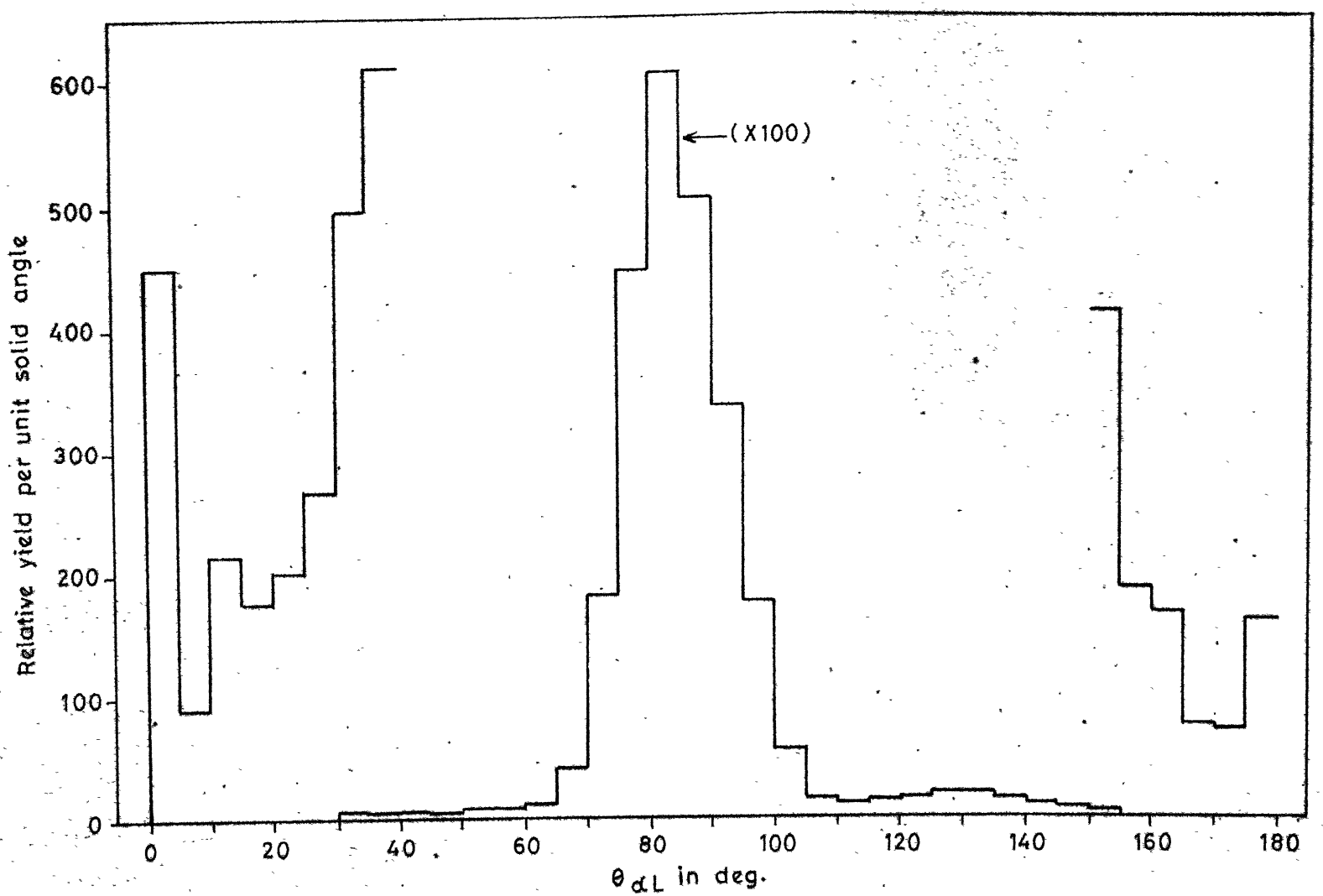

Fig. 5.32. Calculated angular distribution of the alpha-particles

allowing all the SPC parameters free variation. The calculated probability over a small range of the $\theta_{\alpha L}$ was divided by the solid angle corresponding to this range to get the yield per unit solid angle. The calculated angular distribution shows all the important features of the experimental result on the angular distribution[18,19]. Sharp peak around 85° corresponds to the equatorial alpha-particles and has a FWHM nearly 20°. The rising portions near the angles 0° and 180° reproduce the experimental observation for the polar alpha-particles. The polar to equatorial yield ratio for the alpha-particles is found to be 2×10^{-3}. This number is to be compared with the experimental value[20] of 5×10^{-3}. Agreement is fairly satisfactory considering the uncertainties associated with the calculated values and the experimental data as well as the approximate model used for defining the SPC. The yield of the polar alpha-particles emitted along the light fragment is more than the yield of the ones emitted along the heavy fragment in agreement with the experimental trend. However, the ratio of these two yields comes out to be 1.5 which is small in comparison to the experimental value[20] of 3.8. Calculated mean energies of the polar alpha-particle comes out to be about 27.5 MeV and 28.5 MeV for emissions along the light and the heavy fragments respectively. These values are to be compared with the corresponding experimental values which are 25.5 MeV and 24.8 MeV respectively.

The above results indicate that a reasonable agreement is achieved between the calculated and experimental results for the polar emission within the limitations of the model used. Important point to be noted is the fact that a single set of calculation has succeeded in reproducing several important features of both the equatorial and the polar emissions.

In an earlier attempt, Dakowski et al.[21] concluded that the results on polar emission can be reproduced by trajectory calculations including nuclear force only if certain dubious assumptions are made regarding the nuclear force. The present calculations, however, show that the nuclear orbitting model of polar emission deserves further investigations. The agreement between calculated and experimental result is remarkable considering the approximations in the calculations. The calculations for the polar alpha-particles could not be done for different ranges of the interfragment distance due to poor statistics for them. We have not studied the effect of incorporating the friction term in the nuclear interaction. It may be mentioned in passing that the results of Dakowski et al.[21] on polar emission indicate an improvement in the agreement between calculated and experimental results upon inclusion of the friction term.

The nuclear potential employed in the present calculations is an approximate representation of the nuclear interaction between the alpha-particle and the fragments.

However, the main difference between the potential used in the present calculations and the optical model potential used by Dakowski et al.[21] appears to be associated with presence of the repulsive core in the former. The presence of hard-core permits a possibility of α-particle being re-emitted during the evolution of the trajectory even if the separation between the alpha-particle and a fragment goes below the sum of their half density radii. We consider alpha-particle to be absorbed only if once re-emitted during the evolution of the trajectory it comes back again under the attractive part of the nuclear potential to see the repulsive core in it (thus the fragment-alpha configuration will resemble a bound state). On the other hand, for some polar trajectories, the alpha-particle does not see at all the repulsive core of the nuclear potential. The latter type of trajectories will resemble the trajectories as obtained in the calculations of Dakowski et al.[21]. Figs. 5.33 and 5.34 show the trajectories corresponding to the above mentioned possibilities. The effect of repulsive core in the nuclear potential is manifested in the region of kink (marked as RC in Fig. 5.33) in alpha-particle trajectory. The experimental results on the alpha-particle scattering at energies below Coulomb barrier are not reliably usuable to probe the deeper parts of the nuclear potential. The calculated results on scattering at such energies are rather insensitive to these parts of the nuclear potential. Thus the experimental data do not provide a clear picture regarding

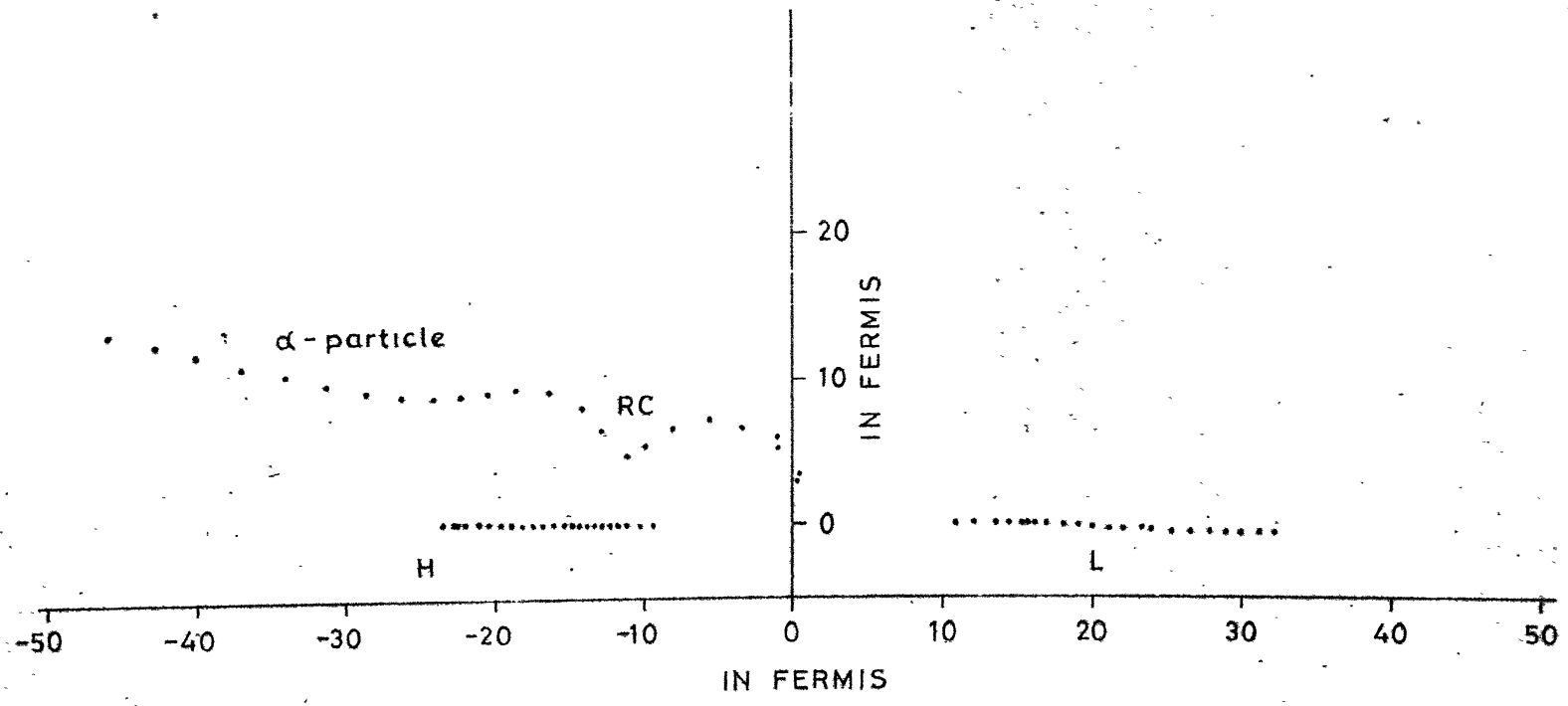

Fig. 5.33. Trajectories of the α-particle and the light (L) and the heavy (H) fragments showing the polar emission

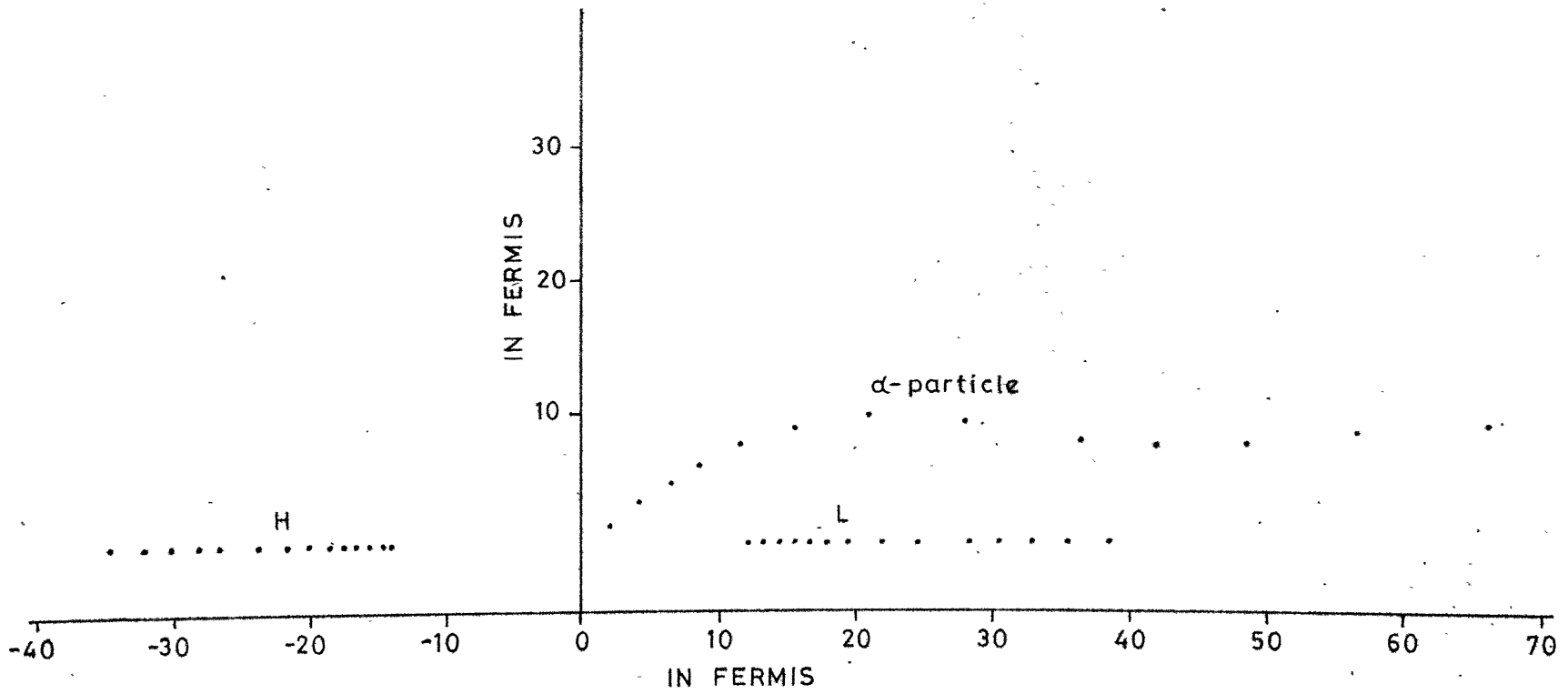

Fig. 5.34. Trajectories of the α-particle and the light (L) and the heavy (H) fragments showing the polar emission

the presence or absence of the repulsive part in the nuclear potential. Theoretical investigations for understanding the behaviour of the deeper part of nuclear potential suggest that repulsive core may arise from the antisymmetrization effect etc.[22,23].

(i) On the Validity of Delayed Emission Hypothesis

Possibility of explaining the polar emission by delayed tripartion is discussed by Piasecki et al.[20]. They discard this possibility as their calculations indicate necessity of a delay of the order of 10^{-20} sec. (implying an increase in interfragment distance of $\simeq$ 200 fm) for explaining polar emission. However, considering the alpha-particle trajectory shown in Fig. 5.33, we can see that if the alpha-particle were emitted in the appropriate direction around the region marked as 'RC', it can come out in the polar direction. This will imply a delayed emission at a point when fragments are nearly 27 fm apart starting with interfragment distance of $\simeq$ 20 fm. Thus we see that the alpha-particle trajectories which are bent in the polar direction after experiencing the repulsive core of the nuclear potential will remain valid trajectories with reasonable values for E_α and E_F even after the elimination of the repulsive core provided we assume the alpha-particle emission to be after a little delay (which may cause an increase of about 10 fm in the interfragment distance).

It is seen that the presence of nuclear attraction, which is ignored in the calculations of Piasecki et al.[24], is responsible for bending of such trajectories in the polar direction.

5.3E Summary and Conclusions

The present calculations have indicated that substantial changes in the SPC may be incumbent once we include the nuclear interaction among the three particles in the light charged particle accompanied fission. This result is in agreement with the findings by Dakowski et al.[25] while results of Guet et al.[26] are not consistent with it.

The calculations with a free variation of all the SPC-parameters and including nuclear force have succeeded in reproducing quite satisfactorily the angular distribution of the alpha-particles, its energy distribution, its average energy as a function of the angle of emission etc. These calculations predict some characteristics of the polar emission in reasonable agreement with the experimental findings. In addition, the calculations predict reasonably well the results for the ^{5}He data[16] (calculated mean neutron energy comes out to be in excellent agreement with the experimental value). The results indicate that the method used by us which permits a free variation in all the SPC-parameters is capable of providing accurate and reliable information regarding the SPC. Need of using a realistic

model for describing the SPC is brought out by the present calculation. Inclusion of the nuclear forces is one step towards making the point charge model more realistic and the results obtained are encouraging. Use of ^{5}He-data has come out to be fruitful in proper selection of the SPC from the phase space of the three particles. Furthermore it improves the agreement between the calculated and experimental results. However, it is seen that the selection of the proper phase space by the weight factor obtained by using ^{5}He-data is more effectively done for the alpha-particle dynamical coordinates in comparison to that for the fragment dynamical coordinates. This is expected as the energy of the neutron from ^{5}He breakup is comparatively less sensitive to the fragment motion. Similar type of data, which have sensitive dependence upon fragment motion (such as, on the scission neutrons!), will be quite useful in fixing a proper time origin for the trajectory calculations in a more reliable way.

The calculations with no restriction on 'D' failed to reproduce observed anticorrelation between $\bar{E}_F$ and E_α and Guet's result of decreasing angular width with increase in E_F. These results along with the energy and angular distributions and energy-angle correlations could be reproduced by calculations with restricted variation in interfragment distance (D). The calculations indicate that best agreement with experimental data is achieved when D is restricted

around 24.9 fm in a narrow range. Thus, the condition of reproducing the anticorrelation and the Guet's result is seen to necessitate a compact scission configuration (with small spread in the value of D), albeit with large initial kinetic energies compared to the result of point charge model calculations.

The present calculations have not included the friction term in the nuclear potential. This term may have important effects in the results, e.g., those on the polar emission. Also, the initial values of fragment deformations are taken approximately while their time dependence has not been considered. These approximations have affected the results of the present calculations. In particular, this may mean that the value of 'D' obtained by calculations with restricted D-variation should be taken only tentatively. As stated earlier the present calculations are exploratory in nature and we find that there is a need of more realistic model for describing the SPC. For example, the approximations regarding the fragment deformations have resulted in an unrealistic bias for higher 'D' values. This is very clearly reflected in the asymmetry observed in the calculated distribution of the total fragment kinetic energy with no restriction on D (Fig. 5.20). The mean value is also found to be lower by a small amount ($\simeq$ 1 MeV) from the experimental value. This bias for higher 'D' values appears due to comparatively higher range available for the variation

of the X-coordinate (see Fig. 5.1) of the alpha-particle. The bias can be reduced if we constrain the calculations to the trajectories which have value of $\theta_{\alpha L}$ in a narrow range. A calculation with $\theta_{\alpha L}$ restricted between 80° and 85° shows that the mean value of the E_F becomes in excellent agreement with the experimental value and also the asymmetry is substantially reduced. A calculation with these approximations removed will be free from such unrealistic bias coming in the selection of the phase space of the three particles to characterise the SPC.

REFERENCES

1. Z. Fraenkel, Phys. Rev. 156 (1967) 1283
2. D.E. Cumpstey and D.G. Vass, Proc. of Symp. on Physics and Chemistry of Fission, (Jülich, 1979), IAEA, Vienna (1980), IAEA-SM-241/F12
3. C. Guet, C. Signarbieux, P. Perrin, H. Nifenecker, B. Leroux and M. Asghar, Le Journal De Physique Letters, 39 (1978) L-213; C. Guet, C. Signarbieux, P. Perrin, H. Nifenecker, M. Asghar, F. Caitucelli and B. Leroux, Nucl. Phys. A314 (1979) 1
4. B. Krishnarajulu and G.K. Mehta, Pramana 4 (1975) 74
5. F. Fossati and T. Pinelli, Nucl. Phys. A249 (1975) 185
6. P. Fong, Phys. Rev. C16 (1977) 251
7. Y. Boneh, Z. Fraenkel and I. Nebenzahl, Phys. Rev. 156 (1967) 1305
8. S. Mukherji, Nucl. Phys. A129 (1969) 297
9. I. Halpern (1963) CERN Report 6812/P (unpublished)
10. M.J. Fluss, S.B. Kaufman, E.P. Steinberg and B.D. Wilkins, Phys. Rev. C7 (1973) 353
11. K. Tsuji, A. Katase, Y. Yoshida, T. Katayama, F. Toyofuku and H. Yamamoto, Proc. of Symp. on Physics and Chemistry of Fission, (Rochester, 1973), IAEA, Vienna (1974) p. 405
12. G.K. Mehta, J. Poitou, M. Ribrag and C. Signarbieux, Phys. Rev. C7 (1973) 373
13. R.K. Choudhury and V.S. Ramamurthy, Phys. Rev. C18 (1978) 2213

14. J. Blocki and T. Krogulski, Nucl. Phys. A122(1968) 417

15. K.T.R. Davies, R.A. Managan, J.R. Nix and A.J. Sierk, Phys. Rev. C16 (1977) 1890

16. E. Cheifetz, B. Eylon, Z. Fraenkel and A. Gavron, Phys. Rev. Lett. 29 (1972) 805

17. C. Ngo, B. Tamam, M. Beiner, R.J. Lombard, D. Mas and H.H. Deubler, Nucl. Phys. A252 (1975) 237

18. E. Piasecki, M. Dakowski, T. Krogulski, J. Tys and J. Chwaszczewska, Phys. Lett. 33B (1970) 568

19. F. Caitucoli, B. Leroux, P. Perrin, G. Barreau, M. Asghar and N. Carjan, Proc. of Symp. on Physics and Chemistry of Fission, (Jülich, 1979), IAEA, Vienna (1980)

20. E. Piasecki and L. Nowicki, Proc. of Symp. on Physics and Chemistry of Fission, (Jülich, 1979), IAEA, Vienna (1980) p. 193

21. M. Dakowski, E. Piasecki and L. Nowicki, Acta Phys. Polonica B9 (1978) 933

22. K.C. Panda, B. Behera and R.K. Satpathy, J. Phys. G : Nucl. Phys. 7 (1981) 937

23. R.K. Satpathy, Sambalpur University, India, Private Communication

24. E. Piasecki, M. Dakowski, J. Blocki and L. Nowicki, INR Report 1720/IA/PL/A (1977)

25. M. Dakowski, E. Piasecki and L. Nowicki, Nucl. Phys. A315 (1979) 370

26. C. Guet, H. Nifenecker, C. Signarbieux and M. Asghar, Proc. of Symp. on Physics and Chemistry of Fission, (Julich, 1979) IAEA-SM-241/F13.

CHAPTER - VI

SUMMARY AND CONCLUSIONS

The phenomenon of emission of light charged particles (LCP) is a relatively less understood aspect of nuclear fission and deserves further investigation. The present thesis reports

(i) a comparative experimental study of two aspects of the light charged particle accompanied fission, namely, the equatorial and the polar emissions.

(ii) a study of the trajectory calculations to extract information on the dynamical aspects of the fission process utilizing the characteristics of the equatorial LCPs and to probe the possibility of an unified description of the polar and equatorial emissions of LCPs.

Short critical surveys of the LCP accompanied fission and the trajectory calculations along with some suggestions and comments are also included.

Simultaneous measurements on the equatorial and polar LCPs emitted in the fission of ^{235}U by thermal and fast (600 KeV) neutrons have been performed using a novel ionization chamber geometry, identification of LCP being accomplished with the help of a ΔE--E semiconductor detector telescope. The geometry permits use of broad fission source without losing the angular resolution necessary for an appropriate identification of the polar and equatorial LCPs. Detailed Monte Carlo calculations on the detection efficiency have been performed. Results

on the absolute and relative yields of the equatorial and polar LCPs in the thermal neutron induced fission are in agreement with the earlier work. The yields of the polar and equatorial protons show a marked increase when the neutron energy changes from the thermal to the fast value while the yields of the polar and equatorial alpha-particles indicate a mild decrease. Most interesting finding of the present study is the observed similarity in the change of yields of LCP with a change in neutron energy for the equatorial and the polar emissions. Such a result provides a rather clear evidence suggesting a similarity in the emission mechanisms of the equatorial and polar LCPs in fission. Two hypotheses on the mechanism of polar emission, namely, the nuclear orbitting hypothesis and the quantum mechanical diffraction hypothesis, appear most promising in view of the present experiment as both of them attempt essentially to provide an unified description of the polar and equatorial emissions of LCPs.

It might be worthwhile to mention the rare nature of the phenomenon that has been studied in the present experiment as we are dealing with coincidence measurements on neutron induced reactions with extremely low cross-sections (for fast neutrons, the cross-section is as low as few tens of microbarns for the polar LCPs).

Trajectory calculations have been performed under point charge model approximation exploiting some recent results on the energy-angle correlation in the alpha-particle accompanied fission

The calculations were done by providing a restricted variation in the interfragment distance around values lying between the limits expected on the basis of different fission theories. Other parameters characterising the scission point configuration were allowed their normal statistical distribution as demanded by the experimental weight factors used for selecting the phase volume characterising the scission point configuration from the initial phase space of the alpha-particle and fragments. A relatively compact scission point configuration with interfragment distance below 21 fm could reproduce various energy-angle correlations of the alpha-particle and fragments and is thus favoured by the point charge model calculations.

An improvement in the trajectory calculations has been attempted by

(i) making the point charge model more realistic by including the effects due to fragement deformations and the nuclear interaction between the alpha-particle and fragments

(ii) using the data on the breakup of unstable ^{5}He particle produced in LCP accompanied fission for fixing a proper time origin in the calculations coinciding with the scission moment

(iii) using comparatively finer grids for various initial variables characterising the scission point configuration providing an uniform coverage of the initial phase space of the three particles and looking for a possible unified description of the equatorial and polar emissions of LCPs.

With these improvements, calculations have been performed with a free variation of all the initial variables characterising the scission point configuration; proper selection from the phase space being done by the probability weight factor obtained by using the experimental energy distributions of the alpha-particle, the fragements and the neutrons from the ^{5}He breakup. The results obtained reproduced very well the angular distribution of the alpha-particle, the distributions in the energy of the alpha-particle and fragments and some energy-angle correlations. Use of data on the ^{5}He - breakup is found to be useful in getting over the basic uncertainty regarding the proper fixing of the time origin in trajectory calculations but need of more accurate data is felt. However, the observed anticorrelation between energies of the alpha-particle and fragments and the observed narrowing of the alpha-particle angular distribution with increasing fragment energy could be reproduced only when a restriction in the variation of the interfragment distance is put. Calculations with restricted variations in interfragment distance have been performed covering low as well as high values of interfragment distance. These calculations indicate that a reasonable agreement between the experimental and calculated energy-angle correlations and distribution is possible when the interfragment distance is restricted around 24.9 fm.

Thus it is realised that significant changes in the reconstructed scission point configuration may be incumbent once the point charge model is made more realistic by incorporating

nuclear interaction etc. Need of further improvement has been suggested by a consideration of some of the calculated results. They concern with inclusion of accurate deformations at the scission point as well as their time dependence during the time evolution of the system. In addition friction term in the nuclear potential etc. should be considered. It is felt that incorporation of these improvements might affect the conclusions drawn from the present calculations.

Reasonable reproduction of the experimental characteristics of the polar emission of alpha-particle is achieved by the present trajectory calculations with improved model.

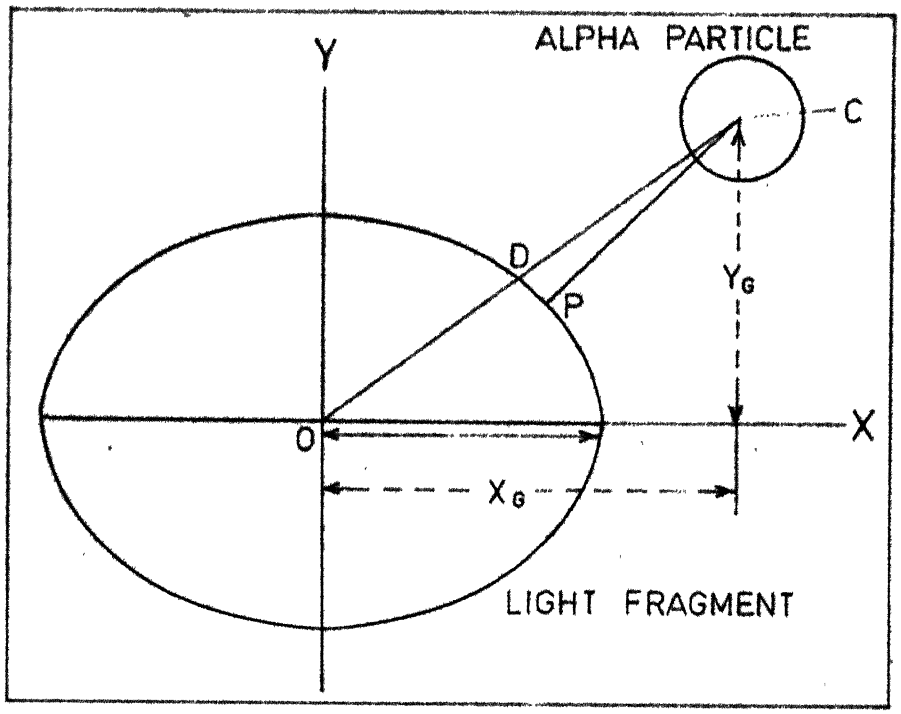

Fig. A.1. Schematic diagram showing the alpha-particle and the light fragment used in calculating the shortest distance between their equivalent sharp surfaces.

Eqn. (4) is a fourth degree algebraic equation and has been solved numerically on the computer. Newton-Raphson method has been used for this purpose. The initial guess for the value of k is obtained by approximating point 'i' with the point D shown in the Fig. This value k_g is given as

$$k_g = [\sqrt{(X_G^2 + \beta^2 Y_G^2)}/(r_o A^{1/3} \rho^{2/3})] - 1$$

where 'r_o' is the nuclear radius parameter and 'A' is the mass number of the light fragment.